UNIVERSITÉ DU LUXEMBOURG

PhD-FSTC-21-2010

The Faculty of Sciences, Technology and Communication

DISSERTATION

Defense held on 19/07/2010 in Luxembourg

to obtain the degree of

DOCTEUR DE L'UNIVERSITÉ DU LUXEMBOURG

EN SCIENCES DE L'INGÉNIEUR

by

Vincent HANUS
Born on 31 October 1983 in Arlon (Belgium)

Analysis and Modelling of the Noise Generation during vibratory Pile Driving and Determination of the Optimization Potential

Dissertation defense committee

Prof. Dr.-Ing. Arno Zürbes, dissertation Supervisor
Professor, Fachhochschule Bingen
Professor, Université du Luxembourg

Prof. Dr.-Ing. Stefan Maas, Chairman
Professor, Université du Luxembourg

Ass. Prof. Dr.-Ing. Danièle Waldmann, Vice Chairman
Assistant Professor, Université du Luxembourg

Prof. Dr.-Ing. Rainer Nordmann
Power Alstom, Switzerland
Professor, Technische Universität Darmstadt

Prof. Dr.-Ing. Jean-Claude Golinval
Professor, Université de Liège

Abstract

Impact driving, pressing and vibrodriving are the three main methods to drive sheet piles. Vibratory pile driving is efficient when compared to impact driving: its installation time is shorter; it generates less noise, and reduces the damage to the driven sheet piles. The sound level generated during vibrodriving varies almost between the very high level of an impact driving and the lowest sound level of a pressing.

This doctoral thesis, entitled "Analysis and modelling of the noise generation during vibratory pile driving and determination of the optimization potential", was made within the Research Unit of Engineering at the University of Luxembourg and in collaboration with ArcelorMittal Research & Development Esch.
In the first part, sound measurements feasibility is thoroughly studied. Particular attention is paid to the measurement conditions on construction sites and to the measurement methods (measurements of sound power level, beamforming and thermography). These methods are outlined and the provided results are compared. In addition, the different causes of noise such as impacts with the safety device, the guides, or the neighbouring sheet piles are analysed. A large part of the noise can be generated in the interlocks of the sheet piles. Various parameters influencing the expected noise level are studied in details.
In the second part of the thesis, the acceleration measurements of the full-scale experiments are used to calibrate a Finite Element model. A parametric study analyses how the most important mechanical parameters influence the noise level.

This research has shown that a decrease of the noise generation on construction sites can be obtained by two ways: by recommendations for installation of sheet piles at the construction site, and by requirement of constructive measures that significantly reduce the noise level.
During the vibrodriving, no impact should occur between the sheet piles and guides or safety devices (if possible). The free height of the already installed sheet pile should be as small as possible. An appropriated arrangement of the two clamps of the vibrator could also reduce noise generation.
The design of the connections can affect the noise too. The modification of the section geometry and the use of absorbent material in the interlock are also shortly considered.

Résumé

Trois méthodes sont majoritairement utilisées pour foncer des palplanches : le battage, le vérinage et le vibrofonçage. Les avantages de cette dernière méthode par rapport au battage sont notamment une mise en œuvre plus rapide, un environnement sonore moins perturbé, et une palplanche moins endommagée. En réalité, les niveaux sonores obtenus pour le vibrofonçage se répartissent pratiquement entre le niveau très élevé du battage et celui relativement faible du vibrofonçage.

Cette thèse, intitulée «Analyse et modélisation de la génération du bruit lors du vibrofonçage de palplanches et détermination du potentiel d'optimisation», a été réalisée à l'Unité de Recherche en Ingénierie de l'Université du Luxembourg en collaboration avec ArcelorMittal Research & Development Esch.
Dans la première partie de la thèse, les possibilités de mesure du bruit sont étudiées. Une attention particulière est accordée aux conditions de mesure sur les chantiers et aux méthodes de mesure (puissance acoustique, la formation de faisceau, et la thermographie). Les résultats obtenus via ces méthodes sont comparés. Plusieurs sources de bruit sont identifiées : les chocs contre les guides, les dispositifs de sécurité ou les palplanches adjacentes sont analysés. Une grande partie du bruit est généré dans les serrures des palplanches. Une étude approfondie détaille l'influence de différents paramètres.
Dans la deuxième partie de la thèse, les mesures d'accélération mesurées in situ sont utilisées pour étalonner un modèle éléments finis. Une étude paramétrique analyse l'influence des paramètres mécaniques les plus importants sur le niveau de bruit.

Cette recherche indique que le bruit sur chantier peut être diminué de deux façons : par des recommandations sur la mise en œuvre de palplanches sur chantier et par la prescription de mesures constructives permettant de diminuer significativement le niveau sonore.
Pendant le vibrofonçage des palplanches, il faut éviter les impacts sur les guides et les dispositifs de sécurité. On veillera également à réduire autant que faire se peut la hauteur libre des palplanches déjà installées. De plus, un choix judicieux du système de pinçage peut également diminuer le bruit.
Le design de la connection peut aussi jouer un rôle. Une modification de la géométrie de la section et l'utilisation d'un matériau absorbant dans la serrure sont également évoquées et brièvement examinées.

Zusammenfassung

Zum Einbringen von Spundwänden in das Erdreich werden drei unterschiedliche Methoden erfolgreich eingesetzt: die Schlagrammung, das Einpressen und die Vibrationsrammung. Gegenüber der Schlagrammung besitzt die Vibrationsrammung die Vorteile, dass die Installationszeit vorort kürzer ist, der Lärmpegel niedriger und die Spundwände nicht beschädigt werden. Der Geräuschpegel beim Vibrationsrammen variiert nahezu zwischen dem sehr hohen Niveau der Schlagrammung und dem niedrigen Niveau des Einpressens.

Diese Dissertation trägt den Titel: "Analyse und Modellierung der Geräuschsentwicklung beim Vibrationsrammen von Spundwänden und Ermittlung des Optimierungspotentials". Diese Arbeit wurde an der Abteilung für Ingenieurwissenschaften der Universität Luxemburg in Zusammenarbeit mit ArcelorMittal Research & Development Esch angefertigt.
Im ersten Teil der Dissertation werden die Möglichkeiten der Schallmessung untersucht. Dabei wird insbesondere auf die Messbedingungen auf Baustellen und die Messmethoden (Schallleistungspegel, Beamforming, und Thermografie) eingegangen. Anschliessend werden die Resultate dieser Methoden miteinander verglichen. Ausserdem werden die verschieden Ursachen der Störgeräusche untersucht wie z.B. Stöße der Spundbohlen gegen die Sicherheitsvorrichtungen oder gegen benachbarte Spundwände. Ein grosser Teil der Störgeräusche kann in den Schlössern der Spundbohlen entstehen. Verschiedene Einflussparameter auf den zu erwartenden Störgeräuschpegel werden im Detail untersucht.
Im zweiten Teil der Dissertation werden die gemessenen Beschleunigungsdaten genutzt um ein Finite Elemente Modell abzugleichen. Mit Hilfe einer Parameterstudie wird untersucht, wie die wichtigsten mechanischen Parameter die Geräuschentwicklung beeinflussen.

Die Untersuchung hat gezeigt, dass es zwei Wege gibt, die Geräuschentwicklung nachhaltig zu reduzieren. Zum einen werden Empfehlungen für den Einsatz der Spundwände auf der Baustelle gegeben und zum anderen werden konstruktive Maßnahmen vorgeschlagen, welche die Geräuschentwicklung maßgeblich beeinflussen.
Beim Einbringen sollte das Einschlagen der Bohlen an Führungen und Sicherheitsvorrichtungen nach Möglichkeit vermieden werden. Die freie Höhe der bereits gerammten Bohlen sollte möglichst gering sein. Ausserdem kann durch eine ge-

schickte Anordnung der beiden Vibratorklemmen die Geräuschentwicklung ebenfalls reduziert werden.
Die Auslegung der Verbindungen kann die Störgeräusche beeinflussen. Die Änderung der Querschnittgeometrie und die Verwendung von dämpfenden Produkten in den Schlössern werden auch kurz angeschnitten und diskutiert.

Acknowledgements

I would like first to express my gratitude to the University of Luxembourg and ArcelorMittal Research & Development Esch that created the project related to this thesis. I thank my supervisor Professor Arno Zürbes for following me in my long explanations and for the freedom he gave me, and Professor Stefan Mass and Danièle Waldmann for their comprehensive suggestions around this subject. I want to express my gratitude to Dr.-Ing. Alex Schmitt and, last but not least, Ir. Marie-Pierre Bourdouxhe for their collaboration, interest and support during the project.

Thanks to my colleagues at the university: Laurent Breyer for his computer, his discussions and his help on construction site; Markus Waltering for his advices; Ken Adam and Costel Rosca for their help on construction sites; Gilbert Klein, Ralf Reiter, Cedric Bruyère, Claude Collé and Ed Weyer for their availability. I am grateful to them and the others (Simon, Nadine, Julien, Volker, Thomas, André, Marc, etc.) for the friendly atmosphere.

The help of Valérie Whenham for the first building site was highly appreciated; thanks also to her colleagues. Other collaborators should also be mentioned: Nico Zurmühlen, Jonas Bruneel and his company SOETAERT, Andreas Mauer and his company OBG BAU, Frédéric Rocher-Lacoste, Claude Quézel, Guillaume Dazin, etc.

Et j'abandonne ici la langue de Shakespeare pour ceux qui ne pourront guère me comprendre que dans celle de Voltaire. Merci à ma famille qui a assisté de près au début de cette thèse. Je tiens également à exprimer ma gratitude à celle qui est devenue mon épouse au cours de cette thèse pour ses encouragements, ainsi qu'à celui qui est désormais mon beau-père pour ses suggestions intuitives et fondées sur ce sujet. Je remercie encore Marc Depreytere pour ses corrections, et tous mes autres proches pour leur soutien. Et surtout ma reconnaissance éternelle à mon Seigneur et Sauveur, qui m'a fait traverser ces quatre années sans jamais m'abandonner.

Contents

Introduction

Steel sheet piles are profiled rolled beams that can be connected together by clutches to build a sheet pile wall. They are used in the civil engineering domain for the construction of quays and harbours, locks and moles, bank reinforcement on rivers and canals as well as for protection and retaining wall for all kind of excavations.

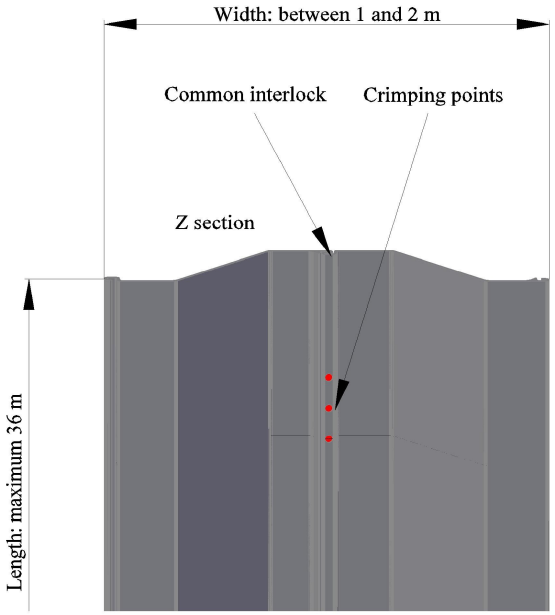

Figure 0.1.: General aspect of double sheet pile (Z section)

As they are mainly vertically used, the ends are called “top” and “toe”. Three driving methods are usually used [1]:

Impact driving: This is the best method for driving piles into difficult ground or final driving of piles to level in panel form. With a correctly selected and sized hammer it is the most effective way of completing deep penetration into hard soils in most conditions. The downside is that it can be noisy and not suitable for sensitive or restricted sites.

Vibrodriving: This is usually the fastest and most economical method of pile installation but usually needs loose or cohesionless soil conditions for best

results. Vibration and noise occurs but this can be kept to a minimum provided the right equipment is used and the site is not too sensitive.

Jacking: Otherwise known as silent vibrationless hydraulic jacking. Machines of various types are now widely used. This method is very effective in clay soils. In dense cohesionless ground, pre-augering or jetting techniques can be used. This is the most effective method to use when installing sheet piles in sensitive locations where piling would have not been considered in the past.

(a) Impact pile driving

(b) Vibratory pile driving

(c) Press driving [2]

Figure 0.2.: Examples of drivings

Researches were and are still being conducted about the vibro-driveability (see the bibliography review of Viking [3] and the Symposium TRANSVIB 2006 [4]). Two types of disturbances are also being studied: ground vibrations (many publications are available, e. g. [5, 6, 7, 8, 9, 10, 11, 12, 13, 14]) and the acoustic emission.

During the last few years, the permitted values for acoustic emissions on construction sites close to inhabited areas have been reduced substantially in the Netherlands as well as in Germany: indeed, people become more sensitive to such disturbances. Other European countries are likely to follow this trend [15]. Table 0.1 gives some values for the sound power levels measured on construction sites; it can be compared to the guideline values for the sound pressure levels given by the World Health Organization [16] in table 0.2. With the range values of table 0.1, outdoor living areas should be located at between 200 m and 5 km of the construction site for a moderate annoyance. It might occur, in case of loud noise, that the construction activities at a site are being limited or even interrupted and in this way the economic value of vibratory sheet pile driving is reduced.

Number	Equipment name	Number of pieces	Min. L_{WA} $[dBA]$	Max. L_{WA} $[dBA]$	Average L_{WA} $[dBA]$
3	road sweeper	1	105	105	105
4	concrete mixer	3	91	98	96
5	bulldozer	20	102	118	111
6	truck	9	95	109	106
9	crawler-type loader	2	104	106	105
10	wheel-type loader	20	100	117	110
11	back-hoe loader	12	99	109	105
12	power lift truck	2	98	102	100
14	tamping roller	2	115	116	115
16	rubber-tired roller	10	99	114	103
18	vibrating roller	18	100	115	106
19	compressor	5	90	117	106
20	crusher	1	117	117	117
22	motorscraper	6	108	118	111
23	suction dredge	1	119	119	119
24	excavator	1	110	110	110
25	finisher	8	107	113	109
27	self-propelled spreader	3	98	102	99
28	resistance welding set	1	110	110	100
29	electric generating set	10	89	116	109
30	crane	8	94	114	107
32	pneumatic drill	6	112	121	116
33	hammer - vibrator	20	104	132	118
34	grader	18	94	113	105
35	tracked excavator ($< 100\ kW$)	14	103	111	107
36	tracked excavator ($> 100\ kW$)	18	102	116	109
37	excavator	14	102	112	106
38	excavator (with stone crusher)	8	114	123	118
40	vibratory rammer	1	107	107	107
41	tar spreader	3	95	100	98
44	dumper	17	100	113	108

Table 0.1.: Emission for equipment on construction site [17]

Specific environment	Critical health effect(s)	L_{Aeq} $[dB]$
Outdoor living area	Serious annoyance, daytime and evening	55
	Moderate annoyance, daytime and evening	50
Dwelling, indoors	Speech intelligibility and moderate annoyance, daytime and evening	35
Inside bedrooms	Sleep disturbance, night-time	30
Outside bedrooms	Sleep disturbance, window open (outdoor values)	45
School class rooms and pre-schools, indoors	Speech intelligibility, disturbance of information extraction, message communication	35
Pre-school Bedrooms, indoors	Sleep disturbance	30
School, playground outdoor	Annoyance (external source)	55
Hospital, ward rooms, indoors	Sleep disturbance, daytime, evenings and night-time	30
Hospitals, treatment rooms, indoors	Interference with rest and recovery	as low as possible
Industrial, commercial, shopping and traffic areas, indoors and outdoors	Hearing impairment	70

$$L_{WA} = L_{Aeq} + 20\ \log_{10} r + 8$$

where L_{WA} = sound power level $[dB]$,
L_{Aeq} = sound pressure level measured at a distance r of the source $[dB]$, and
r = distance between the sound source and the measurement point $[m]$.

Table 0.2.: Guideline values for community noise in specific environments [16]

But few sound measurements have been performed on site [13, 18, 19, 20] and the mechanisms implied in the noise generation have not been studied: only some correlations between the parameters have been deduced. It is known that there are high noise levels , but nothing is known about how sound is generated. The purpose of this thesis is to propose improvements to obtain more quiet vibratory pile drivings. It is a part of the project "Analysis and modelling of the noise generation during vibratory pile driving and determination of the optimization potential" (VSP) in the Research Unit in Engineering Science at the University of Luxembourg, in collaboration with ArcelorMittal Research & Development Esch. As this project has not been completed yet, this thesis can only be considered as one step of the project.

Firstly, many parameters have the potential to influence the noise generation, and their influence needs to be inspected. They were quantified experimentally during two experiment sessions: these acoustic measurements are summarized in part I. The measurement conditions given by the standards used for sound measurements are difficult to carry out in the case of a vibratory pile driving because or the large dimensions of the system. So, a study of the measurement conditions is given in chapter 1: as the sound is measured at some distance of the source with surroundings whose acoustical behaviour cannot be exactly known, some approximations about the noise propagation are made and quantified. As making sound measurements for the vibratory pile driving of sheet piles is very recent, the know-how to improve the measurements quality is given as guidelines for the experimental set-up.

Two sound measurement types have been used to study the mechanism generating the noise:

Sound pressure measurements: Keeping in mind the approximations explained in chapter 1, such measurements can be transformed into sound power levels of the noise source. They can be used to order the parameters in accordance with their influence on the noise. This is done in chapter 2.

Beamforming measurements: A localization system of the noise sources is used to bring more information about the mechanisms implied in the sound generation. In chapter 3, the choice of the beamforming system is justified. This system is presented and used with thermographic pictures to show the paramount influence of the impacts generating the noise

Part I shows that impacts in the common interlock of a double sheet pile, impacts with a wall, impacts of the security device, etc. are the main source of noise. This part brings also information about the other parameters and mechanisms implied in the noise generation.

The impacts occurring in the common interlock of a double sheet pile are intended to be studied thoroughly in part II with simulations. Identifying the rel-

evant parameters in the impact generation allows then to reduce the noise. This study has been made in two steps:

1. In chapter 4, a model of the sheet pile has been built by taking into account the vibrator and the soil. Acceleration measurements are injected in the model to calculate the forces generated at the ends of the sheet pile. The calculation results show the paramount influence of the vibrator force and a minor influence of the toe force (in the studied cases) on the vertical accelerations measured on the sheet pile.
2. With the conclusions obtained in chapter 4, approximations have been made on the model and variations of the parameters of the model are calculated in chapter 5. A suitable processing of the simulated interlock displacements studies the occurrence and the violence of impacts. As the sheet pile section plays a role, its optimisation has been performed.

The conclusion recalls the mechanisms involved in the noise generation. It gives guidelines for the contractors to generate less noise on construction sites with vibratory pile drivings as well as development directions for the manufacturers of sheet piles. A scope for future researches in this domain is also proposed.

Part I.

Acoustics

Chapter 1.

Measurement techniques

Acoustic measurements performed in free-field conditions are regulated by laws [21, 15] and standards [22, 23]. But such conditions are difficult to carry out in the case of a vibratory pile driving. The literature presents measurements with less restrictive conditions [13, 24, 25]. The assumptions for such measurements will be studied and quantified in section 1.1: this will allow to assess the quality of published or unpublished measurements [13, 18, 19, 20] and to compare them.

Independently of the sound propagation, extra noise sources must also be taken into account: the sound that does not come from the sheet pile influence the measurement. For example, some measurements made by Rocher-Lacoste [13] have not been made carefully enough to interpret the noise behaviour.
Some guidelines are given in section 1.2 to improve the quality of sound measurements. Other considerations are also given to be able to compare driven sheet piles with fast experiments.

1.1. Measurement conditions

Standard [22] recommended by the law [21] describe how to perform acoustic measurements in free-field conditions for one piece of equipment; in the case of a vibratory pile driving, the measurement conditions that must be applied should be as follows:

- The measurement must be performed on a reflecting plane (typically on asphalt or concrete) and preferably far of any reflecting object.
- The background noise must be 6 dB (if possible, 15 dB) lower than the measurements.
- Windscreens must be used with microphones.
- Climatic conditions should be compensated if they influence the measurements.

- For measurements in free-field conditions around a large object, measurements on a hemisphere around the object is recommended. Its radius r must be at least twice the characteristic dimension d_0 of the object (defined in the standard) and is rounded to 1, 2, 4, 6, 8, 10, 12, 14 or 16 m. Ten main microphones must be positioned on this hemisphere (see figure 1.1). In special cases, additional microphones must be added.

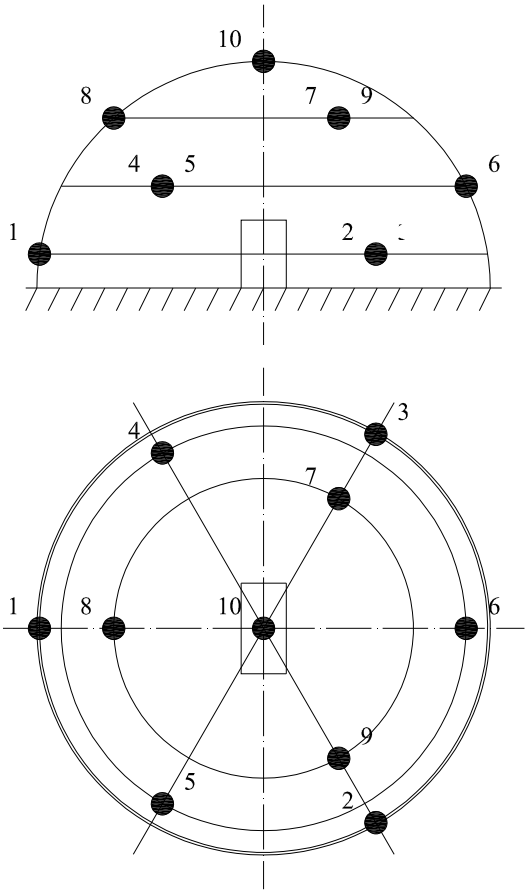

Figure 1.1.: Position of the microphones on the hemisphere [22]

These conditions are difficult to carry out:

- The ground is not a reflecting plane when a sheet pile is driven in the ground; indeed, it is never driven in concrete or asphalt.
- For an object with a large height (compared to the other dimensions), the characteristic dimension d_0 can be approximated by the height of the object. So, the standard allows to measure sound of objects smaller than 16 m. However, sheet piles larger than 16 m were measured.
- Even if the sheet pile was smaller than 16 m, then the microphone 10 must be placed at least at 32 m above the soil, which is difficult.

Less restrictive conditions are used in the literature:

- Gill [24] gathered data at a distance of 15 m from the toe of the sheet pile and at a height of 1.5 m. The positioning (in front or on one side of the sheet pile) is not specified.
- Rocher-Lacoste [13] referred to Mériel *et al.* [17]: for a sound source considered as fixed, the measurement points are chosen in four orthogonal directions at a distance at least the largest dimension of the equipment; the measurement is made between 1.2 and 3 m above a reflecting plane.
- Ballesteros *et al.* [25] measured several sound sources on a construction site by placing the microphones at a hight of 1.5 m and at more than 2 m away from any reflecting surface.

As shown by these few examples, two ways can be used to give an idea of the noise on construction sites:

- If the several noise sources have variable amplitudes, the measurements are made to have an average sound pressure level [25, 26].
- If only one sound source is relevant, then it can be approximated as a point sound source on a reflecting plane and the sound pressure level can be post-processed to obtain the sound power level of the source as follows [17, 27]:

$$L_{WA} = L_{Aeq} + 20\ \log_{10} r + 8 \tag{1.1}$$

where L_{WA} = sound power level $[dB]$,
L_{Aeq} = sound pressure level measured at a distance r of the source $[dB]$, and
r = distance between the point sound source and the measurement point $[m]$.

In this second case, the approximations of this evaluation must be kept in mind. Five of them are described here below.

1.1.1. Reflecting plane

The ground of a construction site never behaves as a perfect reflecting plane, but as a partly reflecting plane. Equation 1.1 can be compared with the equivalent formula for a point source located on an absorbing plane [27]:

$$L_{WA} = L_{Aeq} + 20\ \log_{10} r + 11 \tag{1.2}$$

A difference Δ_p of 3 dB between these two behaviours is found. The literature gives more information about the ground behaviour (e.g. [28]) and the reflection models (e.g. [29]).

1.1.2. Distance

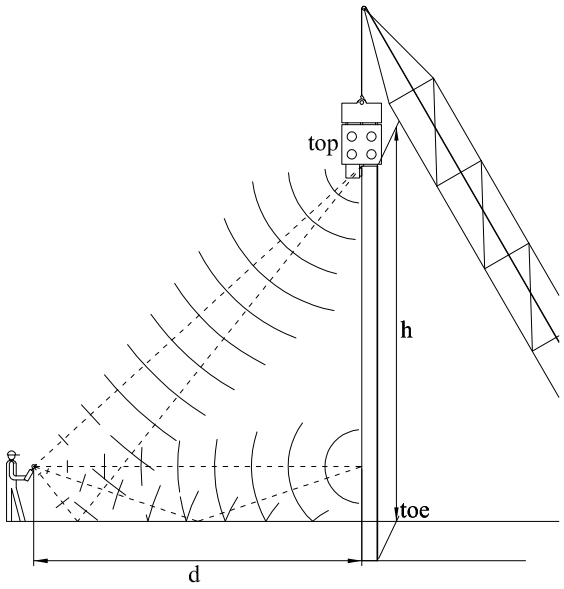

Figure 1.2.: Situation when measuring sound with a large vibrating sheet pile

At the beginning of the vibratory pile driving of large sheet piles, the distances between the microphone and the sheet pile top and between the microphone and the sheet pile toe are different if this microphone is placed near the ground, as shown in Figure 1.2. If the sound source is located at the top of the vibrating sheet pile, then an error is introduced when calculating the sound power with equation 1.1 and the horizontal distance d as the reference one. This difference Δ_d depends on the height of the sheet pile as shown in the following formula:

$$\begin{aligned} \Delta_d &= 20\ \log_{10}\sqrt{h^2+d^2} - 20\ \log_{10} d \\ &= 10\ \log_{10}(1+\frac{h^2}{d^2}) \end{aligned} \tag{1.3}$$

where Δ_d = difference between the sound power calculated with a horizontal distance and the sound power calculated with the oblique distance for a source at the top of the sheet pile $[dB]$,
h = height of the vertical sheet pile $[m]$, and
d = horizontal distance between the vertical sheet pile and the measurement point $[m]$.

This equation is drawn in Figure 1.3. At a distance equal to the height of the vibrating sheet pile, a difference of 3 dB is again obtained[1]. A larger distance increases thus the precision of the measurements, especially if the vibrator is the main sound source.

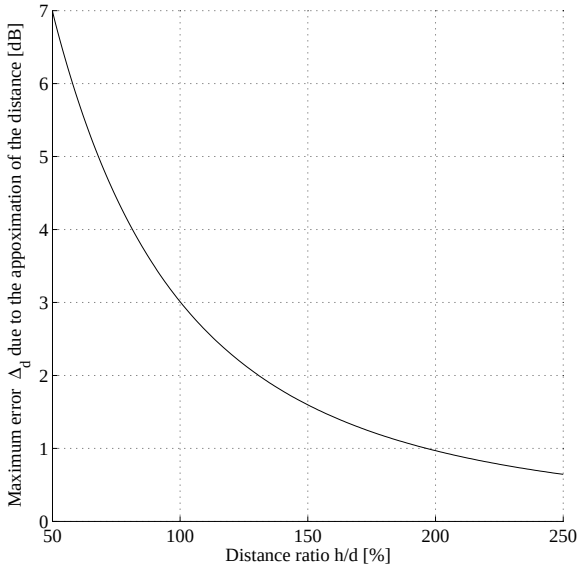

Figure 1.3.: Maximum error Δ_d $[dB]$ due to the approximation of the distance as a function of the distance

Several experiments were performed to verify the validity of equation 1.1, by measuring at 25 different distances with a sound level meter in front of a sheet pile with a height of 12 m (1 m in the ground) vibrated by a vibrator with a height of 2.3 m in a stationary state. During this measurement, sound pressure levels have also been measured simultaneously at six fixed points (the position scheme is given in figure 1.5b) to verify that this state was stationary. It was rather the case as these sound pressure levels varied in a maximum range of 3.8 dBA (arithmetic average of this range for 17 measurements: 2.2 dBA).
Figure 1.4 shows the sound power obtained by using equation 1.1 for three different sheet pile configurations: one was an experiment with a loud noise (tested two times) whereas the two others were more quiet. Three observations can be made:

- The sound power level can be considered almost constant at distances larger than 120% of the sheet pile height.
- Furthermore, the maximum level difference for one configuration is 4.4 dBA: it quantifies the uncertainty of such a measurement.

[1] In fact, this difference can be more important, e.g. if the source is the vibrator itself (as it is above the sheet pile and can be several meters high); however, the sheet pile is driven into the soil and thus the error decreases.

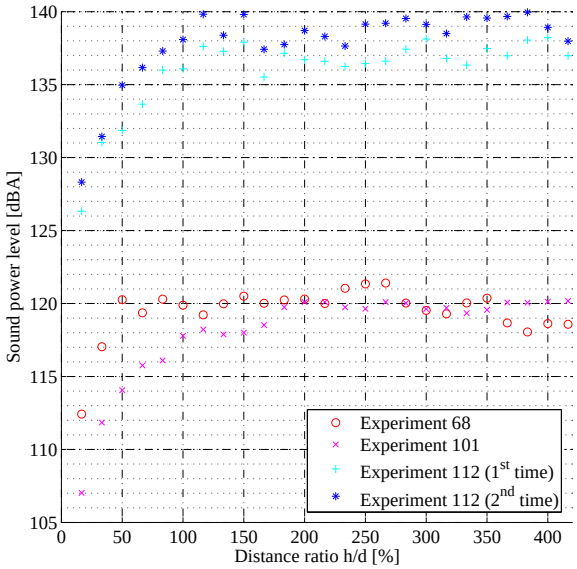

Figure 1.4.: Sound power as a function of the distance (the description of the legend available in confidential section D.4)

- If the sound power level is calculated for the repeated experiment (for distances larger than 120%), only a difference of 1.8 dBA is observed between the first and the second time.

The conclusion is that the sound power measurements are almost constant at a distance larger than 100% of the height (as specified by Mériel *et al.* [17]), but increasing this distance up to 120% of the height can improve the precision. Moreover, the uncertainty of such a measurement is around 5 dBA; this one is decreased if averaging is applied.

1.1.3. Free-field conditions

If several reflections can take place, each of them can induce local errors Δ_f (increase or decrease) up to 3 dB, as already shown by comparing formulas 1.1 and 1.2. As already mentioned, more accurate models can be found in the literature (e.g. [29]).

1.1.4. Decreasing rate

Equation 1.1 is valid for one sound source; it states that a doubling of the distance from a source produces a 6 dB drop in sound pressure level [27]. If several coherent sound sources take place, then behaviours like dipoles of quadrupoles can occur

[27], inducing another drop for a doubling of the distance.
This decreasing rate seems to be well represented in Figure 1.4, as an almost constant level can be observed.

1.1.5. Directivity of the noise

When the sound is generated at several locations with different orientations (for instance at sheet piles with Z sections), a variation of the noise should be measured when changing the direction of the measurement around the source. It is useful to make measurements for several directions and average them to decrease this effect.

Regarding the validity of this approximation, two microphone location schemes were used to measure the sound pressure levels during the experiment sessions:

- for the scheme of figure 1.5a, a maximum difference of 6 dBA was observed during one experiment between the measurements of microphone 1 (in front of the sheet pile) and microphone 2 (next to the sheet pile), but the arithmetic average for 27 measurements was 2.4 dBA;

- with the scheme of figure 1.5b, maximum differences (among the three microphones at the same distance) of 9.4 dBA and 8.3 dBA were observed at 20 m and 40 m, respectively, but the arithmetic averages of these differences for more than 400 measurements were 2.8 dBA and 2.7 dBA, respectively.

Therefore, in some experiments, the approximation of the directivity could introduce great bias (almost 10 dBA), but most of the measurements showed acceptable differences.

1.1.6. Conclusions

As large uncertainties can be obtained (up to 5 dBA) when reproducing an experiment, it seems very important to calculate the sound power levels of each microphone and to average them (instead of comparing directly individual sound pressure level measurements). By doing this, more precise measurements can be compared in a more efficient way. The study of the approximations used during measurements shows also that 1 or 2 dBA is not a significant difference.

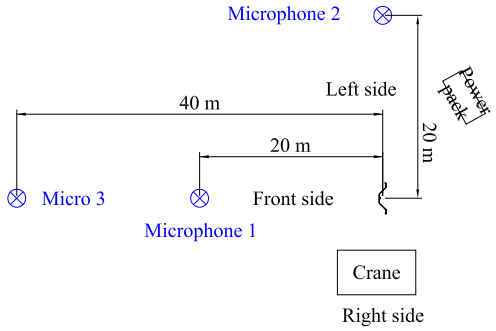

(a) First experiment session

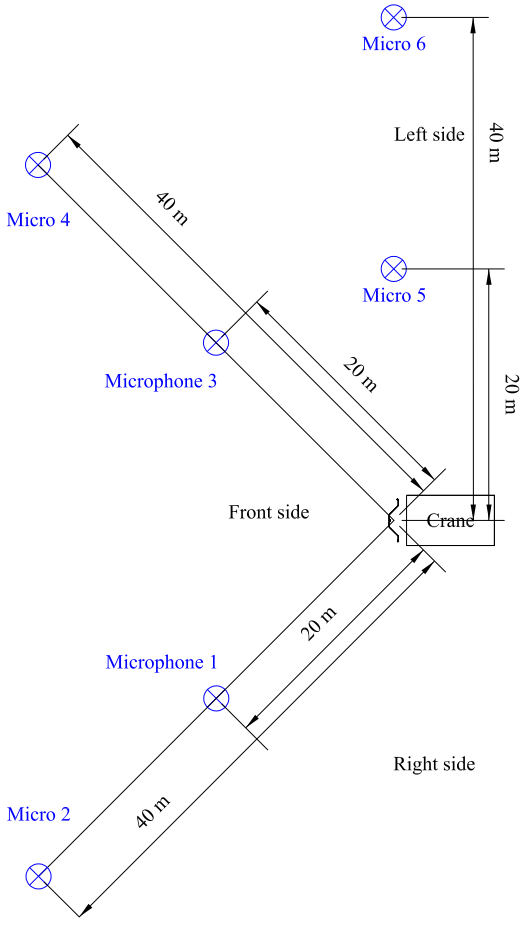

(b) Second experiment session

Figure 1.5.: Microphone location schemes, chosen for practical reasons

1.2. Guidelines to perform reproducible sound measurements

As already mentioned, few experimental works have been undertaken to measure and interpret the noise generated by vibratory pile driving [13]. Even if a description of the measurements has been given, the way to perform these experiments has not been described. Actually, care must be taken to have no extra noise that can cover the sound produced by the vibratory pile driving itself; such a phenomenon can generate poor-quality results.
For example, Rocher-Lacoste [13] measured sound and calculated sound power levels on the site of Limelette (Belgium). Measurements made three weeks later showed sound pressure levels 11.6 dBA lower (experiment `A` of Rocher-Lacoste compared with experiments `33` and `34`; see confidential section D.4 for the description of the experiment). There was only one difference between the two experiment configurations (same sheet pile, same vibrator, same parameters, etc.): tubes were used for the instrumentation of the sheet pile for the experiment of Rocher-Lacoste and they were removed afterwards. These tubes protected cables delivering the signals of the toe accelerometers; they were placed on the neutral axis of the double section on both sides, between the toe and a height of 7 m (see Figure 1.6; chapter 3 gives guidelines to interpret such pictures)). Beamforming measurements show in Figure 1.7 hot spots at the location of the tube of the right side of the sheet pile: it is the extra sound source.

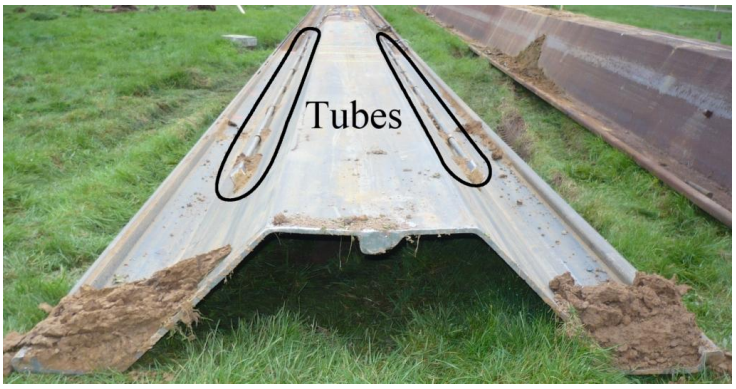

Figure 1.6.: Tubes fixed on a double sheet pile

Another extra source, which was found during the experiments, was a security device. It can be seen in Figure 1.8 that hot spots occur near the top of the sheet pile; indeed, the shackle was placed 2 m under the top of the sheet pile on the left side in a hole of the sheet pile and generated impacts with the sheet pile. It was attached to a sling, itself being attached to the second cable of the crane (see Figure 1.9). The increase of the sound pressure level was measured between 6.7

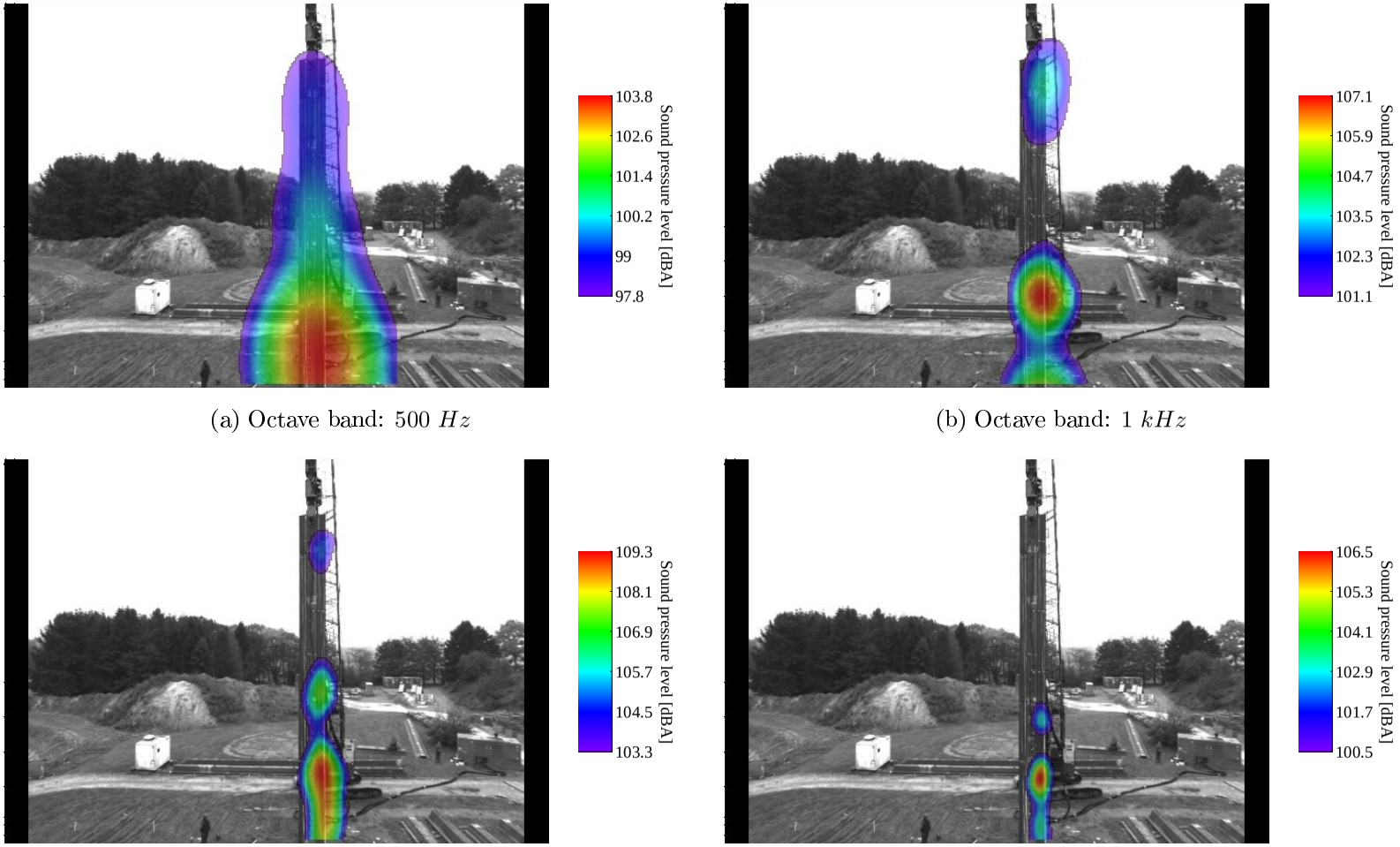

(a) Octave band: 500 Hz

(b) Octave band: 1 kHz

(c) Octave band: 2 kHz

(d) Octave band: 4 kHz

Figure 1.7.: Beamforming results showing the influence of the tubes during experiment `A` of Rocher-Lacoste [13]

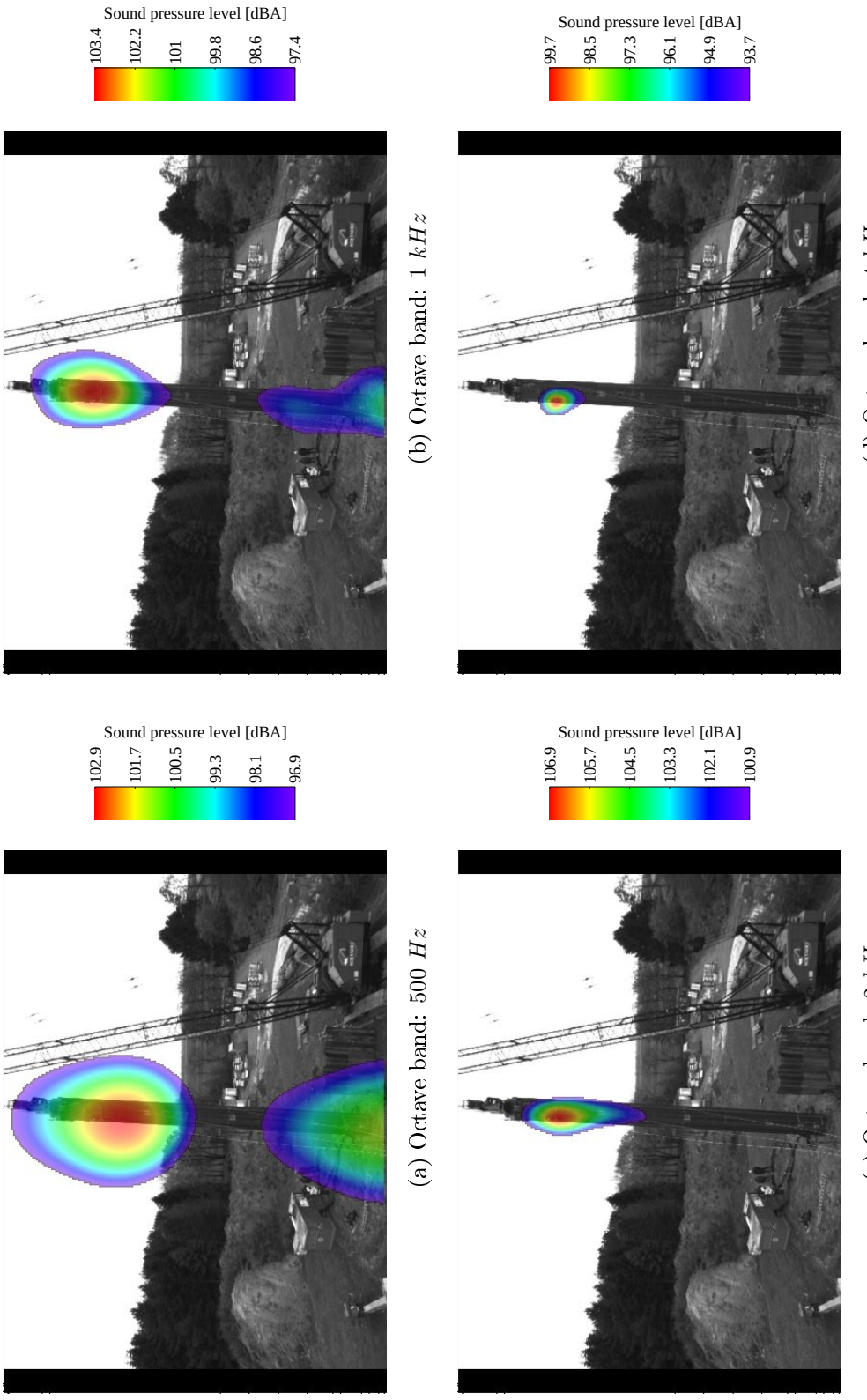

(a) Octave band: 500 Hz (b) Octave band: 1 kHz

(c) Octave band: 2 kHz (d) Octave band: 4 kHz

Figure 1.8.: Beamforming results showing the influence of the security device of figure 1.9 during experiment 10 (quiet sheet pile configuration)

and 10.6 dBA for two quiet configurations; such increases were not observed for loud configurations.

Figure 1.9.: Security device used with a sheet pile

In light of those observations, it can be deduced that any expected noise source (from chains, shackles, security systems, tubes, etc.) have to be removed or insulated so that no impacts can occur[2].

(a) Chain insulation (b) Destruction of the chain insulation

Figure 1.10.: Chain insulation

For example, a chain was used as a security system during the second experiment session. Rubber bands (obtained by cutting bike tubes) were put around this chain with scotch-tape (see figure 1.10a). As this insulation was destroyed bit by bit (see figure 1.10b), it needed to be renewed from time to time and it can be used only for experimental works. It should also be mentioned that this insulation was not able to reduce the noise coming from impacts between the clamp and

[2]It was observed that quiet vibratory pile drivings were more sensible to such disturbances.

the chain itself, but this noise can be considered the normal noise generated by a leader-mounted system in use. The use of a cable instead of a chain could also decrease the generated noise.

Figure 1.11.: Top "insulation" of the sheet pile

Another insulation was also installed at the top of the sheet pile for the two experiment sessions: a piece of plastic (shown in figure 1.11) as used for thermal insulation can be placed in the clamping device in order to avoid any direct contact between the sheet pile top and the clamp during the vibratory pile driving. Another method to avoid this type of impact between the sheet pile top and the vibrator consists in lifting up the vibrator when clamping the sheet pile to keep a small gap between the clamp and the top of the sheet pile.

(a) System before burying it

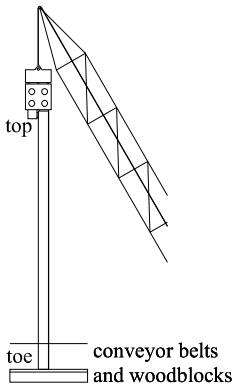

(b) Scheme of the system

Figure 1.12.: Woodblocks and conveyor belts buried in the soil

To be able to perform a large number of measurements in a limited range of time and to characterise the configuration of the vibrating sheet pile independently of the behaviour of the soil and of the driving depth of the sheet pile in this soil, a

method allowing a reproducible and stationary situation was developed by burying some woodblocks at 1 m of depth with conveyor belts overlaid on them (like in figure 1.12). The sheet piles were blocked and could not be driven any further into the soil so that a stationary situation was created. By this method, similar noise levels are obtained when compared with a standard vibratory pile driving: a maximum difference of 5.2 dBA, but an arithmetic average of 1.9 dBA for six different experiments.

In the same way by which standardization is considered, crimping, which is usually used to fix the common interlock of double sheet piles, can be replaced by welding. Crimping is usually applied over 200 mm as a triple crimping point (see figure 2.15) for the fixing of the interlock of double sheet piles. An equivalent weld should thus have the same length (200 mm). A comparison of these two systems is available in section 2.3.4.

1.3. Conclusions

This chapter presents some results about the approximations made when measuring sound during full-scale vibro-driving experiments. It indicates that a difference of 1 or 2 dBA is not significant when comparing microphone measurements. It also shows that averaging the sound power levels (logarithmic average) for one experiment gives an advantage to compare the measurements. This brief study gives a framework to interpret the results of the experiments given in chapter 2. All the care that was taken during the experiment sessions has also been described: these guidelines help to make reproducible and representative measurements.

It should be mentioned that other types of measurement can provide useful information when trying to interpret the results:

- A localization system of the sound sources is useful to show that the sound sources from the sheet pile and not from other parts. For this application, only a beamforming system (presented in chapter 3) seems to fit.
- Acceleration measurements increase the knowledge of the vibration state of the sheet pile. Such measurements are studied in chapter 4.
- Strain gauges can bring information about the local deformation that can be treated in the same way as the acceleration measurements.
- A thermographic camera can be used to monitor whether the temperature is not dangerous for the sensors or not. But it can also provide information about the mechanism of the noise generation. For example, in case of impacts, the mechanical energy is dissipated in heat, noise and/or permanent deformation. A link between heat and noise could indicate impacts occurrences.

Chapter 2.

Acoustic measurements

As already written in section 1.1, published measurements [13] did not explain the generation of the sound produced by the vibratory pile driving. Consequently, the first step is making global comparisons with full-size experiments in order to identify the most relevant parameters. The parameters that are assumed to have the potential to influence the noise generation can be sorted in four categories (see figures 2.1 and 2.13 for some parameters sketches):

- Sheet pile parameters (see figure 2.1b):
  - section parameters (see figure 2.1a): thickness of the web and of the flanges, opening angle, width and height of the section
  - length
  - common interlock configuration: spacing between the welds or the crimping points (see figure 2.13), clearance of the interlocks, water-tightness joint (with bituminous or polyurethane sealant)
  - imperfections compared to the nominal sheet pile: straightness and section tolerances
- Vibrator parameters:
  - leader system: leader-mounted or free-hanging systems (see figure 2.2)
  - clamping system: single or double clamps system (see figure 2.3)
  - static force (see figure 2.4)
  - frequency of the vibrator (see figure 2.4)
  - eccentric moment of the vibrator (see figure 2.4)
  - design of the vibrator: number of shafts, gears, bearings, hydraulic motors (see figure 2.4)
- Environment parameters:

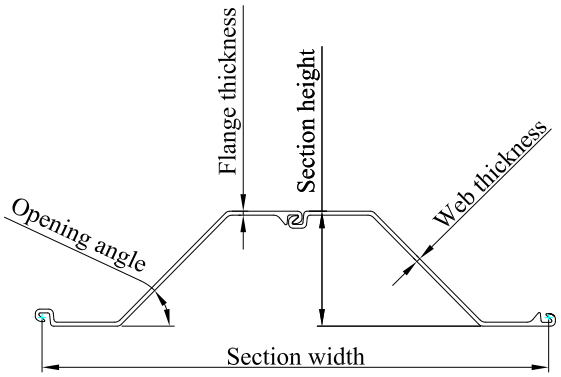

(a) Parameters of section of a Z type

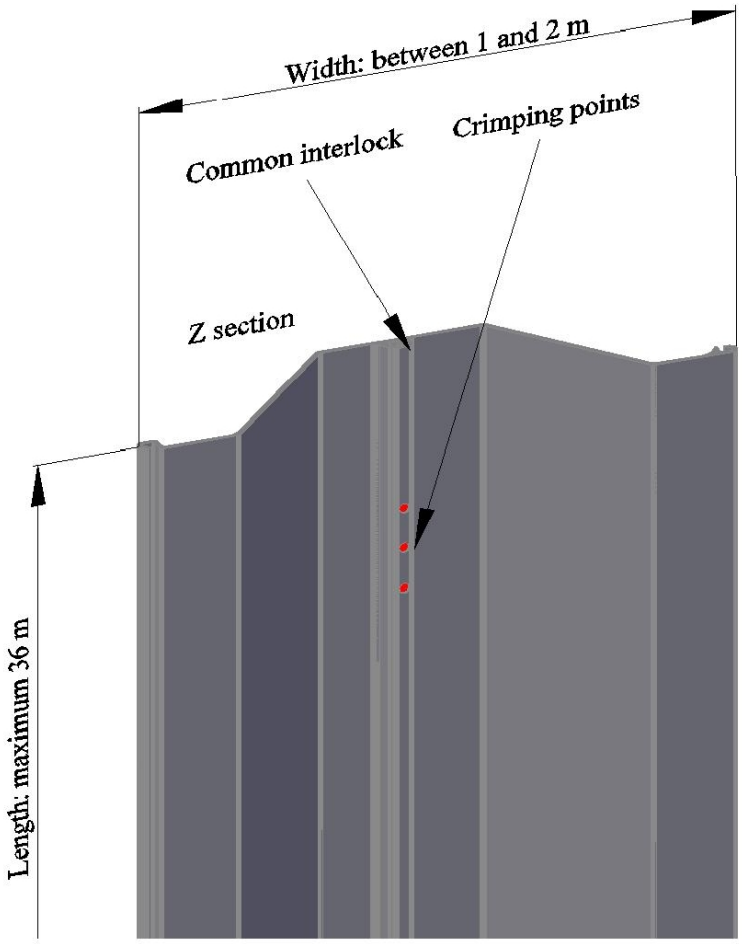

(b) Other sheet pile parameters

Figure 2.1.: Some sheet pile parameters that are assumed to have the potential to influence the noise generation

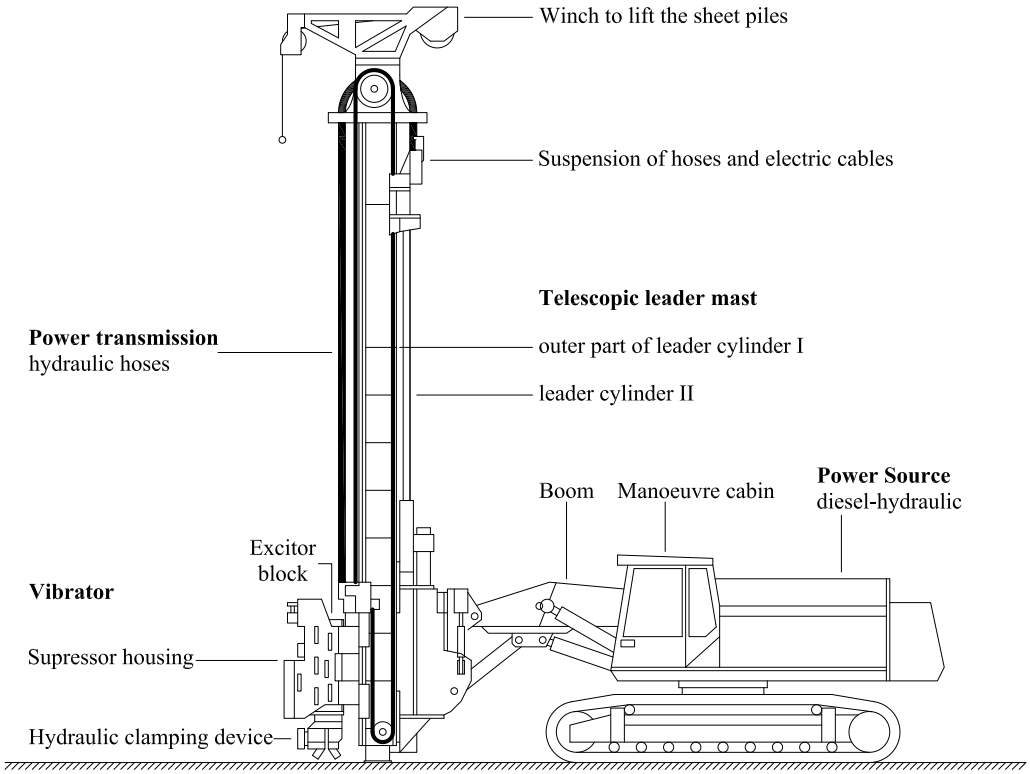

(a) Leader-mounted system (from the ABI vibratory-machine manufacturer's brochure)

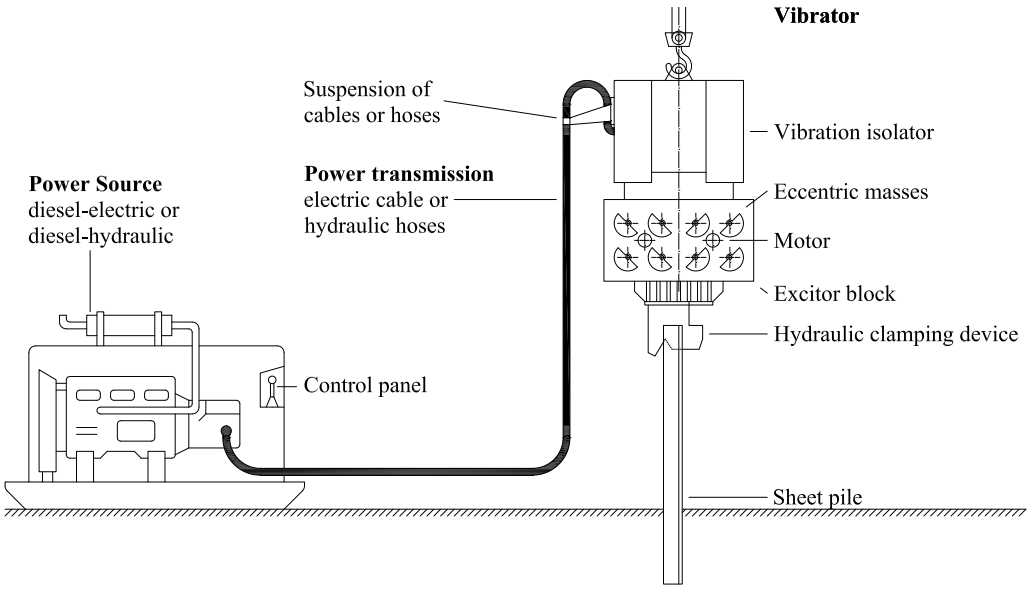

(b) Free-hanging system (from the ICE vibrator manufacturer's brochure)

Figure 2.2.: Leader systems

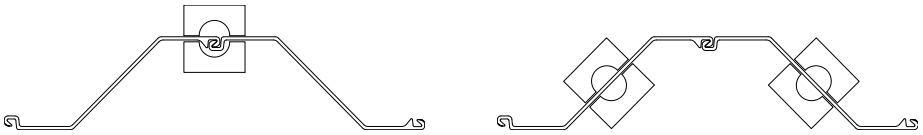

(a) Single clamp (b) Double clamps

Figure 2.3.: Position of clamping systems on a Z sheet pile section

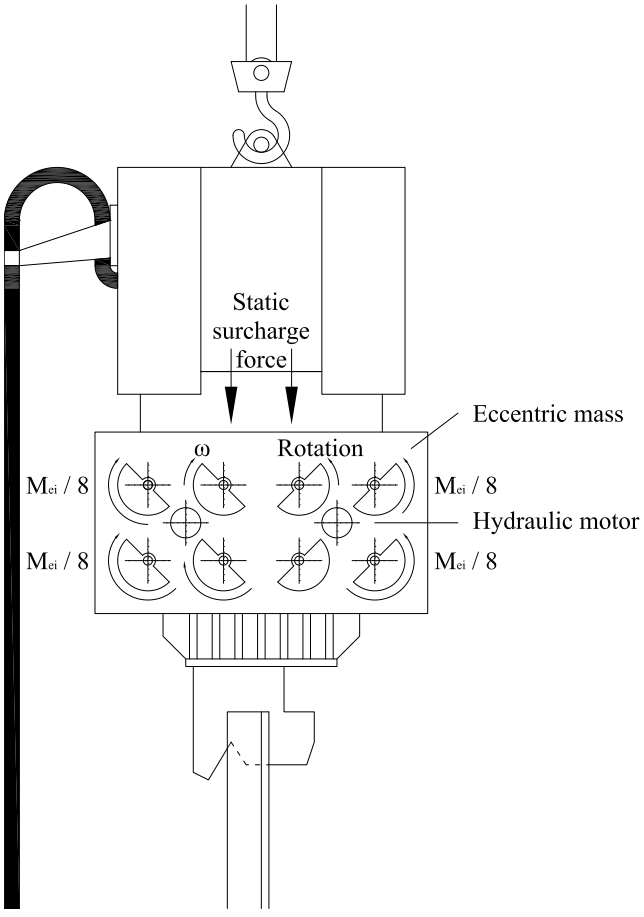

Figure 2.4.: Parameters of the vibrator

  - parameters of a neighbouring wall: watertightness joint of the wall (with bituminous or polyurethane sealant), height above the ground (see figure 2.13), clearance of the interlock
  - soil properties
  - penetration depth
- Accessories:
  - guide
  - security system

As already mentioned, two experiment sessions have been made on two different sites (see figure 2.5) to measure the influence of most of these parameters. Appendix B presents a description of the experiments. For confidential reasons, the experiments are thoroughly described with a nomenclature in confidential appendix D. Section 1.2 already explained the procedure used during the experiments.

This chapter presents the measurement equipment (in section 2.1), the post-processing of the data (in section 2.2) and the results (in section 2.3). These results help to identify key parameters of the noise generation.

2.1. Used equipment

Six microphones have been used to measure the sound during the experiments; their location schemes are available in figure 1.5. They are free-field microphones with an integrated preamplifier and they have a very wide operating temperature range and low ambient-temperature coefficient. Their features are available in section A.1.

They were all put with the appropriated windscreen on a support at 1.75 m above the ground (see figure 2.6): it is the average height of the human ear and literature gives a height between 1.5 m and 3 m [23, 17, 24, 25].

The microphone measurements were sampled at 40.958 kHz for the first experiment session and at 44 kHz for the second one.
The background noise had a sound pressure level around 60 dBA.

(a) First session

(b) Second session

Figure 2.5.: View of the sites of the two experiment sessions

Figure 2.6.: Position of a microphone

2.2. Applied post-processing

The processing explained in this section is usually performed by a sound level meter to calculate the equivalent continuous sound level (also called time-average sound level).
The microphones measure a sound pressure $p_Z(t)$. An analog filter can be applied before the sampling of the signal in order to reproduce the sensitivity of the human ear, usually an A-weighting filter[1] [30] (shown in figure 2.7); indeed, this filter is recommended by laws [15, 21] as well as standards [22, 23]. In this case, the measured sound pressure is called $p_A(t)$. A global level is obtained by integrating

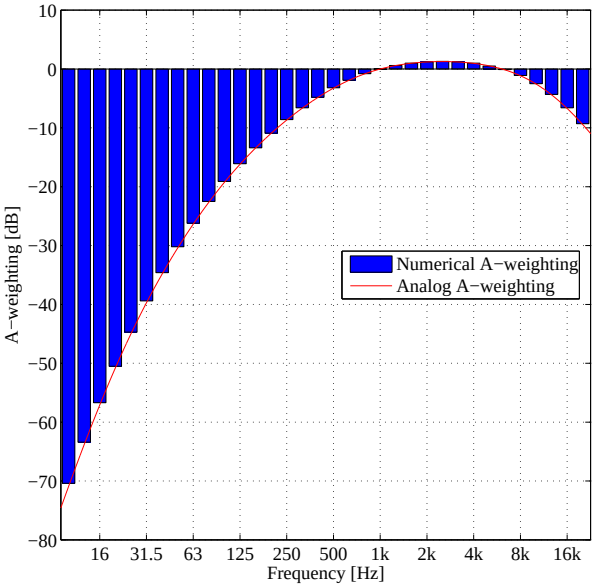

Figure 2.7.: Transfer function of a A-weighting filter [31]

this signal: the sound pressure level[2] L_x is defined as [22]:

$$L_x = 10 \log_{10} \left(\frac{1}{T} \int_0^T \frac{p_x^2(t)}{p_0^2} \, dt \right) = 20 \log_{10} \left(\frac{p_{x,rms}}{p_0} \right) \tag{2.1}$$

where L_x = x-weighted sound pressure level $[dB]$,
T = integration time $[s]$,
$p_x(t)$ = x-weighted pressure $[Pa]$,
p_0 = reference pressure ($= 20\ \mu Pa$ in the air), and
$p_{x,rms}$ = x-weighted root mean square pressure $[Pa]$.

[1] This filter can be applied numerically later, inducing a little difference, which is neglected.
[2] x is a letter summarizing the applied weighting (Z for no weighting, A for the A-weighting).

Usually, equation 2.1 is applied over a selected frequency range (octave or third-octave) and during a defined time interval (e.g. 0.5, 1 or 2 s). When such several sound pressure levels L_{xi} are obtained, a global level L_{xt} can be obtained by the following sum:

$$L_{xt} = 10 \log_{10} \left(\sum_{i=1}^{n} 10^{\frac{L_{xi}}{10}} \right) \tag{2.2}$$

where L_{xt} = x-weighted sound pressure level for all the frequency ranges $[dB]$,
n = number of frequency ranges, and
L_{xi} = x-weighted sound pressure level of frequency range i $[dB]$.

If an average over the time L_{xT} is needed, this formula can be adapted:

$$L_{xT} = 10 \log_{10} \left(\frac{1}{N} \sum_{j=1}^{N} 10^{\frac{L_{xj}}{10}} \right) \tag{2.3}$$

where L_{xT} = average x-weighted sound pressure level $[dB]$,
N = number of time intervals, and
L_{xj} = x-weighted sound pressure level of time interval j $[dB]$.

The calculation of the sound pressure level of the experiments was made as follows (an example of the first five steps is given in figures 2.8 and 2.9):

Step 1 - Sound power spectrum: The power spectrum[3] of a measurement signal was calculated every second (for 65 536 = 2^{16} samples[4]) and converted into third-octave data by using the *Fast Fourier Transform* (FFT); no window was applied because its use changes the energy of the signal. This step is shown in figure 2.8a.

Step 2 - Sound pressure level: These third-octave data were converted into a sound pressure level for each third-octave by using equation 2.1. This step can be seen in figure 2.8b.

Step 3 - A-weighting: As the measurement signal had not been weighted before the digitizing of the data, the numerical A-weighting of figure 2.7 was applied to these third-octave data. An example is given in figure 2.9a.

Step 4 - Average over the time: An average calculated over the time by equation 2.3 for each third-octave contribution indicates the average spectrum of the measured sound, as shown in figure 2.9b.

[3] The power spectrum is the square of the effective amplitude spectrum (also called root mean square amplitude spectrum), itself obtained by the division of the FFT by $\sqrt{2}$.

[4] For the first experiment session: 2^{16} samples = 1.6 s; for the second experiment session: 2^{16} samples = 1.489 s. As it was computed every second, the overlaps for the two sessions are thus 37.5% and 32.9%, respectively.

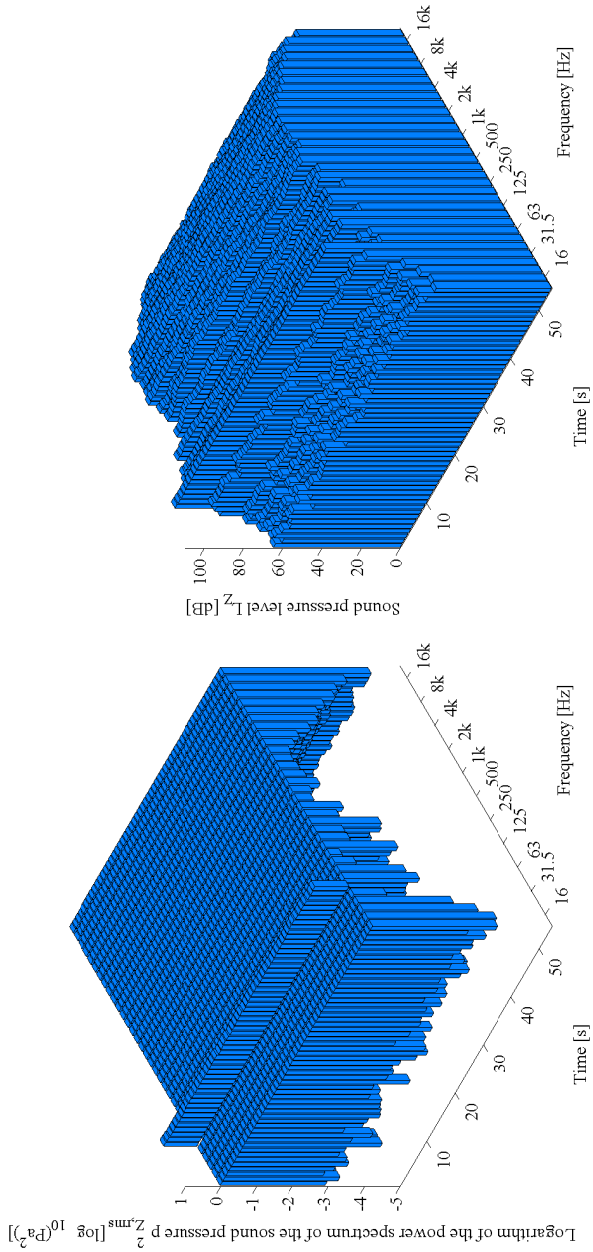

(a) Step 1 - Sound power spectrum

(b) Step 2 - Sound pressure level

Figure 2.8.: Example of steps of the post-processing of the acoustic measurements

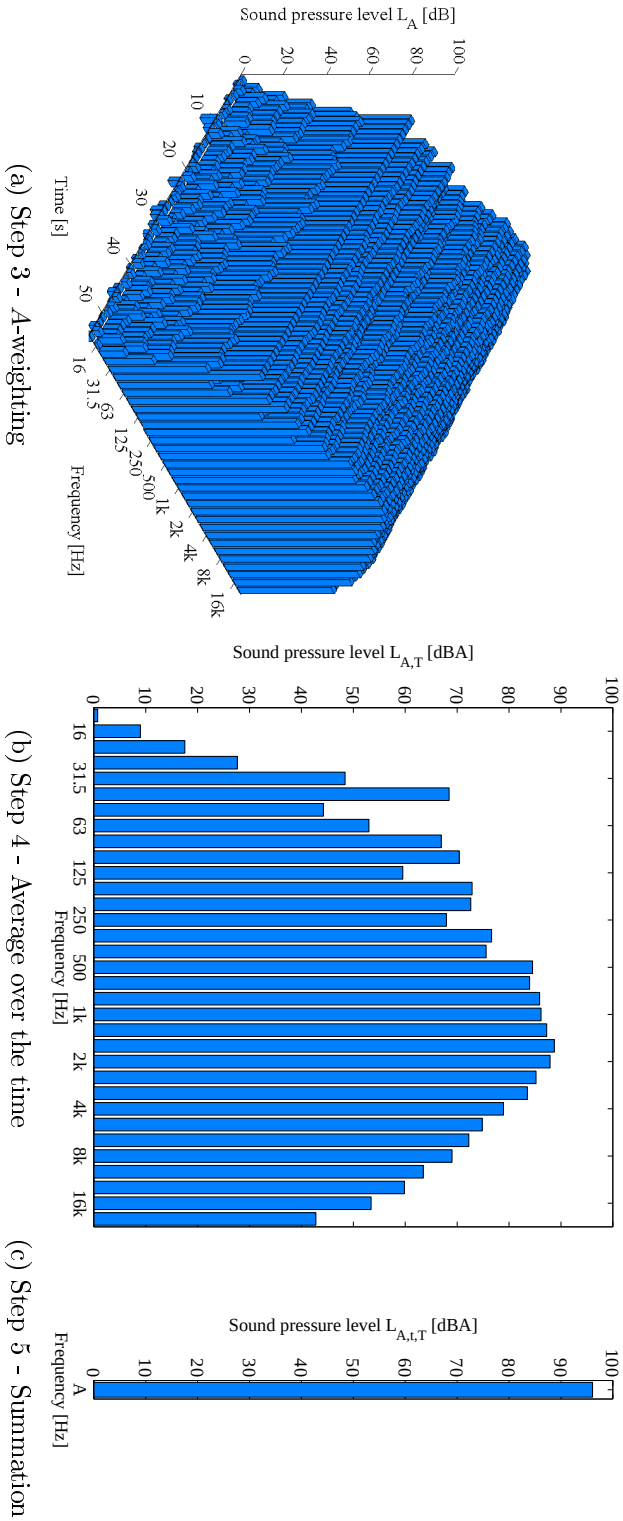

(a) Step 3 - A-weighting

(b) Step 4 - Average over the time

(c) Step 5 - Summation over the frequencies

Figure 2.9.: Example of steps of the post-processing of the acoustic measurements

Step 5 - Summation over the frequencies: A global result for the entire frequency range can be found by summing each third-octave contribution by using equation 2.2. Figure 2.9c shows an example of such a result.

Step 6 - Sound power level: To have a result independent of the distance between the microphone and the sound source, an approached value of the sound power level was computed with equation 1.1 (keeping in mind the approximations explained in section 1.1).

Step 7 - Average over the microphones: A global result over all the microphones measuring during the experiment was obtained by averaging logarithmically with a formula similar to equation 2.3:

$$L_{WA} = 10 \log_{10} \left(\frac{1}{m} \sum_{k=1}^{m} 10^{\frac{L_{WA,k}}{10}} \right) \tag{2.4}$$

where L_{WA} = A-weighted sound power level of the tested equipment $[dBA]$,
m = number of microphones, and
$L_{WA,k}$ = A-weighted sound power level of microphone k $[dBA]$.

2.3. Results

2.3.1. Global results

In confidential appendix E are listed all the sound power levels of the two experiments sessions obtained with the post-processing explained in section 2.2 (see confidential appendix D for the codes and the description of the experiments).
Considering these average results is important: in some cases, wrong conclusions can be obtained if one single microphone is considered instead of the global result. Each experiment lasted at least 30 s in order to have the global result of a stationary state. However, as shown when studying the approximations used during the experiments in section 1.1.6, 1 or 2 dBA are not enough to show a difference: such a difference could be obtained because of the approximations.

2.3.2. Global comparisons

Maximum and minimum sound power level

Before going into details of the experiments, the maximum and minimum sound power level of the experiments can be considered:

- The first experiment session shows 106.9 dBA for the minimum sound power level (during experiment `20`) and 142.1 dBA for the maximum one (during experiment `26`), which makes a difference of 35.25 dBA.
- The second experiment session has 113.4 dBA for the minimum sound power level (during experiment `84`) and 139.6 dBA for the maximum one (during experiment `170`), which makes a difference of 26.2 dBA.

These large differences between sheet piles that could be considered as similar (same section, same length, same vibrator) if the details would not be considered, show that care must be taken if noiseless vibratory pile driving must be performed.

The maximum sound power level observed for an impact driving is around 140 dBA (i.e. sound pressure levels around 112 dBA at 10 m of the source) [24]. The vibratory pile driving does not seem able to generate more noise than a noisy impact driving: it can be considered as the highest limit.
On the other hand, the lowest level is given by the equipment in service: this sound power level was measured between 105 and 110 dBA (i.e. sound pressure levels between 77 and 82 dBA at 10 m of the source), consistent with the measurements of Rocher-Lacoste [13]. This level can be considered as the lowest limit.

Influence of the vibrator frequency and of the eccentric moment on the sound power level

When studying one combination of parameters, the maximum sound power level is always obtained for the highest frequency (see figure 2.10) and for the highest eccentric moment (see figure 2.11). Indeed, the force generated by the vibrator F_c is given by [3] (see figure 2.12):

$$F_c = M_{ei}\ \omega^2 \tag{2.5}$$

where F_c = vertical force amplitude of the vibrator $[N]$,
M_{ei} = eccentric moment $[kgm]$, and
ω = angular frequency $[rad/s]$.

The higher the eccentric moment, the larger the force. The same mechanism can be suggested for the influence of the frequency, but a variation of the frequency

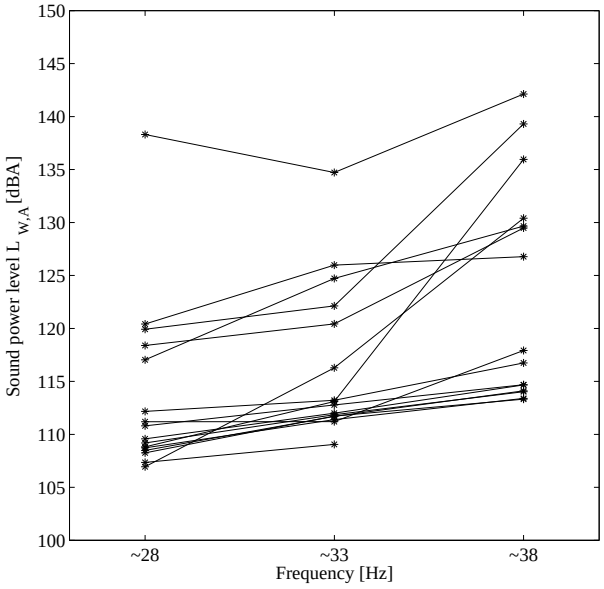

Figure 2.10.: Sound power level as a function of the frequency for 16 different configurations of the first experiment session

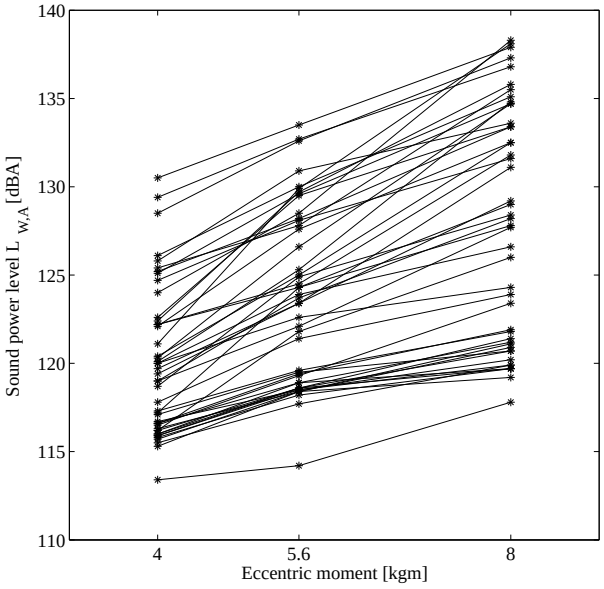

Figure 2.11.: Sound power level as a function of the eccentric moment for 46 different configurations of the second experiment session

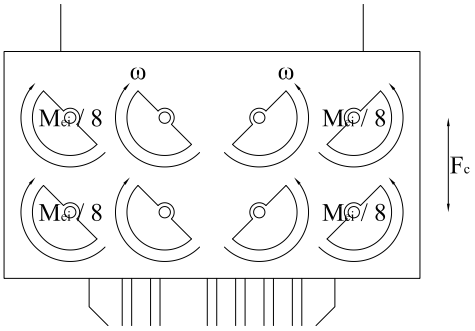

Figure 2.12.: Force generated by a vibrator

can also modify the harmonic behaviour of the system and so influence the sound generation.

It should be mentioned that modifications of the frequency or of the eccentric moment will affect the efficiency of the vibro-driveability [3, 32]. Normally the contractors prefer to use the maximum force because the driving is usually more efficient.

2.3.3. Key parameters generating noise

When considering the experiment results, two configurations yield a very high noise level (around 140 dBA for the sound power level): a common interlock without any welds and a wall with a height of 3 m. The configurations of the wall and of the common interlock seem to be the main parameters for the noise generation. These key parameters are presented here below and a mechanism is proposed; other evidences are given in following chapters.

The spacing between the welds of the common interlock

It can be seen in figure 2.14 that the spacing between the welds (for a description, see figure 2.15) is of paramount importance for the noise generation: the closer the welds, the lower the sound power level. If this space is large enough, then increases can be observed when comparing with a totally welded common interlock; but such increases are not automatically obtained: other parameters can influence the noise generation secondarily. As the results of some experiments have been modified by the impact generation of the security system, such modified results are not displayed (see section 3.4.1 for more information).

The second experiment session studied in details way the relationship between the spacing between the welds and the noise generation. Figure 2.16 is obtained by displaying the results with a logarithmic scale for the spacing between the welds.

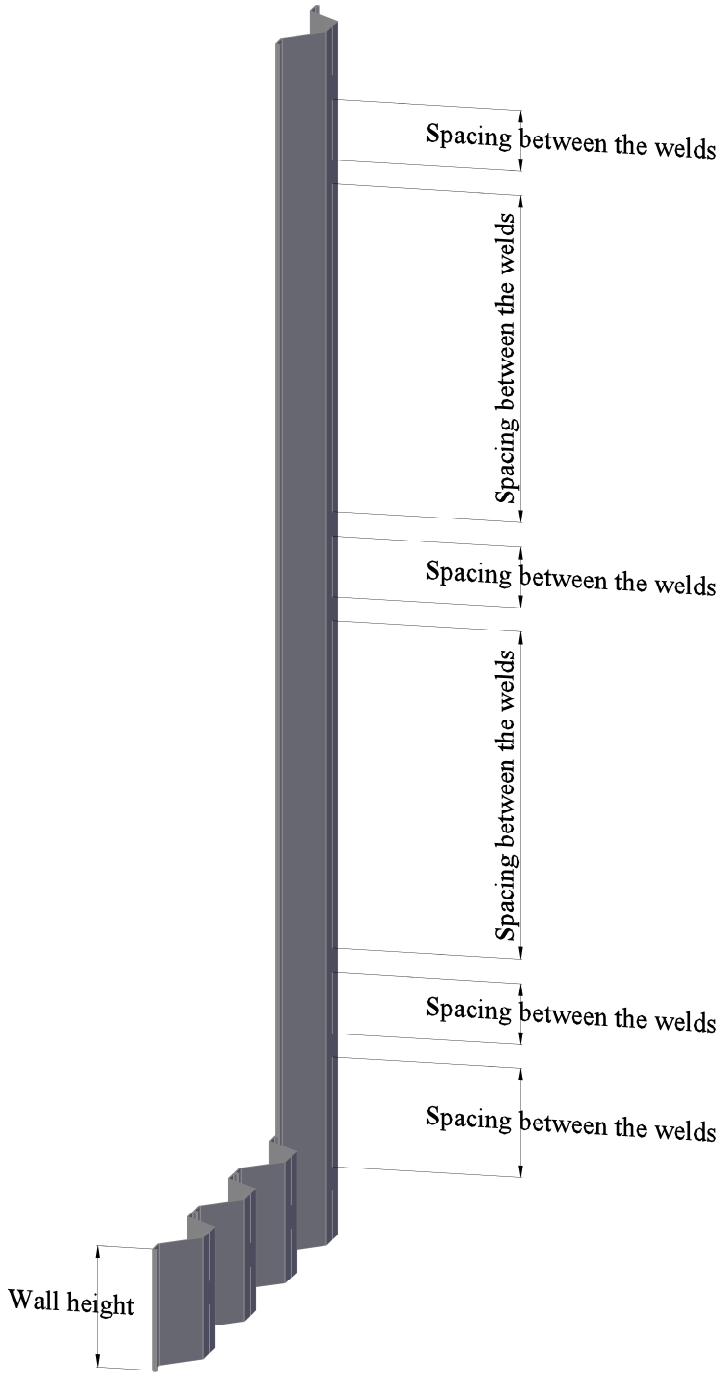

Figure 2.13.: Key parameters of the noise generation

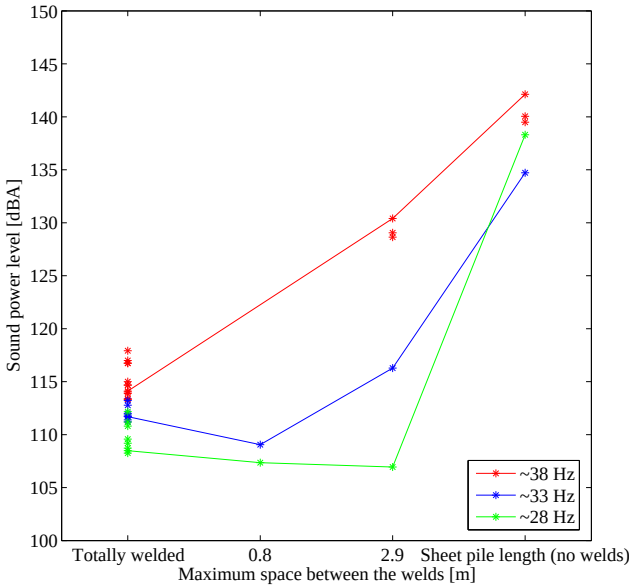

Figure 2.14.: Sound power level as a function of the maximum space between the welds (first session - the experiments with the wall are not shown)

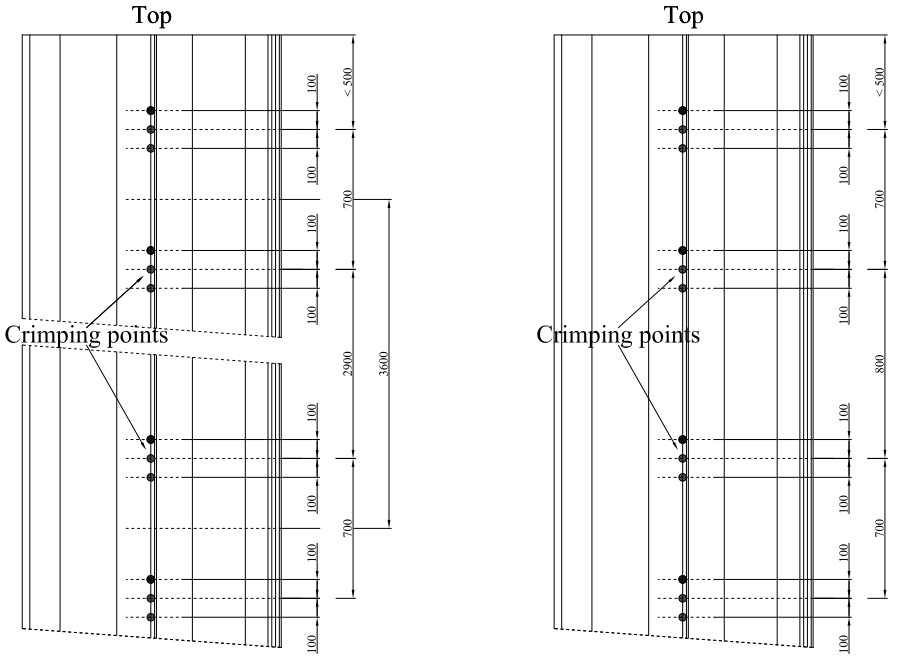

(a) Crimping with a maximum space between the welds of 2.9 m

(b) Crimping with a maximum space between the welds of 0.8 m

Figure 2.15.: Used crimpings [33, 34, 35]

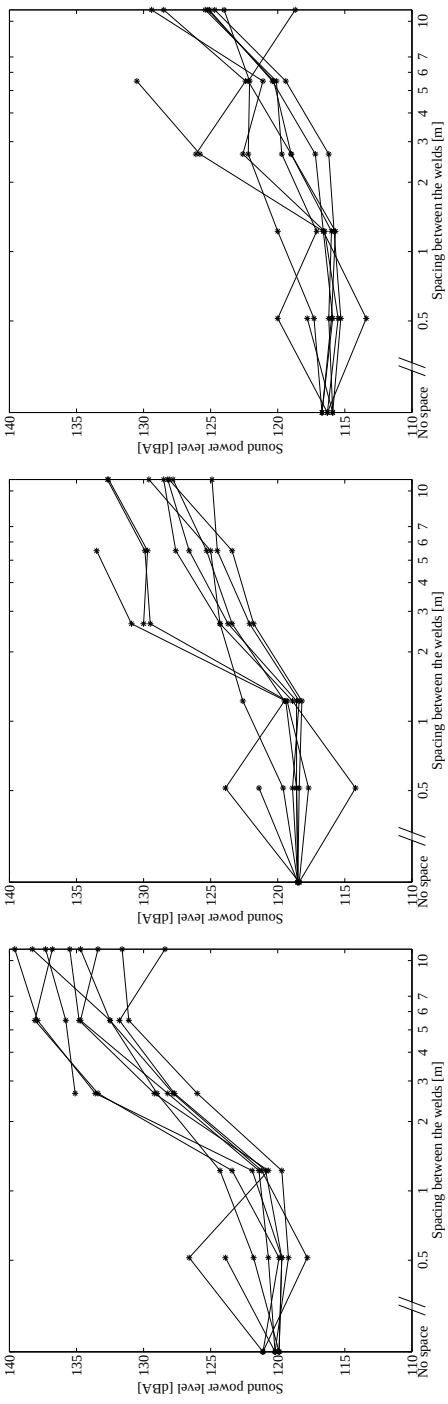

(a) Eccentric moment of 8 kgm (b) Eccentric moment of 5.6 kgm (c) Eccentric moment of 4 kgm

Figure 2.16.: Sound power level as a function of the spacing between the welds (second experiment session)

A threshold can be observed: below this threshold, the sound generated is similar to the one of a welded sheet pile; for larger spaces between the welds, substantial increases have been measured.

The mechanism proposed to explain these noise increases is based on impact occurrence in the common interlock:

- Due to the positioning of the clamping system along the sheet pile section on its top (for a single or a double clamping device), the vibrator does not only generate traction-compression waves: bending and torsion waves are also induced. The configuration of the system (boundary conditions, configuration of the common interlock, sheet pile length, etc.) determines the occurrence of resonances.
- When propagating along the sheet pile, these waves move the section along the principal axes and around the shear centre for the bending and torsion motions respectively. Only the cross-section of a single sheet pile is considered between two welds. Its shear centre is approximately merged with the centre of gravity of the section (see figure 2.17a). If it is not the case (like for double sheet piles, see figure 2.17b), the waves are composed of coupled torsion and bending motions [36].

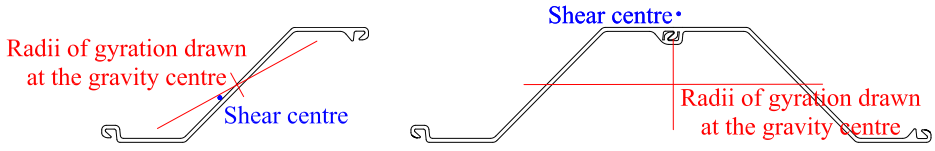

(a) Single sheet pile (b) Double sheet pile

Figure 2.17.: Example of radii of gyration, shear centre and centre of gravity of a sheet pile

- Between two welds, several impacts can occur at different locations, depending on the way how the waves are reflected at the ends and transmitted through the welds. The impact locations are then defined as the local maxima of the difference of the motion of the clutches, independently of the amplitude of this motion, which can be enough to provoke a real impact.
  If only one impact location is wanted around the middle of the space between the welds (i.e. only one maximum between two welds), this space must be lower than a fraction of the wavelength of the concerned wave type. This fraction could be determined experimentally or by simulations.
  - If only one impact location is obtained as centred between two welds, it could be suggested that statistically, the smaller the spacing between the welds is, the smaller the violence of the impacts, and thus the noise

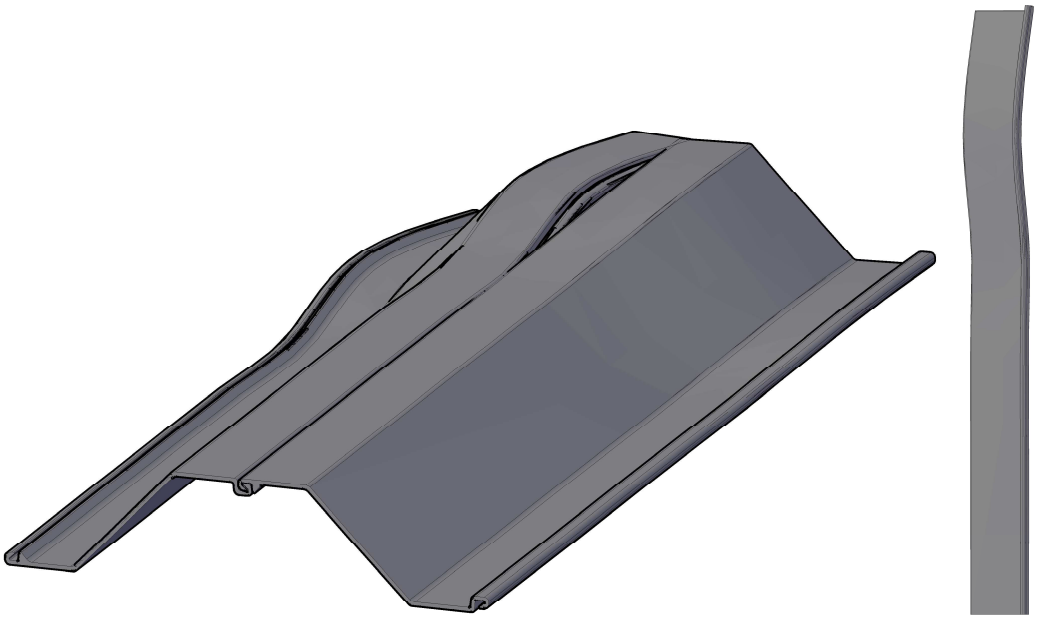

(a) Views of a bending local-mode (the subsystem with substantial vibration is at one end)

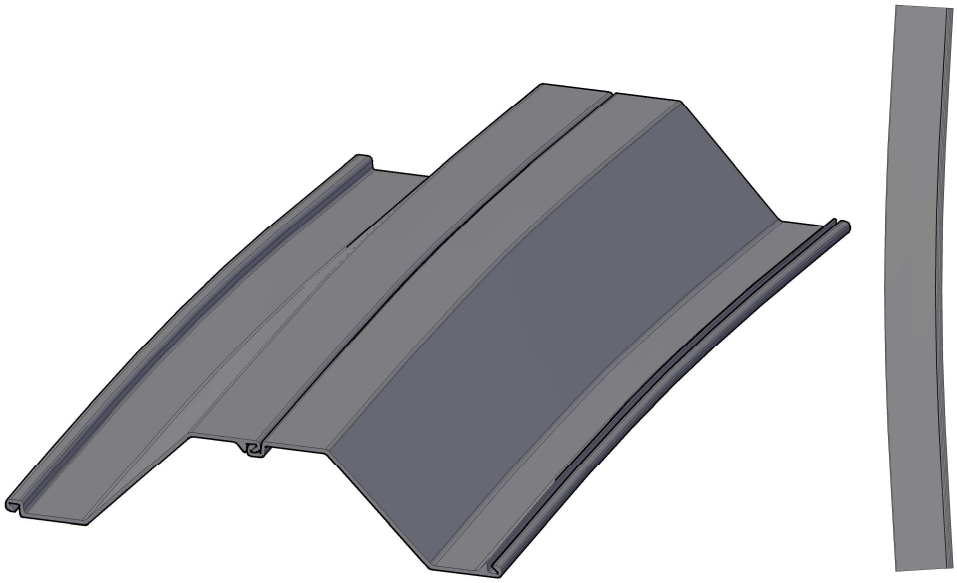

(b) Views of a bending global-mode

Figure 2.18.: Example of global- and local-modes of a double sheet pile

that could be generated, is. This is a statistical conclusion, because such a choice does not prevent to get a resonance of a global-mode, which can also introduce impacts.
Global-modes could be defined as modes moving substantially the entire studied structure (see figure 2.18a). They are opposed to local-modes that induce a substantial vibration of only a subsystem of the studied system [37, 38] (see figure 2.18b).

– If several impacts can occur, then local-modes of the part between the welds can occur, with possible resonances (inducing violent impacts and thus noise emission) and one or several impact locations between two welds. A resonance of a global-mode can still occur in this case and provoke impacts.

In conclusion, such impacts are less likely to occur if the vibrator frequency is below the first local-mode frequency, i.e. the spacing between the welds is lower than a fraction of the wavelength. Clues that endorse this theory are given in the next chapters.

The height of the wall above the ground

It can be seen in figures 2.19 and 2.20 that the experiment with a high wall (3 m above the ground) yielded a large sound power level.

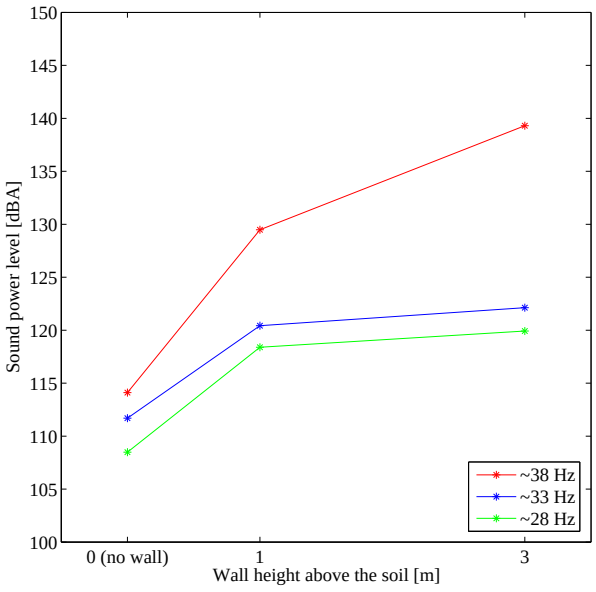

Figure 2.19.: Sound power level as a function of the wall height (first experiment session)

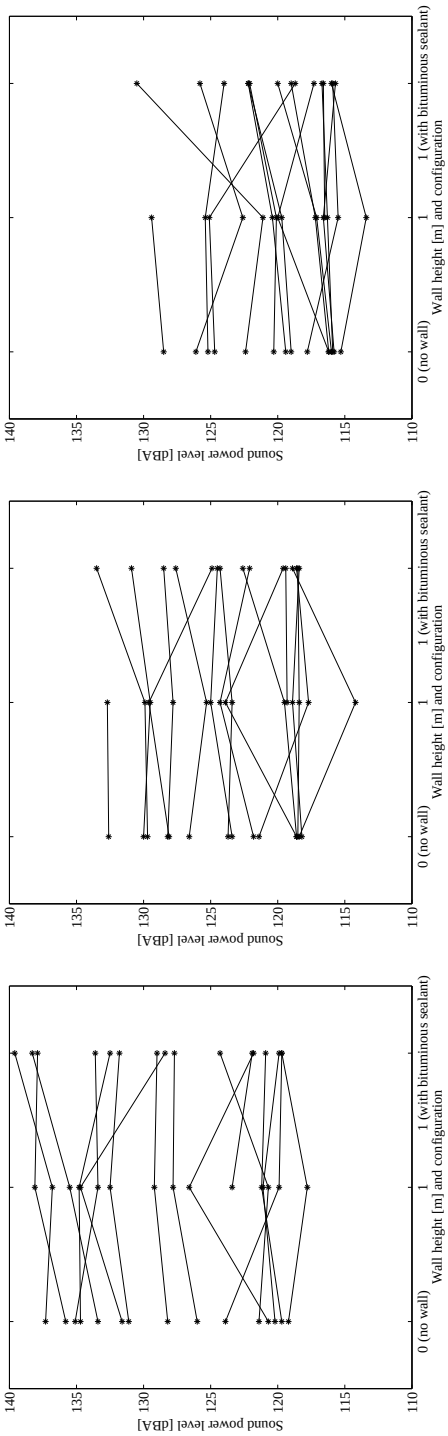

(a) Eccentric moment of 8 kgm (b) Eccentric moment of 4.6 kgm (c) Eccentric moment of 4 kgm

Figure 2.20.: Sound power level as a function of the wall height and configuration (second experiment session)

The mechanism that could be suggested in this case is based on the same principle as the influence of the spacing between the welds:

- Due to the location of the clamping system at the top of the sheet pile, bending and coupled bending and torsion vibrations are generated in the vibrated pile.
  In case of a double sheet pile with a totally welded common interlock, the shear centre cannot be considered as merged with the centre of gravity of the cross-section (see figure 2.17b), but it can be considered as close to one principal axis (due to the symmetry of the section). If one principal axis is merged with the shear centre, pure bending waves grow along this axis. The other principal axis has bending waves coupled with the torsion waves, i.e. coupled bending and torsion waves [39].
- The waves propagate towards the sheet pile toe, are partly reflected and interfere together. A resulting motion is observed between the wall and the vibrating sheet pile.
- If these motions are large enough, impacts can be provoked between the interlocked clutches. Such impacts can generate a loud noise emission.

2.3.4. Secondary parameters

Comparison between a welding and a crimping in the common interlock

Welding was preferred to the crimping during the experiments because it is more reproducible and easier to perform (specially on site). However, a comparison was made to show the equivalence. One comparison showed an increase of 0.7 dBA when using a welding instead of a crimping (experiments 13 and 18). This difference is not significant and the acoustic behaviour can be considered as equivalent.

Influence of a watertighthness joint in the common interlock

Experiments with a polyurethane sealant gave overestimated results, because of the noise generated by the security system. The noise of the loudest experiment was well decreased by the use of the polyurethane sealant (3.6 dBA). But a larger decrease could have been obtained without the influence of the security system, as a softening of the impacts is waited.

A bituminous sealant in the common interlock was tested during the second experiment session. It played a role in the impact generation in the common interlock (see figure 2.21): decreases up to 11.2 dBA can be observed, but the arithmetic average decrease is 4.3 dBA.

It was seen on site that the bituminous sealant was soft and can be pushed out of the interlock.

Sealants can decrease the sound power level, but the amplitude of reduction cannot be quantified or certified.

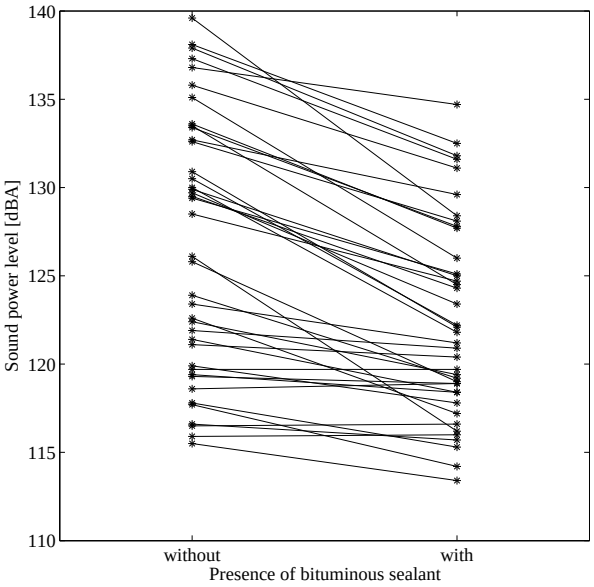

Figure 2.21.: Sound power level as a function of the presence of a bituminous sealant in the common interlock (second experiment session)

Influence of a sealant in the clutch connected to the wall

This influence was investigated by using a bituminous sealant (see figure 2.20). Experiments with a bituminous sealant can be considered as having similar results as experiments with a wall but without sealant; indeed, the wall was too small to generate loud impacts. The observed differences could be explained by the fact that interlocked clutches are not the same (the straight clutch for the experiments with the bituminous sealant and the curved one for the experiments without bituminous sealant).

During some experiments, the sealant quickly melts because of the energy dissipated in the interlock. This behaviour was obtained faster for sheet piles with a large spacing between the welds; indeed, sheet piles with a smaller spacing between the welds are more rigid and smaller motions should be statistically observed. For example, thermographic measurements show a temperature of almost 170 $°C$ during experiment 134 (see figure 2.22).

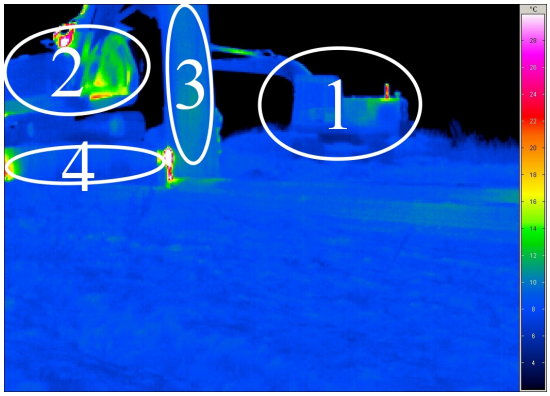

Maximum temperature of the connection with the wall: 132.73°C
Legend:
1. excavator
2. leader machine
3. vibrating sheet pile
4. sheet pile wall

(a) First picture

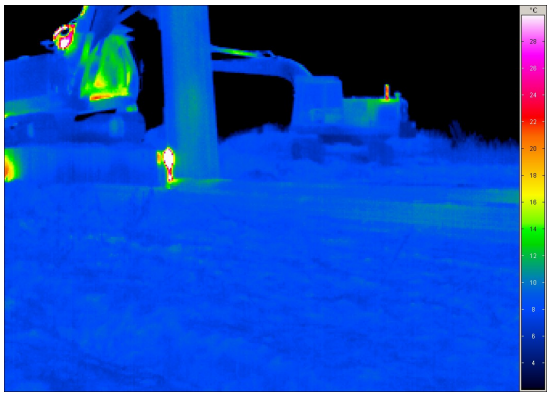

Maximum temperature of the connection with the wall: 148.54°C

(b) Picture taken 38 s after the picture (a)

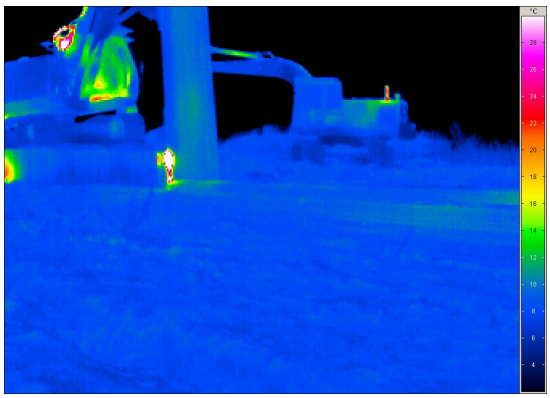

Maximum temperature of the connection with the wall: 168.14°C

(c) Picture taken 37 s after the picture (b)

Figure 2.22.: Thermography pictures taken with a interval of 30 s showing the melting of the bituminous sealant (experiment `134`)

Influence of the machine system

A misalignment between the sheet pile and the wall can generate an noise increase. From this point of view, a leader-mounted system gives more control than a free-hanging system.

Other measurements

The other measurements made during the first experiment session did not show a clear influence of the tested parameters. Indeed, the impacts are the loudest sound source and these experiments were performed with a welded common interlock and no wall: this configuration prevents any impact occurrence.

2.4. Conclusions

In this chapter, the sound measurements on site with their post-processing are described, giving an approach value of the sound power level. The results give a hierarchy of the tested parameters:

1. Key parameters: Two parameters can produce loud or quiet vibratory pile drivings, depending on their configuration:

- the spacing between the welds of the common interlock;
- the height above the ground of the wall connected to the sheet pile.

A threshold spacing between the welds of the common interlock was highlighted: a drastic increase of the sound power level is observed when this spacing increases from 1.2 to 2.7 m (for the studied configuration). The same phenomenon is observed with the wall: the threshold height above the ground is waited between 1 and 3 m.

A theory explaining these behaviours is presented in both cases. Summarized, it gives:

- Bending, torsion or coupled bending and torsion waves are generated by the vibrator, because of the positioning of the clamping system along the sheet pile section on its top (for a single or a double clamping device).
- The induced motions can create impacts because of the difference of displacement of the interlocked clutches.

  For the spacing between the welds: These impacts are less likely to occur if the vibrator frequency is below the first local-mode frequency,

i.e. the spacing between the welds is lower than a fraction of the wavelength. This is being studied in details in chapter 5.

For the height of the wall: Higher is the wall, more likely is it to generate violent impacts. They can also be amplified by a misalignment of the vibrating sheet pile.

2. Secondary parameters: These parameters could modify the noise emission of a vibrated sheet pile if one of the two key parameters is the source of sound. They cannot generate sound themselves: impacts are obtained only for a combination of the key parameters.

- A comparison is made to show that a crimping is equivalent to a welding.
- Two sealant products were tested to see if they are able to soften the impacts.
  A bituminous sealant can soften the impacts and decrease the sound, but the amplitude of reduction must be investigated further.
  The polyurethane sealant reduce also the noise, but the amplitude of reduction was not determined here.
- A decrease of the eccentric moment or of the frequency seems to induce a decrease of the sound power level. In the second case, the decrease can come from the decrease of the force (proportional to the square of the frequency) or from the modification of the harmonic behaviour. But such modifications (frequency or eccentric moment) decrease the efficiency of the vibrodriveability and are not a solution to noise problems for the contractors.

The next chapters bring proofs and details to support the explained mechanisms.

Chapter 3.

Noise source localization by beamforming

The example of figure 1.6 showed that a localization system is useful to distinguish and identify sound sources. The first goal of such a system is to localize where the noise is generated, e.g. by the vibrating sheet pile or by the power pack. Furthermore, this system can provide information about the noise generated by the sheet pile itself.

3.1. Choice of the method

Several systems are available to produce sound pictures:

Holography: This technique uses spatial Fourier transforms on a regular pattern of microphone measurements around the object to determine the spatial propagation of acoustical waves, or for detecting acoustic sources or objects [40]. Such a system can study planar, cylindrical of spherical objects.

Beamforming: A grid of microphones is placed at some distance of the object (see figure 3.1). The measurements show differences in their phases, depending on the distance between the measurement point and the sound source. This difference is balanced and the signals are summed: a constructive summation occurs where a sound source is located. An acoustic picture showing hot spots is obtained; it is superimposed on a visual picture.

Sound intensity probe: A scanning of the studied object is made by a sound intensity probe. It is a near-field method: the probe must be close to the object during a stationary state to measure the sound intensity emitted by a part of the studied object. The measurements are combined and superimposed on a picture to make a map of the sources.

Helmohltz-Kirchhoff equation approach: When studying a complex geometry, acoustic measurements can be combined with simulations obtained with the

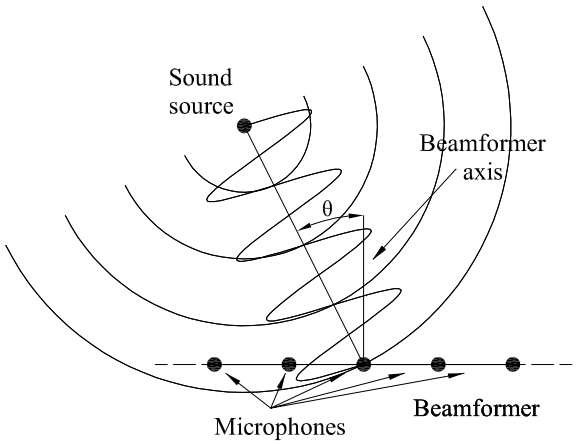

Figure 3.1.: Principle of the beamforming method

Boundary Element Method (BEM) to calculate the normal velocity distribution of the object [40].

Equivalent source methods: Such methods replace one source with an irregular shape by a set of elementary sources (monopoles, dipoles, etc.) adequately located. These methods are more used to study the behaviour of the sources than their location [40].

The beamforming system is favourable to study a vibratory pile driving:

- A measurement is simultaneously performed for all the microphones of the grid, which does not need scanning at different locations during a stationary cycle.
- Transient analyses can be made if desired.
- Beamforming is a far field method, in contrast to the scanning with a sound intensity probe that needs to be made close to the object. This is dangerous during a vibratory pile driving.
- The holography needs a grid around a simple object (planar, cylindrical, spherical, etc.). This is not conceivable and possible for a sheet pile.
- Sheet piles have too large geometries to make satisfying BEM simulations like for the Helmohltz-Kirchhoff equation approach.

The beamforming method is extensively presented by Christensen *et al.* [41]. Two limitations of this technique should be kept in mind when measuring and interpreting the obtained pictures:

Ghost images in the high frequency range: In some cases, a constructive summation can occur where no sound source is located. This ghost image is due to the interaction of several sources. Its occurrence depends on the pattern

of the microphones and on the distance between the microphones. For example, it is known that a spiral pattern will have ghost images in a higher frequency range when compared to a rectangular pattern with the same external diameter [41]. This phenomenon can be simulated so that an adapted grid can be designed before the measurements.

Loss of resolution in the low frequency range: The resolution of the beamformer describes its ability to distinguish waves incident from directions close to each other; for sources at a finite distance a practical definition of resolution is the minimum distance between two sources such that they can be separated [41]. Smaller the resolution is, more easily the picture is interpreted. The beamformer resolution R depends on the frequency as follows [41]:

$$R = a\ \frac{z}{D}\ \lambda\ \frac{1}{\cos^3\theta} = a\ \frac{z}{D}\frac{c}{f}\ \frac{1}{\cos^3\theta} \tag{3.1}$$

where $a = 1.22$ for a circular grid,
z = distance between the grid and the sound source $[m]$,
D = aperture diameter (the diameter of the circular grid) $[m]$,
λ = wavelength of the sound $[m]$,
θ = off-axis angle $[rad]$ (see figure 3.1),
c = sound speed $[m/s]$, and
f = sound frequency $[Hz]$.

The choice of z and D is made by taking into account two effects:

- With a grid close to the object, the beamformer has a small (and thus good) resolution.
- If the object is too close to the beamformer, the large off-axis angle induces a larger resolution, which makes distinguishing two close sources more difficult if not centred. Typically, the maximum used off-axis angle θ is 30°; the resolution is then increased by 50 % [41].

Equation 3.1 shows that the beamformer resolution is worse for low frequencies.

3.2. Configuration of the measurements

Figure 3.2.: Beamforming grid fixed to a cherry picker

The used system is a rectangular grid of 2.4×2.4 m: it is the largest available size to have the highest resolution for the low frequency range and a good grid rigidity as well as some ease to move it as shown in figure 3.2. It was used with a spiral pattern of 48 microphones (shown in figure 3.3). The beamformer was placed at 25 m and 16 m for the first and the second experiment respectively in front of the sheet pile at half of its height by fixing it on a cherry picker (as in figure 3.2), so that the sheet pile was parallel to the grid and centred in the picture.
The used microphones have a reduced frequency range compared to the acoustic measurements: only the frequency range with a good resolution and with few ghost images is useful. They were mounted with the associated windscreens (see section A.2 for more details). The signals were sampled at 32 kHz. Black-and-white pictures were taken by an industrial camera (about 13 frames per second) with a panoramic lens.
The interesting frequency range when studying the vibratory pile driving of sheet piles is between 0.5 and 4 kHz (as shown by the representative example of figure 2.9b), due to the A-weighting recommended by standards and used by the literature [13, 22, 23, 24, 25, 26]. The expected resolutions are then (from equation 3.1):

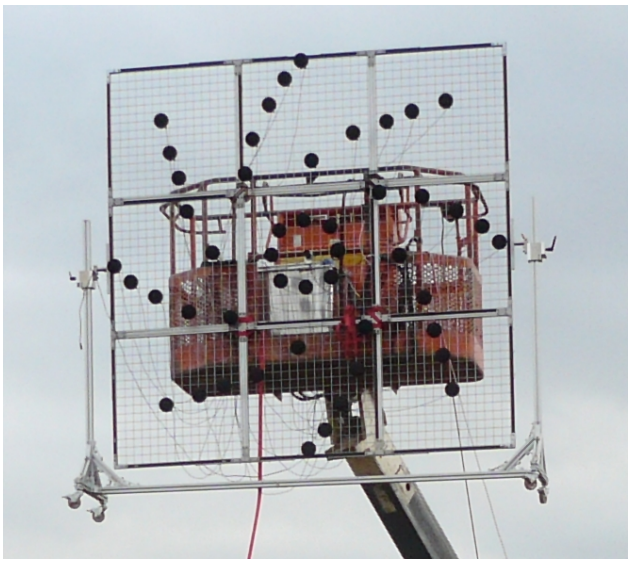

(a) On site (view in front of the grid)

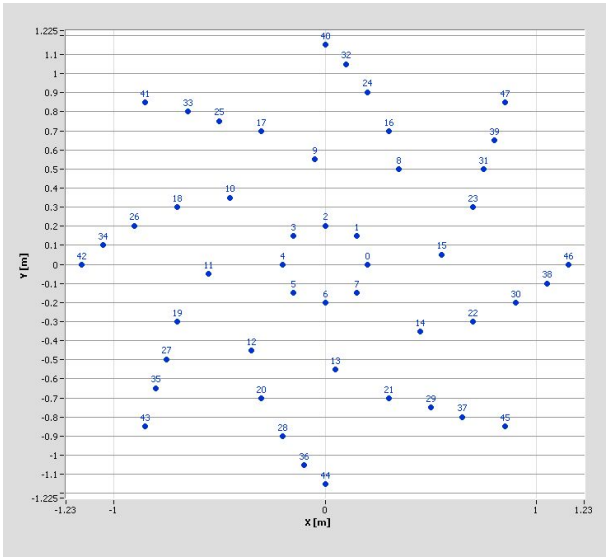

(b) Design (view behind the grid)

Figure 3.3.: Spiral pattern used during the full-scale experiments

Octave	500 Hz	1 kHz	2 kHz	4 kHz
Resolution (first session)	8.7 m	4.4 m	2.2 m	1.1 m
Resolution (second session)	5.6 m	2.8 m	1.4 m	0.7 m

Such resolutions help to vertically localize a sound source, but not to distinguish two different sound sources at the same height on a double sheet pile; indeed, its width is more or less 1.5 m.

To interpret the pictures, it should be mentioned that the scale given in the legend for the sound pressure level is not absolute, but relative: it is obtained by the summation of the balanced signals. So comparisons of the levels of two pictures can be made, but the levels cannot be compared with sound pressure levels or sound power levels as made in chapter 2.
Because sound sources are easier to distinguish for high frequencies, the picture of the high frequency range can be used to localize sources more precisely than in the pictures of the low frequency range. It is assumed that *these sound sources emit noise in both frequency ranges*. This was shown for the security system in figure 1.6: in this case, the picture of the octave band of 4 kHz helps to show that the main source is the bottom part of the vibrator, even if the maximum level of this picture shown in the legend is lower than the ones of the three other pictures.

As shown by this last observation, each picture needs to be interpreted: ghost images must be detected, links between several frequency ranges must be established, the levels displayed in the legend have to be compared, etc.

3.3. Post-processing of the measurements

The post-processing of the measurements has been made as follows:

1. All frequency bands of interest (the octaves of 500 Hz, 1 kHz, 2 kHz and 4 kHz) have been studied over the time range of the stationary driving. A map have been calculated each 0.1 s, using a sound extract of 1 s of length (so an overlap of 0.9 s).

2. As the analysed signal has a length of 1 s only, a Hamming window has been used in order to decrease the leakage phenomenon.

3. The region of interest has been specified on the picture and the calculation has been performed.

4. The calculation results can be saved as pictures or videos. The pictures that are displayed in this thesis are representative extracts of the videos.

3.4. Main results

As already mentioned, the aim of the experiments was to show if the sound is generated by the sheet pile itself; this has always been the case. Here below are studied results giving additional information about this noise generation. The results are given for four octaves (500 Hz, 1 kHz, 2 kHz and 4 kHz) so that the high resolution of the octave of 4 kHz is an advantage, even if this octave band does not substantially contribute to the sound power level as shown in figure 2.9b. Indeed, this representative example shows a difference of 10 dBA between the maximum sound pressure level and the level of the third-octave of 4 kHz; due to the logarithmic summation of equation 2.2, the contribution of the third-octave of 4 kHz to the sound pressure level for all the frequency ranges is weak.

3.4.1. Influence of the security device

The evaluation of the sound power level was influenced by the security device during eight experiments (experiments `10`, `11`, `12`, `14`, `15`, `21`, `22` and `23`). If these results are discussed in this thesis, it is mentioned that the sound power level is overestimated because of the influence of the security device.
This security device has already been described in section 1.2: a shackle was placed 2 m under the top of the sheet pile in a hole on the left side, and was attached to a sling, itself attached to the second cable of the crane.

Indeed, it can be seen in figures 1.6 and 3.4 that this security device was the main source for octaves of 1 kHz, 2 kHz and 4 kHz during experiments `10` and `21`. So the results of these experiments are increased by the impacts of the security system; the results could have been lower if no influence had been detected.
For experiment `13` (in figure 3.5), octaves of 500 Hz and 1 kHz seem to be less concerned. Even if the metallic sound of the shackle impacting the sheet pile can be identified when listening to the registered sound, the sound level was less increased than the level of other experiments.

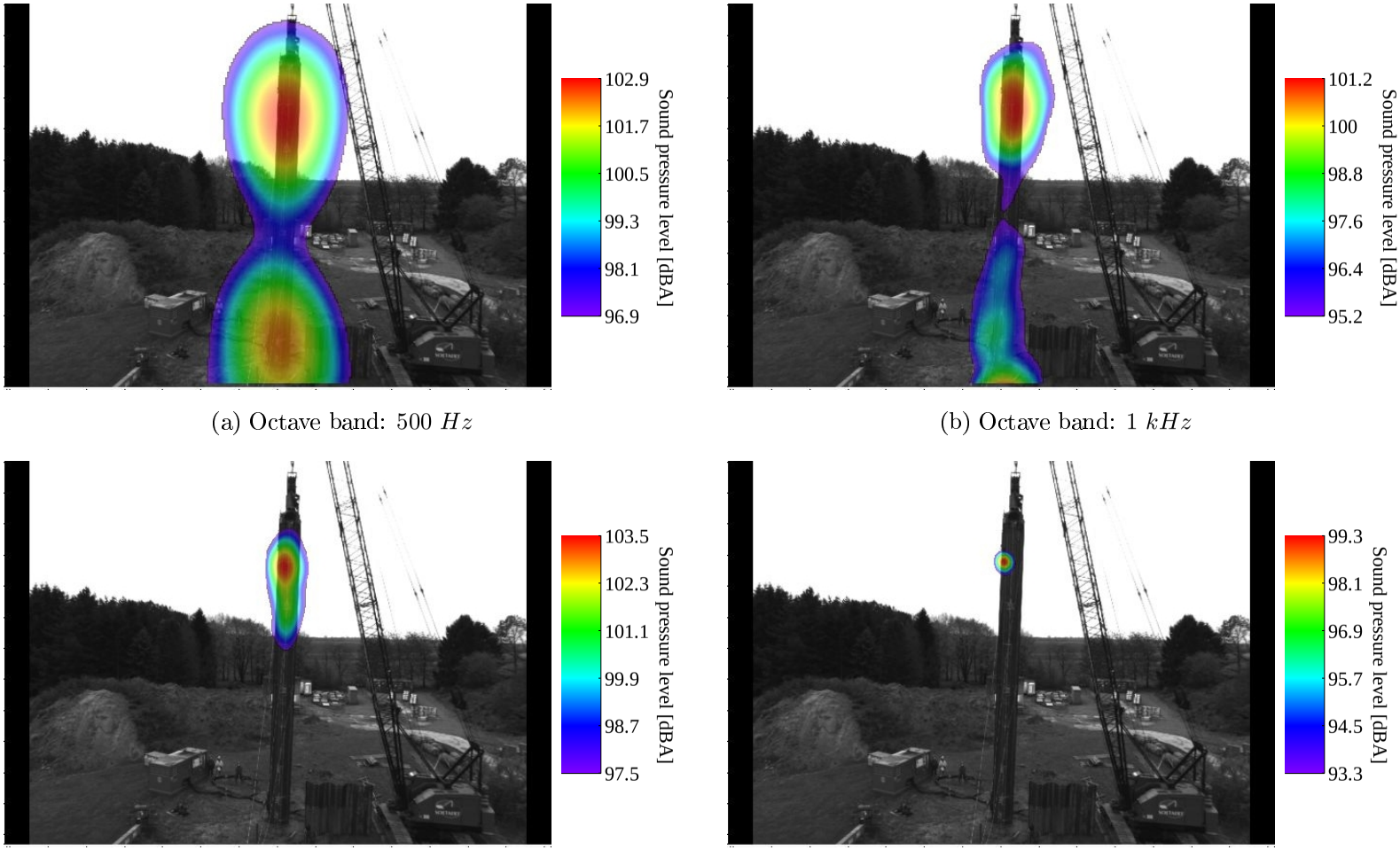

(a) Octave band: 500 Hz

(b) Octave band: 1 kHz

(c) Octave band: 2 kHz

(d) Octave band: 4 kHz

Figure 3.4.: Beamforming showing the major influence of the security device of figure 1.9 during experiment `21`; indeed, the source is identified only for the octave of 4 kHz with a lower level than the three other octaves

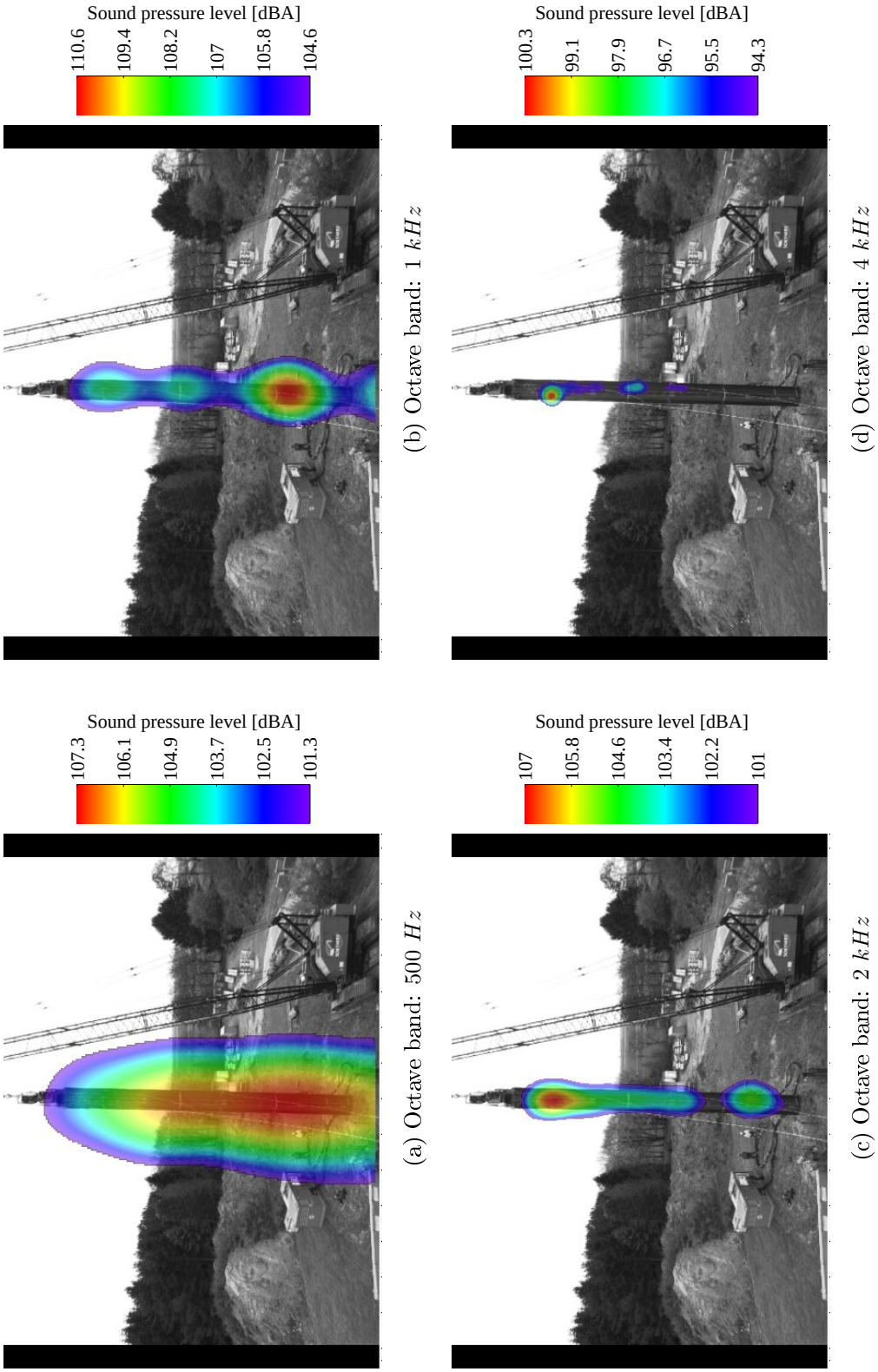

(a) Octave band: 500 Hz (b) Octave band: 1 kHz

(c) Octave band: 2 kHz (d) Octave band: 4 kHz

Figure 3.5.: Beamforming showing the minor influence of the security device of figure 1.9 (during experiment 13)

3.4.2. Vibratory pile driving of welded sheet piles

The quietest drivings were obtained for completely welded double sheet piles. In this case, the sound is mainly generated at the ends of the sheet piles: at the connection with the clamping device and nearby the ground as shown in figure 3.6.

The sound at the top can come from three phenomena:

- The noise produced by the vibrator (due to the gears, the bearings, the hydraulic motors, etc.) is directly emitted in the air.
- This noise from the vibrator can resonate in the first meters at the top of the sheet pile.
- Sound can also be generated by the interaction of the clamping device and the sheet pile.

This noise cannot be decreased easily by modifying the sheet pile design; it should be more efficient to modify the vibrator and the clamping device design.

The noise generated at the boundary with the ground is also difficult to change. It comes from the interaction of the soil and the waves in the sheet pile.

3.4.3. The source at the bottom of sheet piles

When studying the 500 Hz octave band, in several cases, the pictures seem to show a source on the ground in front of the sheet pile as in figures 3.6a or 3.7a. Several hypotheses had been considered to explain such hot spots. In fact, sources located at a rather large angle tend to be shifted to an even larger angle by the beamforming process. Indeed, due to the increase of the off-axis resolution with the off-axis angle θ (equation 3.1), the hot spots that are not in the centre of the picture are deformed and are not like a circle anymore. If only one part of this spot can be seen, a mistake about the exact position of the source is made by extrapolating the source with a circle.

This phenomenon is simulated in figure 3.8. The coordinates of the sources are: $(0\ m, -8\ m)$, $(-4\ m, -8\ m)$ and $(4\ m, -8\ m)$. It can be seen how the waited circle is deformed, and the reader could be confused if he had to position the source.
So the sources displayed in figures 3.6a and 3.7a are at the boundary of the ground and the sheet pile, even if they seem to be located below.

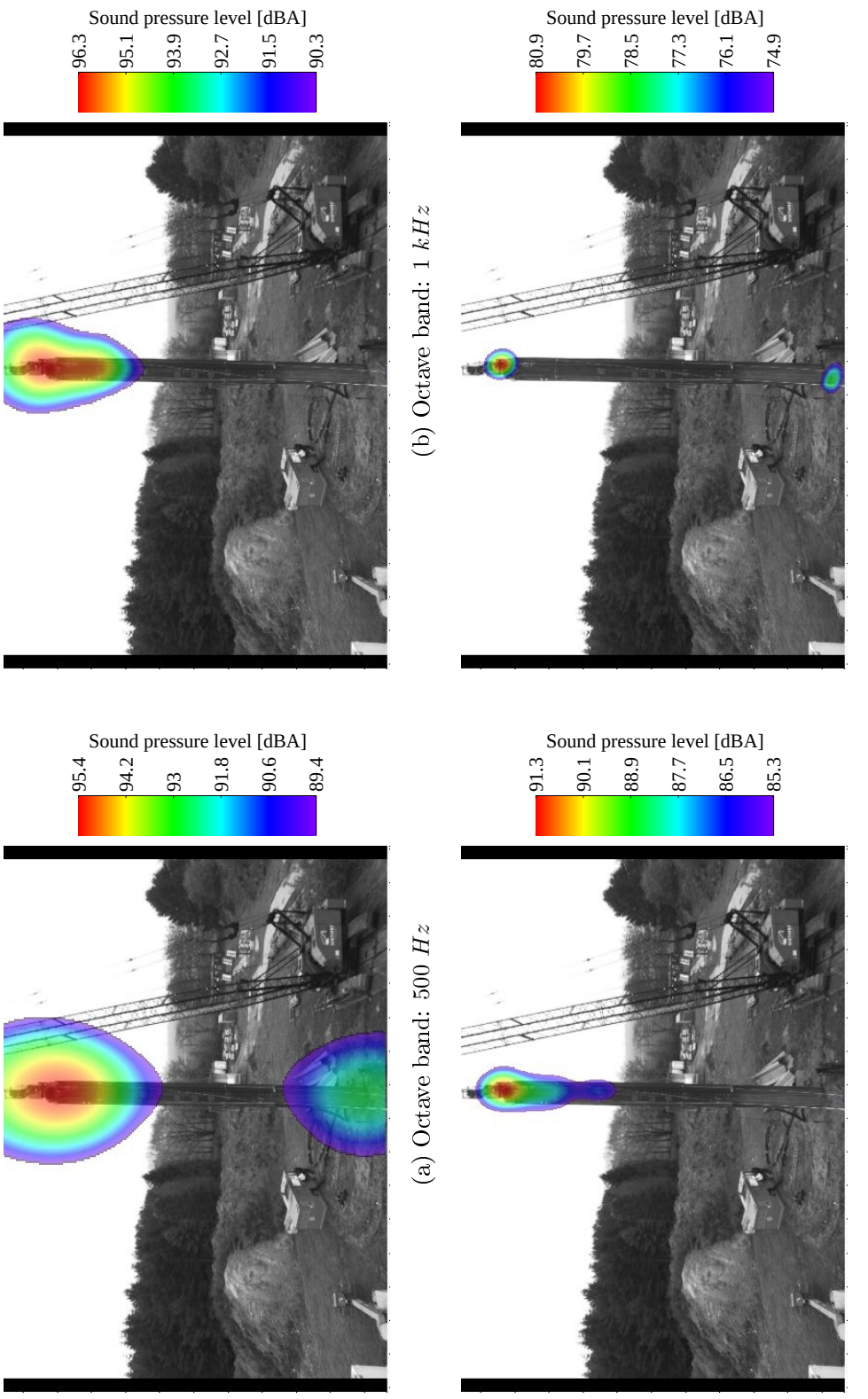

(a) Octave band: 500 Hz (b) Octave band: 1 kHz (c) Octave band: 2 kHz (d) Octave band: 4 kHz

Figure 3.6.: Beamforming showing the noise emitted at the ends of a welded sheet pile (during the quiet experiment 37)

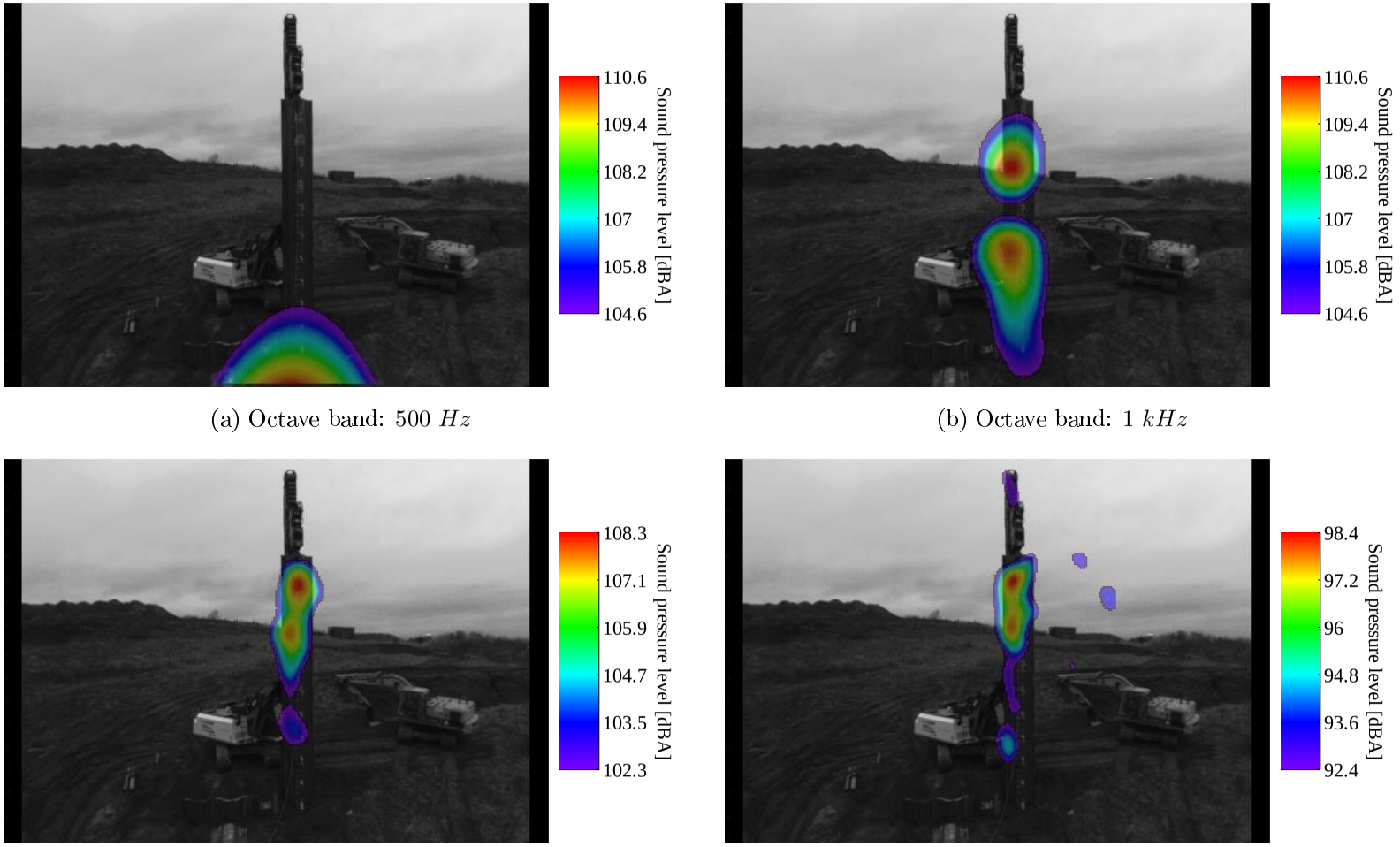

(a) Octave band: 500 Hz

(b) Octave band: 1 kHz

(c) Octave band: 2 kHz

(d) Octave band: 4 kHz

Figure 3.7.: Beamforming showing the noise source at the toe of the sheet pile for the octave of 500 Hz (during experiment `168`)

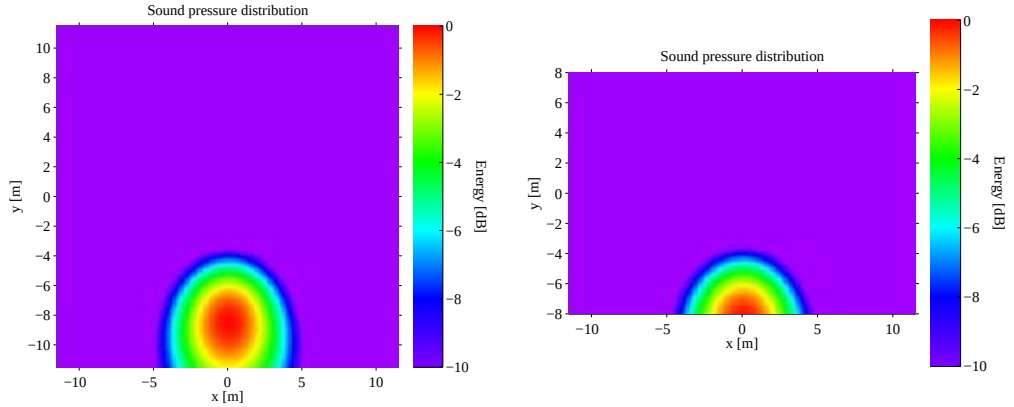

(a) Source coordinates: $(0\ m, -8\ m)$

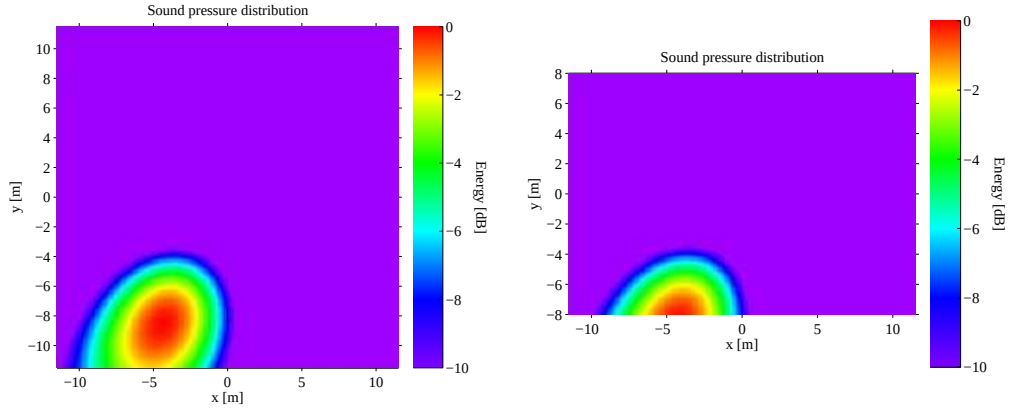

(b) Source coordinates: $(-4\ m, -8\ m)$

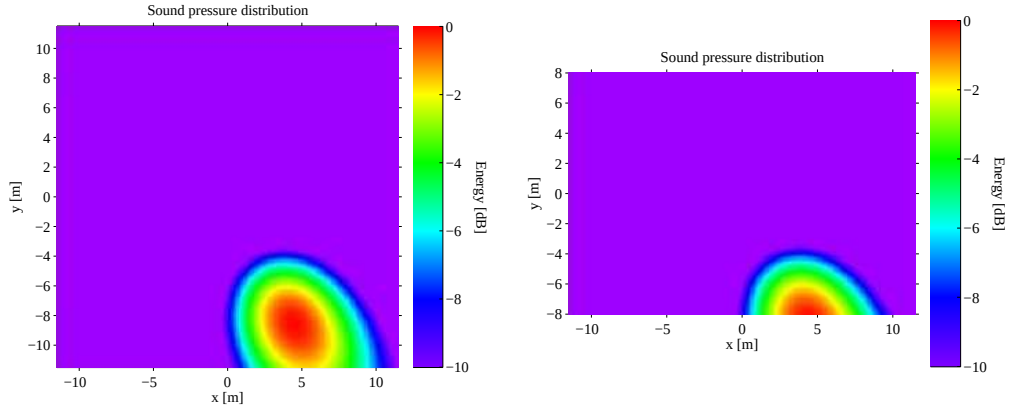

(c) Source coordinates: $(4\ m, -8\ m)$

Figure 3.8.: Simulated deformation and shift of the hot spot performed by the beamforming process for several locations of the source (entire spot and cropped aspect)

3.4.4. Influence of the spacing between the welds

For experiments with a common interlock that is not totally welded, the hot spots are horizontally centred on the sheet pile (see figure 3.13). It can be deduced that the common interlock is crucial in the noise generation.

The most interesting pictures were obtained during the second experiment session. A thermography camera [42] was used to generate thermographic pictures (for example, figures 3.11 and 3.9 for experiments `150` and `112`). These can be compared with the expected sound sources (in figures 3.12 and 3.10).
The position of the sound sources corresponds with the position of a hot spot in the thermography pictures (at around 3 m and 1.5 m of the top for experiments `150` and `112`, respectively. Indeed, impacts occurring in the common interlock at this location generate sound as well as heating. This observation is the clearest evidence of impacts occurring in the common interlock.
Furthermore, the position of these expected impacts is more or less centred between two successive welds, in accordance with the mechanism exposed in section 2.3.3. This mechanism explains also that several impact locations can occur if the spacing between the welds is larger than a fraction of the wavelength: figure 3.13 shows several noise sources instead of one centred source for a sheet pile without any welds.

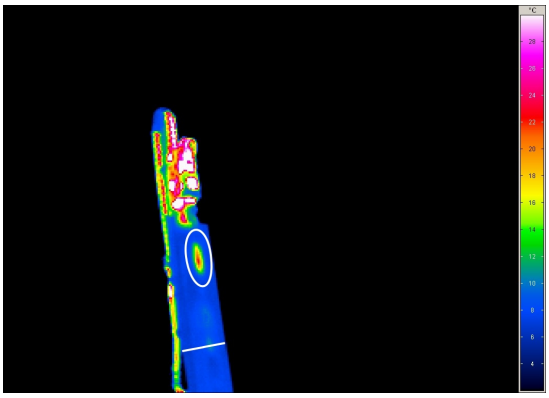

Figure 3.9.: Thermography showing an increase of temperature at the location of the main impact of figure 3.10 (during experiment `112`)

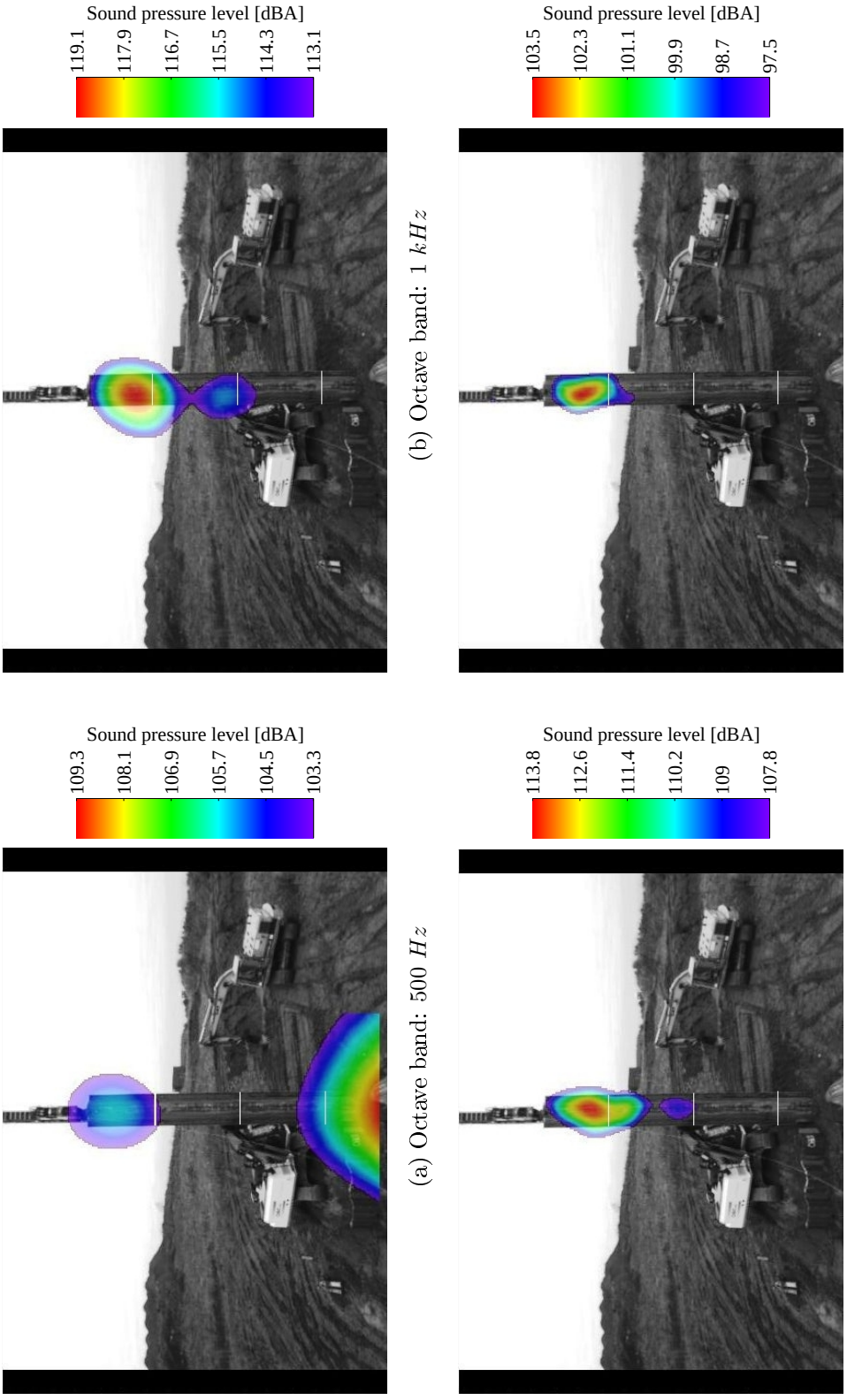

(a) Octave band: 500 Hz (b) Octave band: 1 kHz

(c) Octave band: 2 kHz (d) Octave band: 4 kHz

Figure 3.10.: Beamforming showing the main impact between two welds (the white line at 3, 6 and 9 m of the top) with a space between them of 2.7 m (during experiment 112)

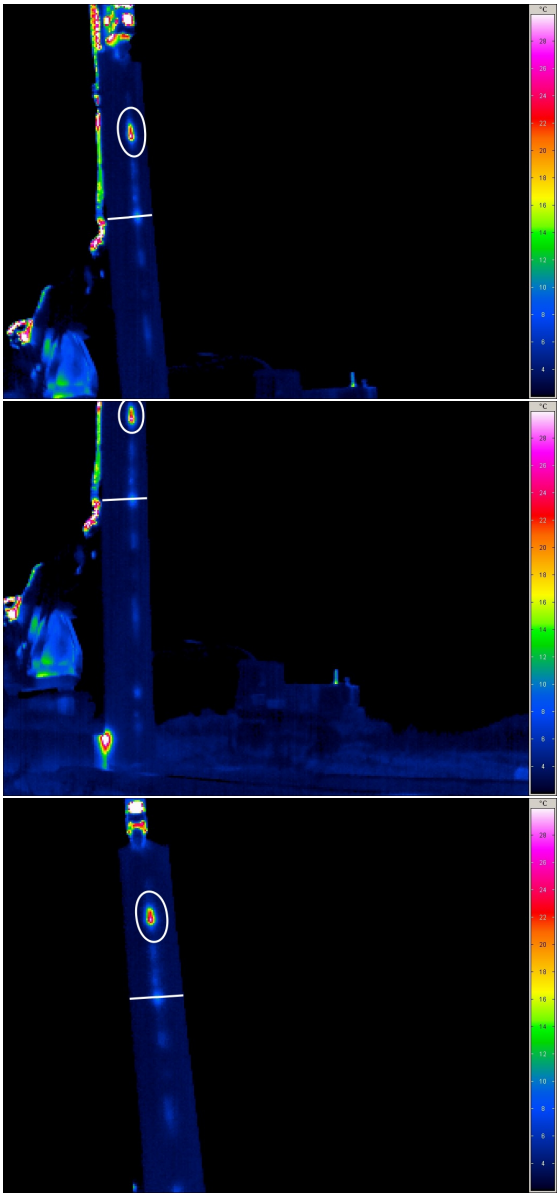

Figure 3.11.: Thermography showing an increase of temperature at the location of the main impact of figure 3.12 (during experiment 150)

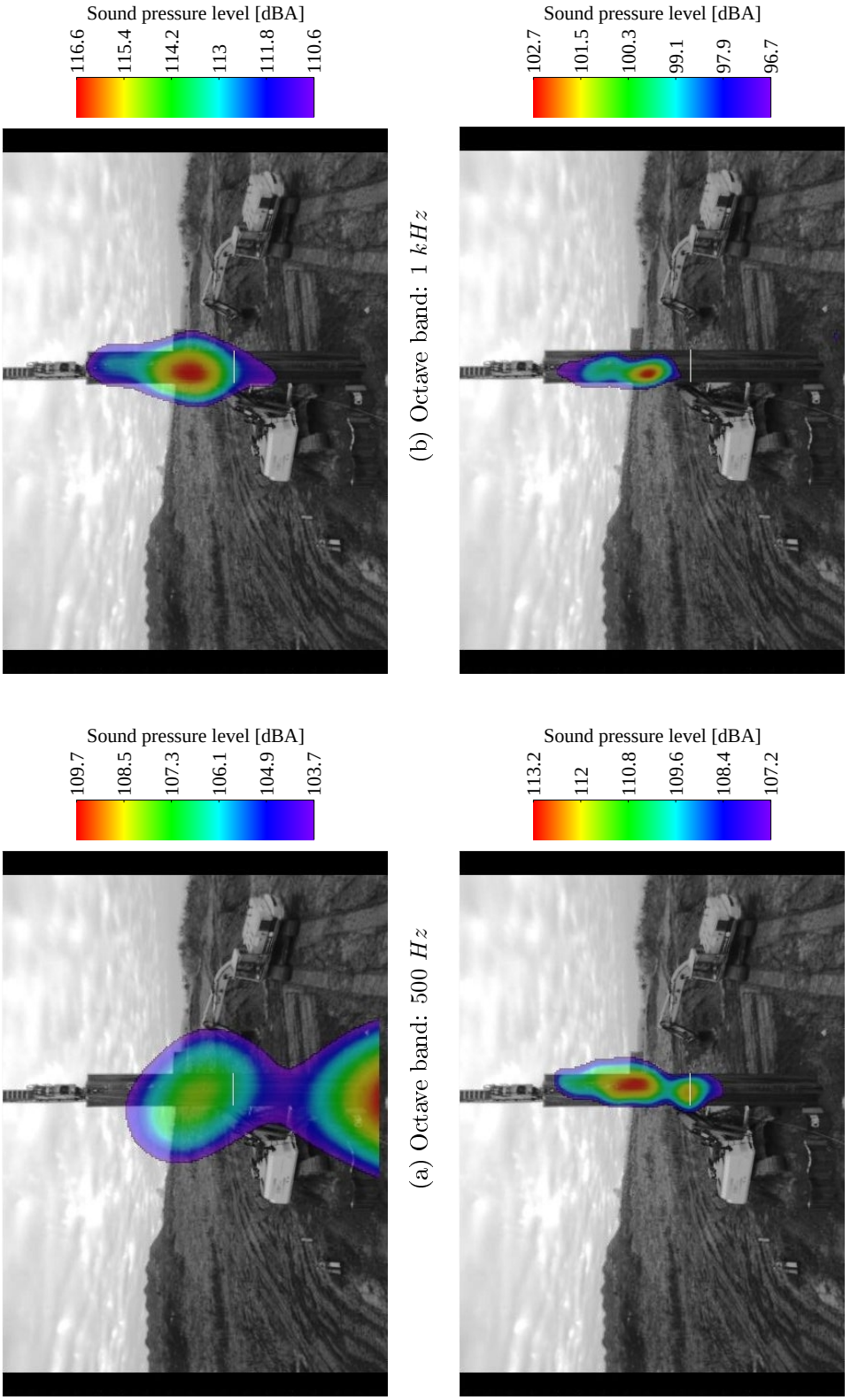

(a) Octave band: 500 Hz (b) Octave band: 1 kHz

(c) Octave band: 2 kHz (d) Octave band: 4 kHz

Figure 3.12.: Beamforming showing the main impact between two welds (the white line at 6 m of the top) with a space between them of 5.5 m (during experiment 150)

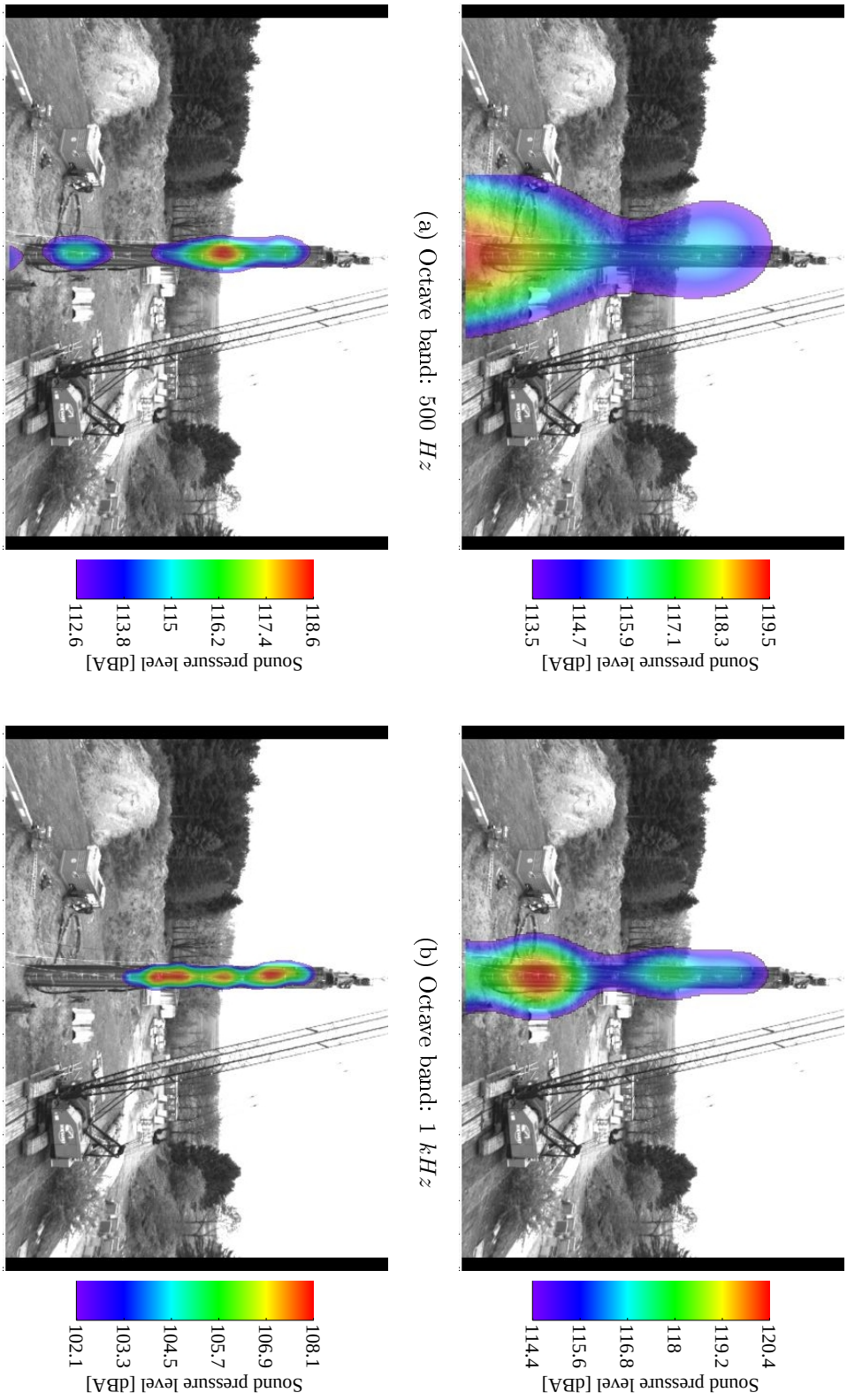

(a) Octave band: 500 Hz

(c) Octave band: 2 kHz

(b) Octave band: 1 kHz

(d) Octave band: 4 kHz

Figure 3.13.: Beamforming showing several noise sources horizontally centred on a sheet pile without any welds (during experiment 26)

3.4.5. Influence of the wall

The experiments of the first session showed an influence of the wall on the noise generation (see section 2.3.3), and this can be verified in figures 3.14 and 3.15. Only one sound source (at 4 m above the top of the wall) can be seen in figures 3.14c and 3.14d for the octaves of 2 and 4 kHz (for a wall with a height of 1 m above the ground). The wall was thus the main noise source for these experiments of the first session.

During the second experiment session, no increase of the sound power level was observed in section 2.3.3 when testing sheet piles with a wall session. The beamforming pictures confirm that the wall was never the main sound source during this second session (for example, in figure 3.16); indeed, other sources generating sound with levels close to the wall source can be observed. For this session, the connection with the wall is one of the sources only.

This difference between the two sessions can be explained by the differences between the tested configurations: for the second session, smaller sheet piles, a less powerful vibrator, etc.

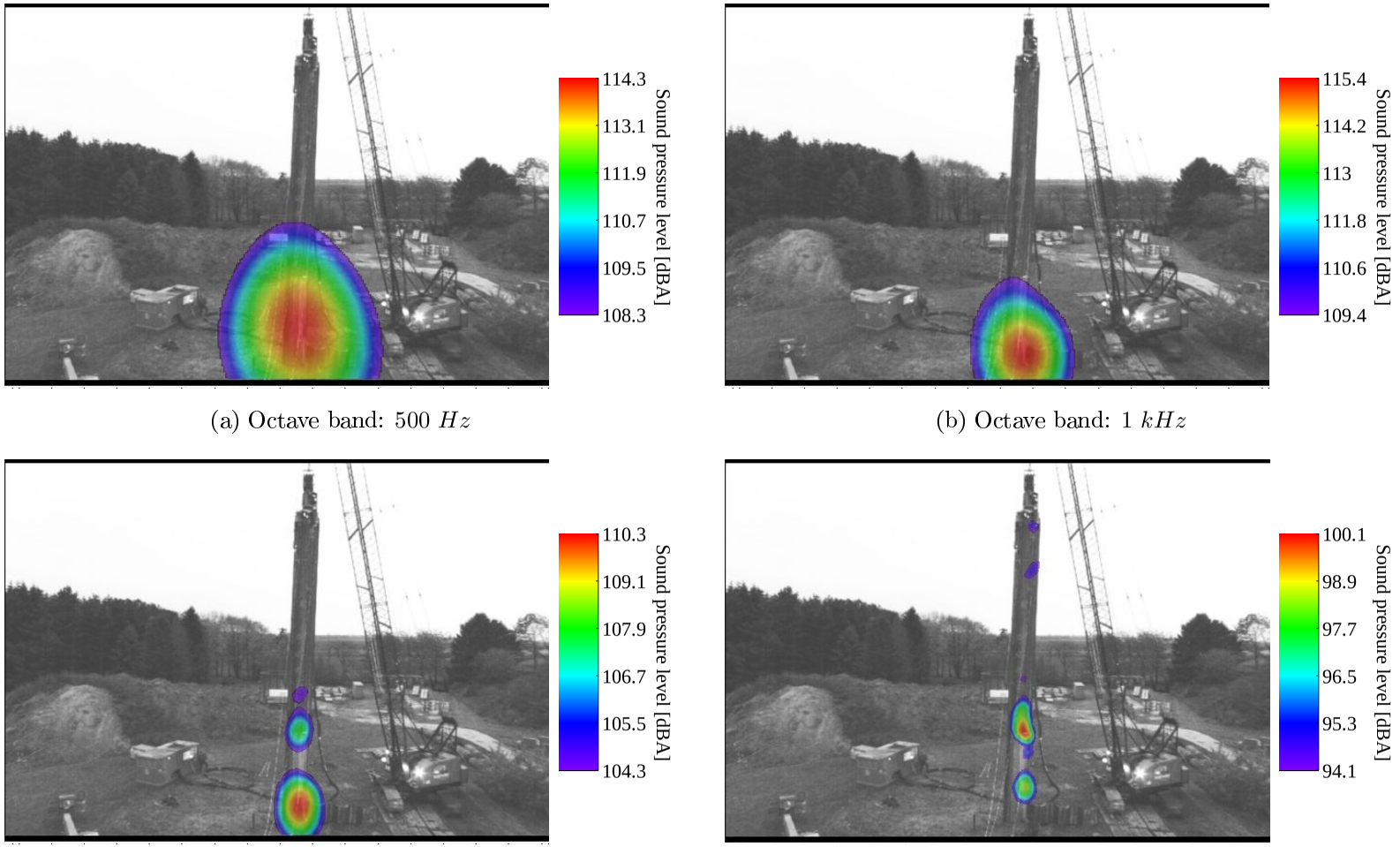

(a) Octave band: 500 Hz

(b) Octave band: 1 kHz

(c) Octave band: 2 kHz

(d) Octave band: 4 kHz

Figure 3.14.: Beamforming showing the connection with the wall (height: 1 m above the ground) as the main sound source for a quiet sheet pile (during experiment 45)

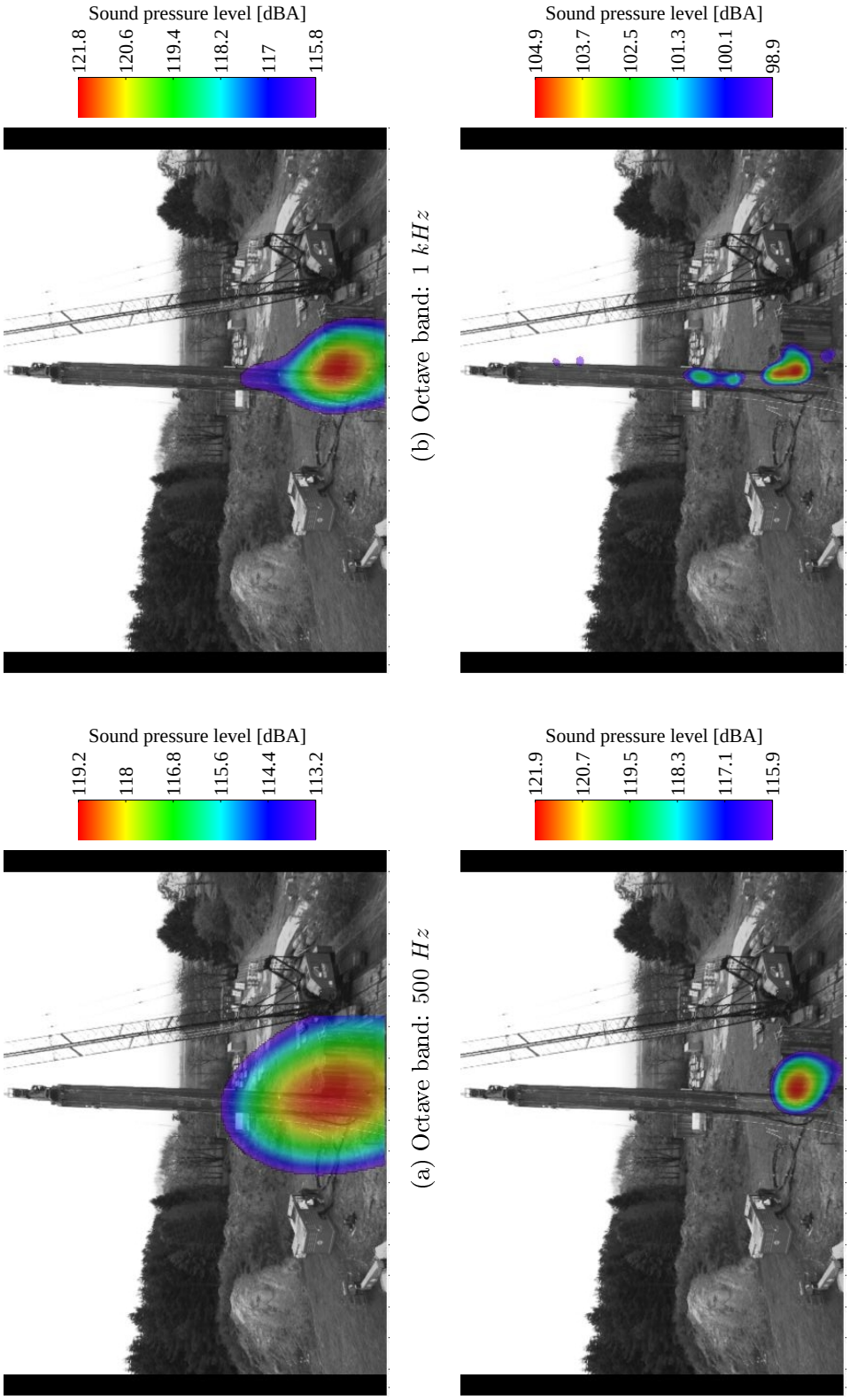

(a) Octave band: 500 Hz

(b) Octave band: 1 kHz

(c) Octave band: 2 kHz

(d) Octave band: 4 kHz

Figure 3.15.: Beamforming showing the connection with the wall (height: 3 m above the ground) as the main sound source for a quiet sheet pile (during experiment 46)

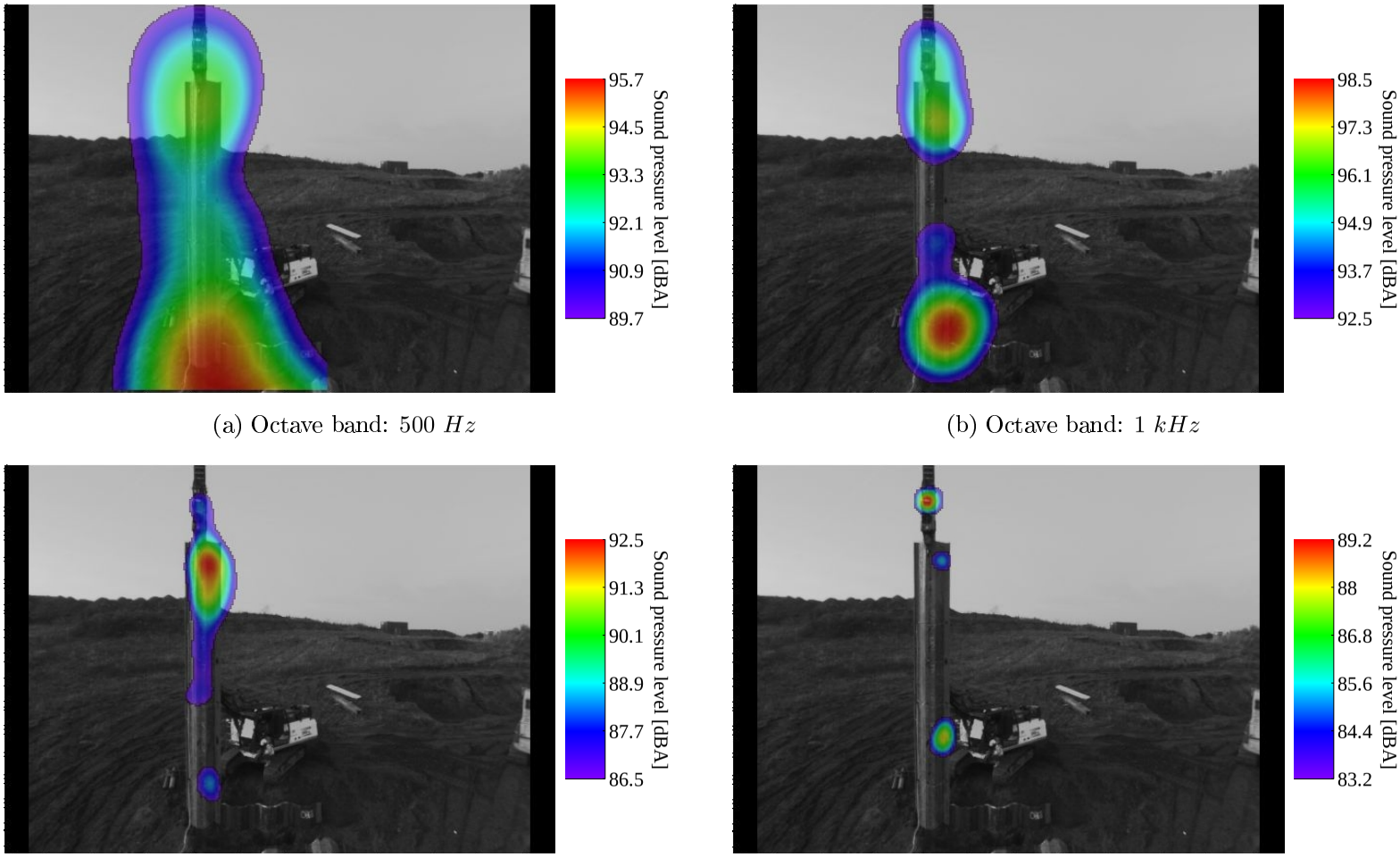

(a) Octave band: 500 Hz

(b) Octave band: 1 kHz

(c) Octave band: 2 kHz

(d) Octave band: 4 kHz

Figure 3.16.: Beamforming showing the connection with the wall (height: 1 m above the ground) as one source among others (the vibrator, the clamping device, etc.) for a quiet sheet pile (during experiment `194`)

3.5. Conclusion

A system localizing sound sources, called beamforming, is presented and used to show that the sound comes mainly from the sheet pile, and not from the construction site. It helps also to detect experiments that are not valid, e.g. experiments with a paramount influence of the security system.

Furthermore, it gives evidence and proofs that the impacts are the origin of the noise for the key parameters discovered in section 2.3.3:

The spacing between the welds of the common interlock: When comparing sound maps obtained by beamforming with thermographic pictures, it is shown that sound is produced concurrently with heat, which is a clue of impacts. Furthermore, such heat and noise sources are located around the middle of the space between two successive welds: this confirms the mechanism described in section 2.3.3 to explain the impact generation.

The height of the wall above the ground: The beamforming results show the connection with a wall as the main sound source for some experiments of the first session. For the second experiment session, the connection is one of the sound sources only; indeed, section 2.3.3 has already shown no clear influence of the wall for this session.

For a sheet pile with a welded common interlock, the noise is generated by the interaction with the vibrator, the clamping device or the soil at its ends. Indeed, the sheet pile does not generate impacts. Improvements on the design of the vibrator and the clamping device should be able to decrease this noise. Schwartz *et al.* [26] gives tips for such improvements on the vibrator.

Part II.

Mechanics

Chapter 4.

Mechanics of the vibratory pile driving

As shown in previous chapters, the impacts in the common interlock of double sheet piles are the most important sound sources. Vibro-impacts are nonlinear phenomena that cannot be studied with the *Finite Element Method* (FEM). Indeed, a lot of behaviours can be obtained, depending of the configuration [43, 44, 45] (periodic, pseudo-periodic, chaotic, etc.) and a transient simulation should use a tiny time step to study the impacts in the interlock as well as a fine geometrical description of the clutches. However, if the exact behaviour of impacts cannot be obtained, their occurrence can be detected by comparing the motion of the interlocked clutches with the available clearance. This is done in chapter 5. But such simulations need a model for the forces at the ends of the sheet pile. Such model is developed in this chapter.

The displacement only is interesting when studying impact occurrences. The analysis of acceleration measurements shows that the study of the vibrator frequency is relevant and that the other harmonics are negligible. So a linear model is used. The parameters of the model (the forces at the ends of the sheet pile) can be calculated by fitting the simulations with acceleration measurements. It is the aim of this chapter.

The configuration of the acceleration measurements is described in section 4.1. The applied post-processing is explained in section 4.2: it yields the main features of the measured signals. The parameters of the simulation are calculated in section 4.3 and discussed in section 4.4.

4.1. Configuration of the acceleration measurements

Accelerometers were placed on the sheet pile

- with different locations: right, left, centre or centre left; see figure 4.1;
- at several heights: 3, 4.5, 6, 7.5, 9, 10 or 17.5 m above the sheet pile toe;
- with several orientations: vertical, lateral or front, as displayed in figure 4.1).

Tables A.1 and A.2 in section A.3 list the accelerometer locations.

Two types of supports were used during the experiments (see figure 4.2), depending on the wished orientations for the measurements (3D or only vertical). 3D devices (in figure 4.3a) were constrained by two nuts in a threaded hole made in the sheet pile. 1D devices (in figure 4.3b) were fixed with cyanoacrylate glue. Such supports influenced the measured signal. For example, figure 4.4 shows the spectra of accelerations measured with the two support types for close accelerometers in the vertical direction: the 3D device introduces an increase in the range of $1 - 2\ kHz$, while the 1D device does not show this behaviour.

The acceleration signals were sampled like the microphones measurements, even if their frequency range is not so high (2 or 10 kHz for the upper limit, depending on the type [46, 47, 48]). The part of the spectrum higher than this limit is thus never considered.

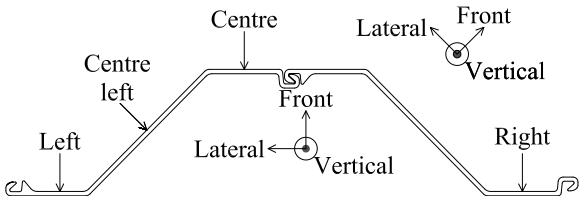

(a) First experiment session

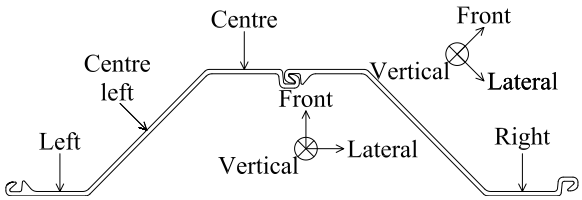

(b) Second experiment session

Figure 4.1.: Locations and orientations of the accelerometer on the sheet pile section

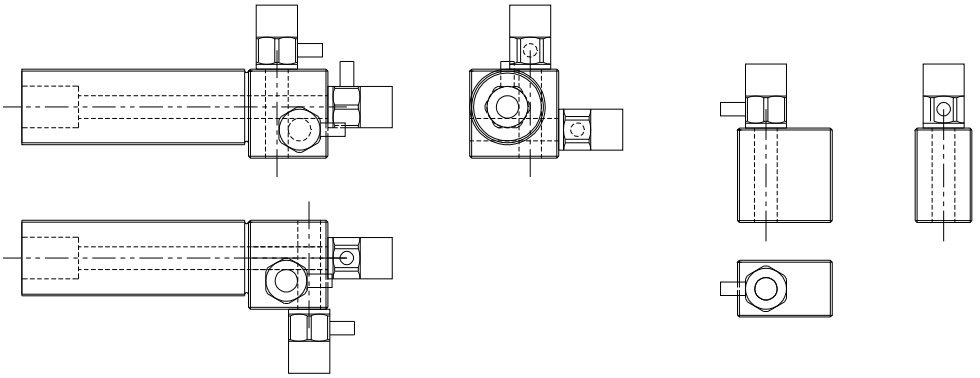

(a) Support for 3D measurements (b) Support for 1D measurements

Figure 4.2.: Supports used during the measurements

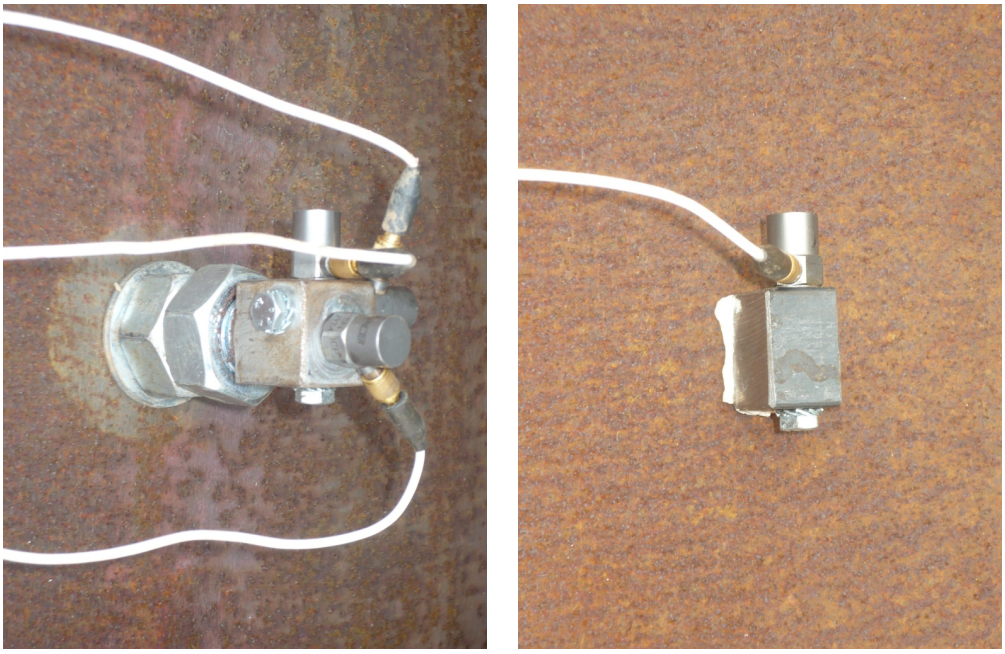

(a) Support for 3D measurements (b) Support for 1D measurements

Figure 4.3.: Supports used during the measurements

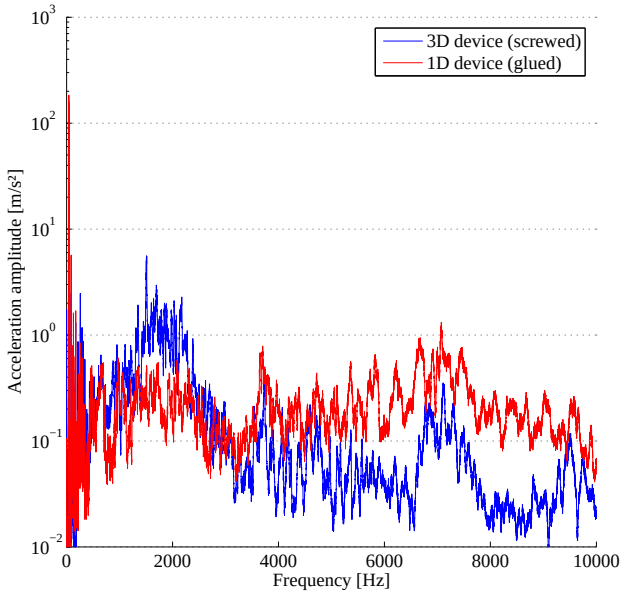

Figure 4.4.: Spectra obtained with 3D and 1D supports showing an increase in the range of $1-2\ kHz$ for the screwed 3D device (during experiment `193`)

4.2. Postprocessing

This process is applied on a signal with duration of more than 30 s: the longer the time signal, the finer the frequency resolution. The possible transitory effects are ignored.

As already mentioned, acceleration measurements are intended to be used with *Finite Element* (FE) simulation in order to reproduce the sheet pile motion in section 4.3. The displacement only is relevant when studying impact occurrences. The second harmonic of the vibrator frequency contributes typically only to 10 % of the displacement, and the next harmonics are negligible. So only the vibrator frequency is studied and the non-linear effects generating higher harmonics are neglected.

The determination of the parameters of the signals (frequency, amplitude and phase) is made in two steps. First the signal is filtered to select the first harmonic; then the signal parameters are determined; several methods are considered and discussed.

4.2.1. Filtering of the signal

Due to the leakage phenomenon occurring when applying the *Fast Fourier Transform* (FFT), to the variation of the vibrator frequency during the experiment and to the measurement noise, a sharp peak cannot be obtained when calculating the spectrum of an acceleration signal. The dispersion of the frequencies decreases when the analysed duration increases, but the effect remains (see figure 4.6a).
To decrease this effect, a window is usually applied before the FFT; it decreases the influence of the extremities of the signal. But the use of a window decreases the amplitude of the measurement and this should be avoided in this application. So a Tukey window (also called "cosine-tapered window") [49] is used: indeed, it does not change the amplitude of a part of the signal. Its equation is:

$$w(n) = \begin{cases} 1 & 0 \leq |n| \leq \beta\frac{N}{2} \\ \frac{1}{2}\left[1 + \cos\left[\pi \frac{n - \beta\frac{N}{2}}{2(1-\beta)\frac{N}{2}}\right]\right] & \beta \leq |n| \leq \frac{N}{2} \end{cases} \tag{4.1}$$

where $w(n)$ = Tukey window function,
β = fraction of the window with a unit amplitude, and
N = number of samples studied.

The parameter β is chosen equal to 0.5, which means that 50 % of the time signal amplitude is modified (see figure 4.5). The comparison with the spectrum obtained without windowing can be made between figures 4.6a and 4.6b.
So the peak region is selected (the red curve in figure 4.6b) and used in order to obtain the time signal. Only the range whose amplitude was not modified by the window before the FFT is used further: it is the centred half of the signal.

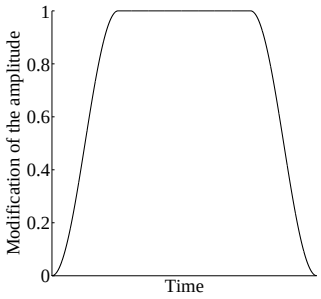

Figure 4.5.: Tukey window ($\beta = 0.5$) used for the post-processing of the acceleration measurements

The acceleration signal seems to be poorly approximated (see figure 4.7a). But when considering the displacement signal, the approximation is satisfactory (see figure 4.7b); indeed, it was already mentioned that the second harmonic of the vibrator frequency contributes typically only to 10 % of the displacement.

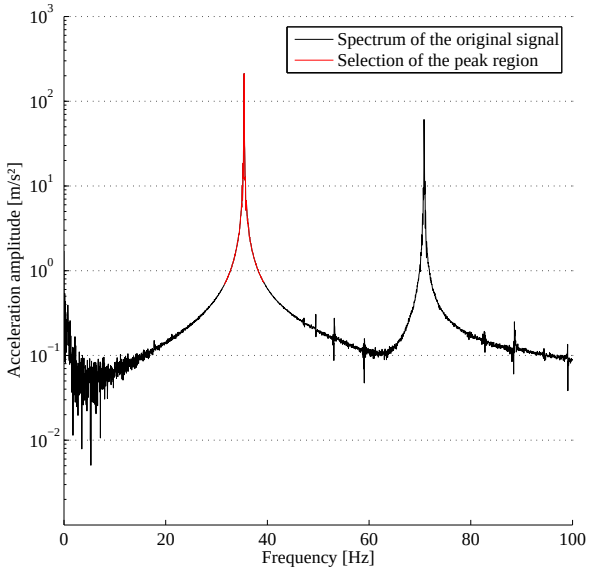

(a) FFT applied without windowing

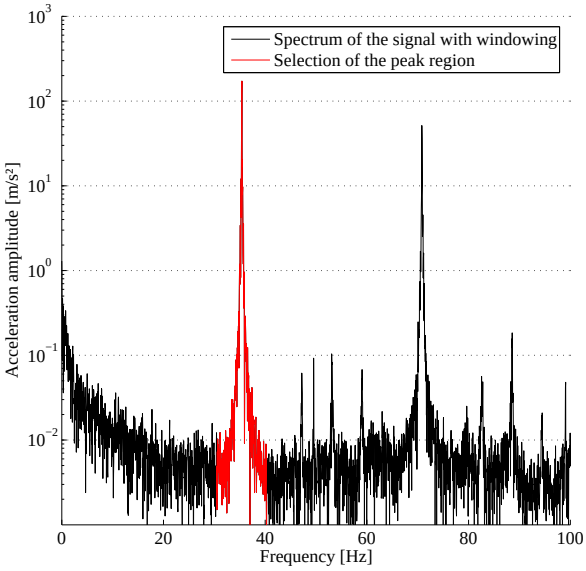

(b) FFT applied with a Tukey window

Figure 4.6.: Typical spectrum obtained during a vibrodriving (analysis made for duration of 25.6 s)

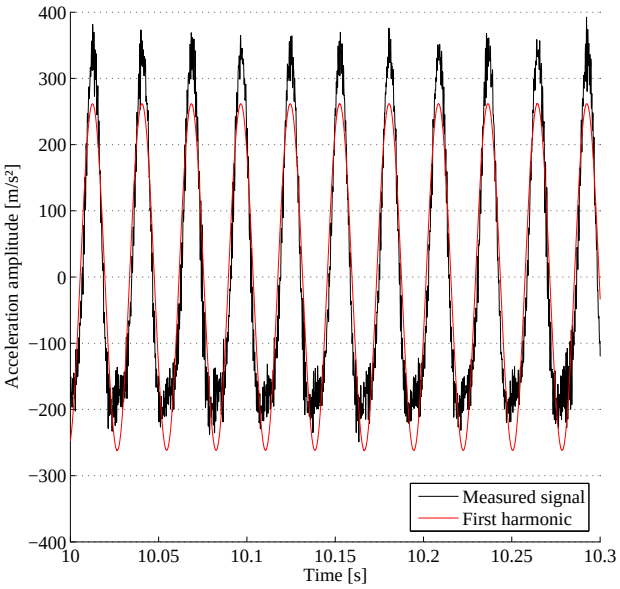

(a) Comparison of the accelerations

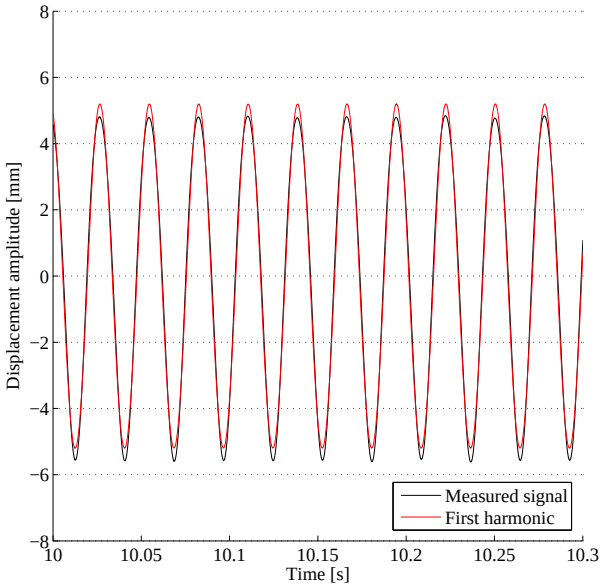

(b) Comparison of the displacements

Figure 4.7.: Comparison between the time signal and its first harmonic

4.2.2. Calculation of the parameters of the signal

Three parameters are needed to describe a harmonic signal $y(t)$. For example, the frequency, the amplitude and the phase:

$$y(t) = A\sin(2\pi f\ t + \theta) \qquad \text{for an analog signal} \tag{4.2}$$

$$y_i[t_i] = A\sin(2\pi f\ t_i + \theta) \qquad \text{for a numerical signal} \tag{4.3}$$

where y, y_i = harmonic signal,
A = amplitude of the harmonic signal,
t, t_i = time $[s]$,
f = frequency of the harmonic signal $[Hz]$, and
θ = phase $[rad]$.

Determination of the amplitude A of a harmonic signal

The amplitude can be calculated either by summing the power spectrum or by multiplying the root mean square of the time signal by $\sqrt{2}$. The second method has been used:

$$A = \sqrt{\frac{2}{T}\int_0^T y(t)^2\ dt} \qquad \text{for an analog signal } y(t) \tag{4.4}$$

$$A = \sqrt{\frac{2}{N}\sum_{i=1}^{N} y_i^2} \qquad \text{for a numerical signal } y_i[t_i] \tag{4.5}$$

where T = duration of the time signal $[s]$, and
N = number of samples of the numerical time signal.

Approximation of the frequency f of a harmonic signal

For a first step, an approximation of the frequency f only is needed. It is obtained by counting the number of roots of the time signal, i.e. by counting the number k of sign changes of the signal.

$$f \approx \frac{k}{2\ T} \tag{4.6}$$

where k = number of sign changes of the signal.

The next step will refine this approximation.

Determination of the frequency f and the phase θ of a harmonic signal

If this phase difference is obtained directly with a FFT between two acceleration signals, the obtained results are not accurate: in figure 4.8 for example, the phase difference varies within a range of 5 ° around the frequency of the signal (35.7 Hz in this case). They should be determined in a more accurate way. Moreover, the approximation of equation 4.6 can be not precise enough.

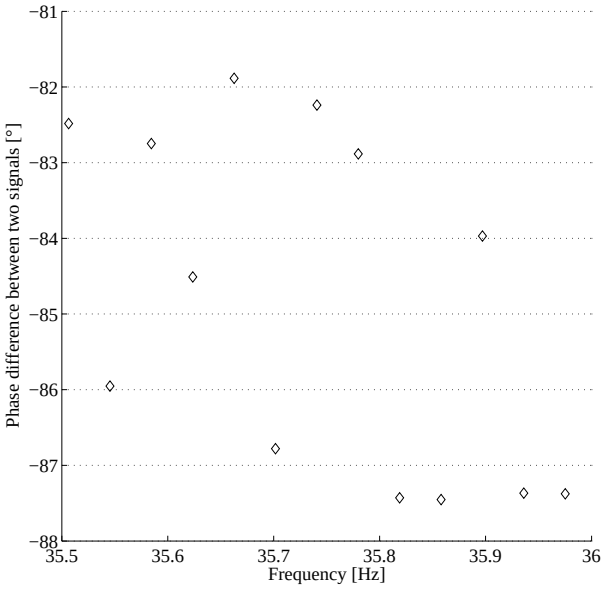

Figure 4.8.: Phase difference between two signals around the vibrator frequency (35.7 Hz)

The absolute phase θ and the exact frequency f can be calculated by performing a regression analysis (method of least squares). The sum of squared residuals $SSR(f, \theta)$ is minimized:

$$SSR(f,\theta) = \sum_{i=1}^{N} (y_i - A\sin(2\pi f\ t_i + \theta))^2 \tag{4.7}$$

The minimum appears when the gradients are set to zero:

$$\begin{aligned} \frac{\partial SSR}{\partial f} &= -2A\sum_{i=1}^{N}[(y_i - A\sin(2\pi f\ t_i + \theta))\cos(2\pi f\ t_i + \theta)\ 2\pi\ t_i] = 0 \\ \frac{\partial SSR}{\partial \theta} &= -2A\sum_{i=1}^{N}[(y_i - A\sin(2\pi f\ t_i + \theta))\cos(2\pi f\ t_i + \theta)] = 0 \end{aligned}$$

$$\begin{aligned}\sum_{i=1}^{N}[y_i\cos(2\pi f\ t_i+\theta)\ t_i]-\frac{A}{2}\sum_{i=1}^{N}[\sin(4\pi f\ t_i+2\ \theta))\ t_i] &= 0\\ \sum_{i=1}^{N}[y_i\cos(2\pi f\ t_i+\theta)]-\frac{A}{2}\sum_{i=1}^{N}[\sin(4\pi f\ t_i+2\ \theta)] &= 0\end{aligned}$$

$$\begin{aligned}\sum_{i=1}^{N}[y_i\cos(2\pi f\ t_i)\ t_i]\cos\theta-\sum_{i=1}^{N}[y_i\sin(2\pi f\ t_i)\ t_i]\sin\theta-\\ -\frac{A}{2}\sum_{i=1}^{N}[\sin(4\pi f\ t_i)\ t_i]\cos(2\theta)-\frac{A}{2}\sum_{i=1}^{N}[\cos(4\pi f\ t_i)\ t_i]\sin(2\theta) &= 0\\ \sum_{i=1}^{N}[y_i\cos(2\pi f\ t_i)]\cos\theta-\sum_{i=1}^{N}[y_i\sin(2\pi f\ t_i)]\sin\theta-\\ -\frac{A}{2}\sum_{i=1}^{N}[\sin(4\pi f\ t_i)]\cos(2\theta)-\frac{A}{2}\sum_{i=1}^{N}[\cos(4\pi f\ t_i)]\sin(2\theta) &= 0\end{aligned}$$

Some constant are defined:

$$\begin{aligned}c_1&=\sum_{i=1}^{N}[y_i\cos(2\pi f\ t_i)\ t_i] & c_2&=-\sum_{i=1}^{N}[y_i\sin(2\pi f\ t_i)\ t_i]\\ c_3&=-\frac{A}{2}\sum_{i=1}^{N}[\sin(4\pi f\ t_i)\ t_i] & c_4&=-\frac{A}{2}\sum_{i=1}^{N}[\cos(4\pi f\ t_i)\ t_i]\\ c_5&=\sum_{i=1}^{N}[y_i\cos(2\pi f\ t_i)] & c_6&=-\sum_{i=1}^{N}[y_i\sin(2\pi f\ t_i)]\\ c_7&=-\frac{A}{2}\sum_{i=1}^{N}[\sin(4\pi f\ t_i)] & c_8&=-\frac{A}{2}\sum_{i=1}^{N}[\cos(4\pi f\ t_i)]\end{aligned}$$

$$t=\tan\frac{\theta}{2}$$

The system gives:

$$\begin{aligned}c_1\ \frac{1-t^2}{1+t^2}+c_2\ \frac{2t}{1+t^2}+c_3\ \frac{1-(\frac{2t}{1-t^2})^2}{1+(\frac{2t}{1-t^2})^2}+c_4\ \frac{2(\frac{2t}{1-t^2})}{1+(\frac{2t}{1-t^2})^2} &= 0\\ c_5\ \frac{1-t^2}{1+t^2}+c_6\ \frac{2t}{1+t^2}+c_7\ \frac{1-(\frac{2t}{1-t^2})^2}{1+(\frac{2t}{1-t^2})^2}+c_8\ \frac{2(\frac{2t}{1-t^2})}{1+(\frac{2t}{1-t^2})^2} &= 0\end{aligned}$$

$$\begin{aligned} t^3\ [(2\ c_2 - 4\ c_4)\ (-c_5 + c_7) - (2\ c_6 - 4\ c_8)\ (-c_1 + c_3)] + \\ +t^2\ [(-6\ c_3)\ (-c_5 + c_7) + 6\ c_7\ (-c_1 + c_3)] + \\ +t\ [(2\ c_2 + 4\ c_4)\ (-c_5 + c_7) - (2\ c_6 + 4\ c_8)\ (-c_1 + c_3) + \\ +(c_5 + c_7)] + (c_1 + c_3)\ (-c_5 + c_7) - (-c_1 + c_3) \ = \ 0 \end{aligned} \tag{4.8}$$

A cubic equation with real coefficients has always at least one real root. So for one chosen frequency, equation 4.8 gives one or several phase angles. The solution is the phase angle giving the minimum of SSR.
So the solutions of the curve fitting can be found by searching the minimum of equation 4.7 with the help of equation 4.8 in order to accelerate the convergence.

Determination of the phase difference between two harmonic signals with the same frequency

A hammer modal testing calculates the phase of the *Frequency Transfer Function* (FTF) between two signals (the signal of the force sensor of the hammer and the signal of one accelerometer) by performing the FFT between the two signals[1]. The phase difference is known only in a relative way in this case.
Similarly, the phase differences between the signals are enough to characterise the forces applied to the sheet pile in FE simulations. So the phase of a signal does not need to be known in an absolute way, but only in a relative one.
Another straightforward method can yield the phase difference of two harmonic signals if they have the same frequency.

When considering two sinusoidal signals y_i and y_j with the same frequency and their phasors $\vec{y_i}$ and $\vec{y_j}$ in the complex plane (also called "phase vectors"), the sum of two phasors gives a phasor $\vec{y_s}$, whose amplitude $||\vec{y_s}||$ (computed by equation 4.9) is linked with the phase difference $\theta - \vartheta$ between the phasors $\vec{y_i}$ and $\vec{y_j}$:

$$\vec{y_i} = \begin{bmatrix} A_i\ \cos(2\pi f\ t + \theta_i) \\ A_i\ \sin(2\pi f\ t + \theta_i) \\ 0 \end{bmatrix}\ (i = 1, 2) \quad \vec{y_s} = \sum_{i=1}^{2} \vec{y_i} = \begin{bmatrix} \sum_{i=1}^{2} A_i\ \cos(2\pi f\ t + \theta_i) \\ \sum_{i=1}^{2} A_i\ \sin(2\pi f\ t + \theta_i) \\ 0 \end{bmatrix} \tag{4.9}$$

$$||\vec{y_s}||^2 = ||\vec{y_1}||^2 + ||\vec{y_2}||^2 + 2\ ||\vec{y_1}||\ ||\vec{y_2}||\ \cos(\theta_2 - \theta_1) \tag{4.10}$$

$$A_s^2 = A_1^2 + A_2^2 + 2\ A_1\ A_2\ \cos(\theta_2 - \theta_1) \tag{4.11}$$

where $\vec{y_i}$ = phasor of harmonic signal i,
A_i = amplitude of signal i,
f = frequency of the signals $[Hz]$,
θ_i = phase of signal i $[rad]$,
A_s = amplitude of sum of the signals i.

[1] In fact, the process uses auto- and cross-spectra of the signal.

As the sign of the phase difference is not known, this equation gives two solutions. Another relationship is obtained by using the definition of the cross product between two vectors. The calculation of the cross product phasor $\vec{y_x}$ gives:

$$\vec{y_x} = \vec{y_1} \times \vec{y_2} = \begin{bmatrix} 0 \\ 0 \\ A_1 \ A_2 \ \sin(\theta_2 - \theta_1) \end{bmatrix} \tag{4.12}$$

$$||\vec{y_x}|| = ||\vec{y_1}|| \ ||\vec{y_2}|| \ |\sin(\theta_2 - \theta_1)| \tag{4.13}$$

$$A_x = A_1 \ A_2 \ |\sin(\theta_2 - \theta_1)| \tag{4.14}$$

where $\vec{y_x}$ = cross product phasor of the phasors 1 and 2, and
A_x = amplitude of cross product phasor of the phasors 1 and 2.

So the sine and the cosine of the phase difference (and thus the angle itself) can be obtained with some manipulations on the signals.

As the process gives relative values of the angle, one signal must be used as a reference to calculate this phase difference with the other ones. To increase the precision, this process is applied between all the signals (for n signals, $n.(n-1)/2$ times) and then an average of the differences is made[2].

4.2.3. Results

An example of results of the phase differences is given in table 4.1. The largest accelerations are obtained for vertical measurements. These have also little phase differences. Their amplitudes seem to depend mainly on the height where the measurement is performed. Indeed, most of the mechanical energy of the vibrator is transferred by traction-compression waves of the bar and their wavelength is much higher than the length of the sheet pile. The speed of a longitudinal wave in a beam c_{LII} and in a plate c_{LI} are respectively [50]:

$$c_{LII} = \sqrt{\frac{E}{\rho}} \qquad c_{LI} = \sqrt{\frac{E}{\rho \ (1 - \nu^2)}} \tag{4.15}$$

where c_{LII} = speed of longitudinal waves in a beam $[m/s]$,
E = Young's modulus $[N/m^2]$,
ρ = density $[kg/m^3]$,
c_{LI} = speed of longitudinal waves in a plate $[m/s]$, and
ν = Poisson's ratio.

[2]This average must be made carefully: 360 ° must be added in some cases.

The longitudinal wavelength of a sheet pile at the vibrator frequency (43.2 Hz in this case) is thus included between:

$$\lambda_{LII} = \frac{c_{LII}}{f} = 119.7\ m \quad \leq \lambda \leq \quad \lambda_{LI} = \frac{c_{LI}}{f} = 125.5\ m \tag{4.16}$$

where λ_{LII} = wavelength of longitudinal waves in a beam $[m]$, and
λ_{LI} = wavelength of longitudinal waves in a plate $[m]$.

Thus amplitudes and phases are relevant when considering vertical accelerations, as the sheet pile is stiff for the traction-compression behaviour.
It is shown in section 5.1.1 that the sheet pile is flexible for the bending and coupled bending-torsion behaviours, i.e. their wavelengths have sizes similar or smaller than the sheet pile length. Amplitudes and phases of horizontal accelerations should not be used: the phase differences are too large with vertical accelerations. Such differences cannot be obtained with a proportional damping in the system: only non-linearities or non-proportional damping can explain such a behaviour.

Accelerometer location	Acceleration amplitude $[m/s^2]$	Displacement amplitude $[mm]$	Phase angle [°]
vertical at 3 m (right)	177	2.4	1.7
lateral at 3 m (right)	9	0.1	-61.8
front at 3 m (right)	171	2.3	-103.6
vertical at 3 m (centre)	197	2.7	0.1
lateral at 3 m (centre)	80	1.1	-109.4
front at 3 m (centre)	45	0.6	0.4
vertical at 6 m (right)	186	2.5	6.2
lateral at 6 m (right)	56	0.8	-0.1
front at 6 m (right)	33	0.4	143.2
vertical at 6 m (centre)	187	2.5	-4.3
lateral at 6 m (centre)	36	0.5	10.9
front at 6 m (centre)	64	0.9	-4.1
vertical at 9 m (right)	169	2.3	-1.9
lateral at 9 m (right)	87	1.2	70.9
front at 9 m (right)	37	0.5	-48.0
vertical at 9 m (centre)	177	2.4	2.3
front at 9 m (centre)	151	2.1	77.8

Table 4.1.: Results of the calculation of the parameters of the acceleration signals for one experiment

4.3. Building of an excitation model

FE simulations and the results of the measurements obtained in section 4.2 can be combined to characterise the forces applied to the sheet pile. Before making the calculation itself (in section 4.3.3), hypotheses are made and detailed here below.

4.3.1. The predominance of the vertical motions

It was shown in the example of table 4.1 that the vertical motions have larger amplitudes than horizontal motions. The vertical accelerations are not expected to have been modified during the experiments by unwanted phenomena.

The horizontal accelerations could have been modified in several ways. Such vertical amplitudes can influence the value of smaller horizontal motions because of the transverse sensitivity of the accelerometers (up to 5 % [46, 47, 48]). Moreover, the operating displacement shapes generated by bending and coupled bending-torsion waves can be expected sensible to the boundary conditions of the system.

So the measurements are not able to give clear information about lateral motions, and the vertical forces can be calculated by using vertical accelerations.

4.3.2. Linearity of the model

In order to simplify the simulations, the system is supposed to behave linearly. This hypothesis allows studying the frequency of the vibrator only and not the other harmonics (as it was shown that their contributions were negligible). The following approximations are made:

- The woodblocks and the conveyor belts are assumed to behave linearly and they can then be modelled as a spring-damper system.
- It was observed that the amplitude of the second harmonic of the displacement contributes up to 10 % of the motion. The non-linear phenomena yielding such behaviour are thus ignored.
- This study is applied to welded sheet piles only, as the impacts occurring in the common interlock of partly welded sheet piles are a non-linear behaviour.
- No dynamic buckling is assumed to occur during the vibratory pile driving.

This last assumption can be verified by approximating the sheet pile as a bi-articulated beam [51] (as in figure 4.9). The test is made for a double Z sheet pile with a length of 20 m, the sheet pile of the experiments that is the most likely to show a buckling behaviour: the longest length and the weakest second moment

of area. A periodic axial force $P(t)$ is applied with a frequency lower than the fundamental frequency of the longitudinal vibration:

$$P(t) = P_0 + P_1 \ \cos(\omega \ t) \tag{4.17}$$

where $P(t)$ = force applied at one extremity of the beam $[N]$,
P_0 = offset component of force P $[N]$ (the static load),
P_1 = amplitude of the harmonic component of force P $[N]$ (the variable load),
ω = angular frequency $[rad]$, and
t = time $[s]$.

For a static buckling, the Euler load P_E is defined as follows:

$$P_E = \frac{\pi^2}{L^2} E \ I \tag{4.18}$$

where P_E = Euler load $[N]$,
L = beam length $[m]$,
E = Young's modulus $[N/m^2]$, and
I = weakest second moment of area of the beam $[m^4]$.

The instability regions can occur around angular frequencies $\omega_{k,n}$:

$$\omega_{k,n} = \frac{2 \ \pi \ k}{n \ L} \sqrt{\frac{1}{\rho \ A}(k^2 \ P_E - P_0)} \quad \text{for} \quad n \in \mathbb{N}_0 \tag{4.19}$$

where $\omega_{k,n}$ = instability angular frequency $[rad/s]$,
k = number of nodes of the buckling shape minus 1,
ρ = density $[kg/m^3]$, and
A = section area $[m^2]$.

To characterise the instability region around angular frequencies $\omega_{k,n}$, the dynamic buckling parameter α is introduced:

$$\alpha = \frac{P_1}{k^2 \ P_E - P_0} \tag{4.20}$$

where α = dynamic buckling parameter.

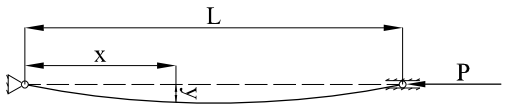

Figure 4.9.: Model for the study of the dynamic buckling

For small α, the boundaries of the instability regions $\omega(\alpha)$ are approximated as follows:

$$\Omega(\alpha) = \omega_{1,k}\ (1 \mp \tfrac{\alpha}{4} - \tfrac{\alpha^2}{64} + \ldots) \quad \text{for} \quad n = 1 \tag{4.21}$$

$$\Omega(\alpha) = \omega_{2,k}\ (1 \mp \tfrac{5\ \alpha^2}{24} + \ldots) \quad \text{for} \quad n = 2 \tag{4.22}$$

where $\Omega(\alpha)$ = boundary of the instability region $[rad/s]$.

A combination of n and k can always be found to correspond to a chosen frequency. But the buckling can occur in this case only if the damping is weak enough, i.e.:

$$\alpha \geq \alpha_0 = 2\ \sqrt[n]{\xi} \quad \text{for} \quad n \in \mathbb{N}_0 \tag{4.23}$$

where α_0 = minimum value of the dynamic buckling parameter, and
ξ = damping ratio of the beam.

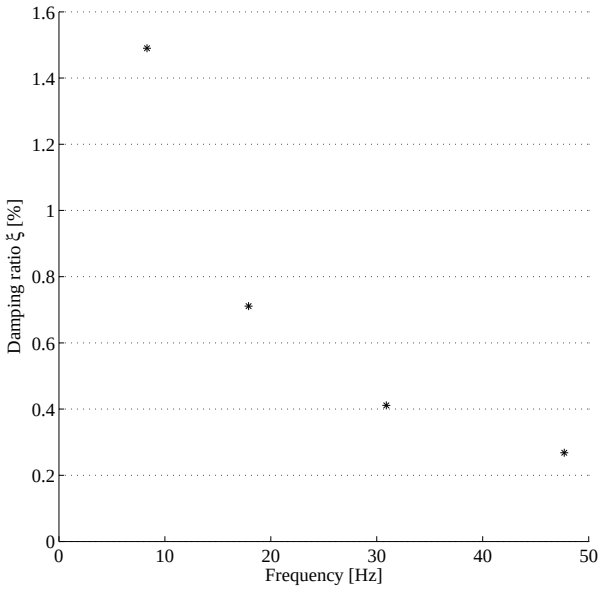

Figure 4.10.: Damping ratio measured by a hammer modal analysis for a single Z sheet pile of 6 m

Figure 4.10 shows the damping ratio obtained by a hammer modal analysis for a single Z sheet pile of 6 m (it is assumed similar for a double Z sheet pile of 20 m): the damping ratio of the modes was always higher than 2.5×10^{-3} for the studied frequency range. It should probably be larger for larger excitation forces and the results of the hammer modal analysis should underestimate the damping during a vibratory pile driving.

Figures 4.11 and 4.12 shows the results for the two experiment sessions: no buckling was expected in the two situations.

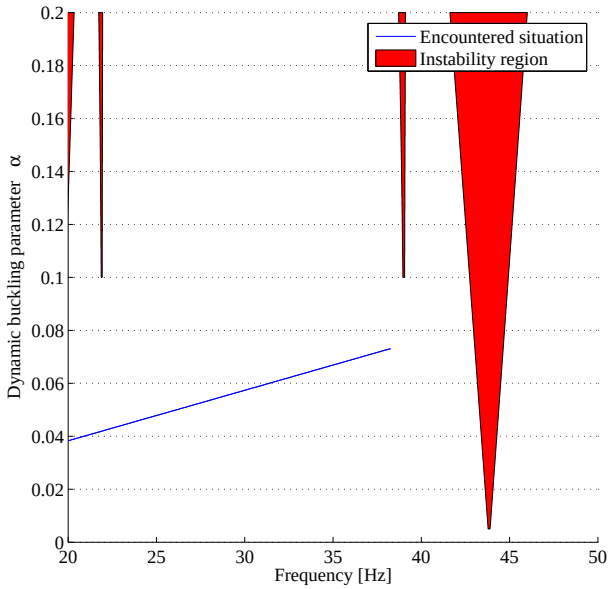

Figure 4.11.: Buckling occurrence of the first experiment session

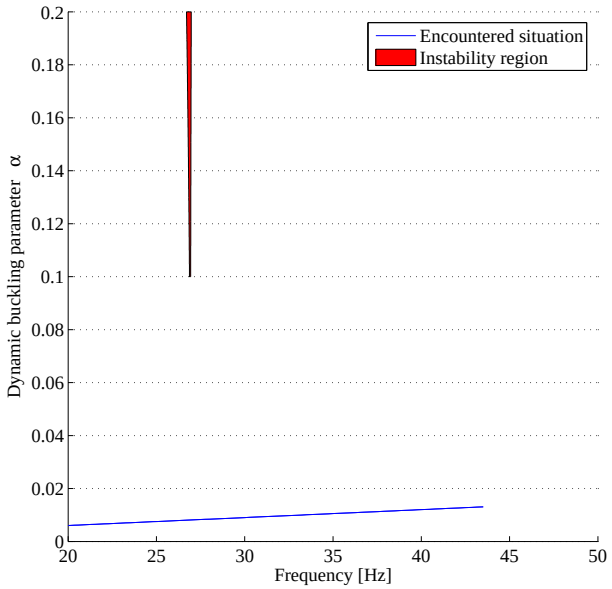

Figure 4.12.: Buckling occurrence of the second experiment session

4.3.3. Model of the forces

Two types of forces are applied to the sheet pile: the forces generated by the vibrator and the reaction forces of the system of woodblocks and conveyor belts described in section 1.2.

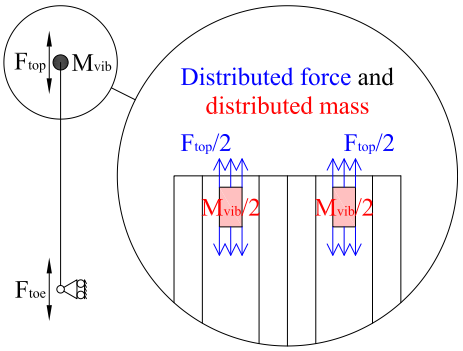

Figure 4.13.: Model of the sheet pile toe and the vibrator

The vibrator is modelled as follows (see figure 4.13):

- The vibrating mass M_{vib} of the vibrator is applied at the location of the clamping system. It is equally distributed over the surface of this clamping system.
- A vertical force F_{top} is generated by the vibrator; it is also applied directly over the surface of this clamping system. This force is chosen as having a unit resultant and is equally distributed over the surfaces of the sheet pile in contact with the clamping system.

The action of the soil and the conveyor belt on the toe section F_{toe} is modelled as a force applied like a pressure with a unit resultant. The woodblocks and the conveyor belt themselves are not modelled, but only their interaction with the sheet pile. This separation is justified in appendix C: such a separation changes the modal description but not the motions for a linear system, i.e. the same displacements are calculated in both cases.
It was observed on site that the section printed a mark on the conveyor belts: the horizontal motions of the toe section were damped by the conveyor belt and the soil. In the model, it is assumed that no horizontal motions of the toe section can occur, i.e. roller supports are applied to the nodes or the toe section.

An example of these two models can be seen in figure 4.14. One parameter is not known to simulate such models: the damping. The processing is thus made for several damping values, and the least square process should show the best fitting.

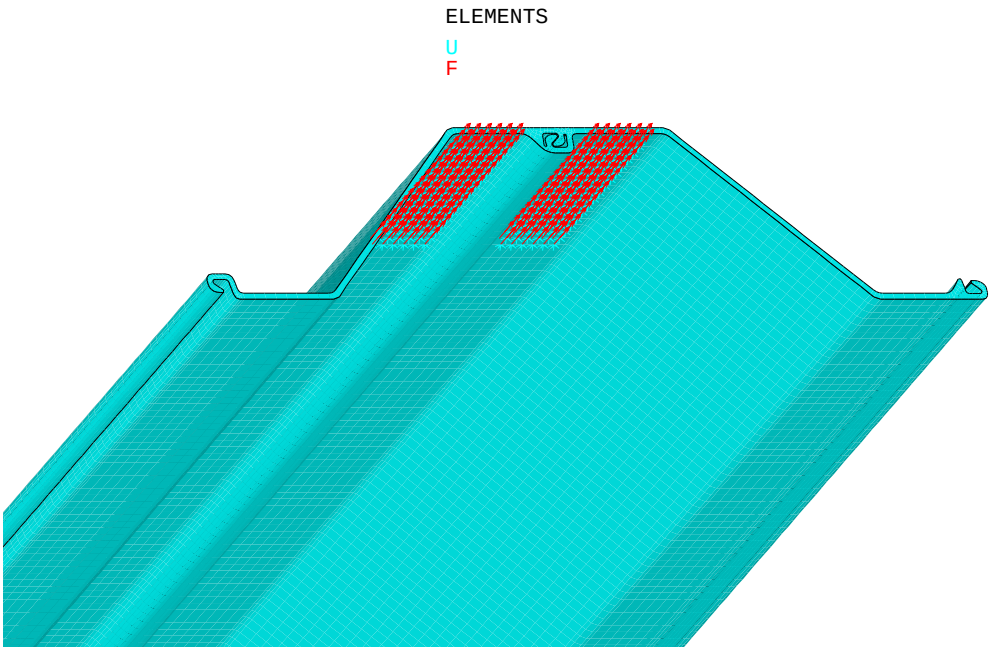

(a) Top boundary condition

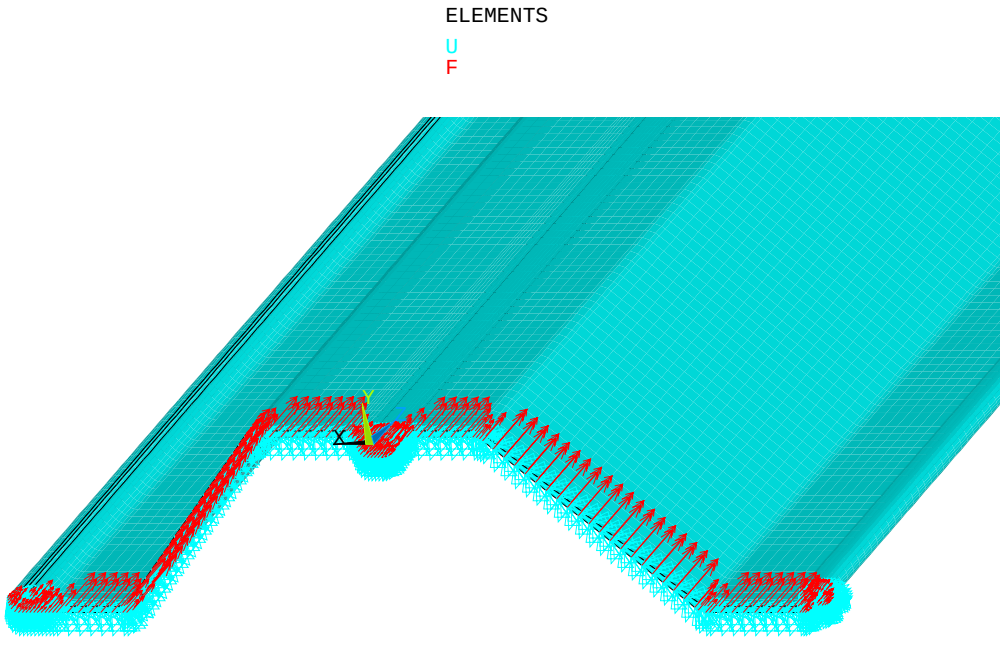

(b) Toe boundary condition

Figure 4.14.: Example of boundary conditions

4.3.4. Regression analysis

For one damping value, two simulations are computed: with a unit force at the top or a unit force at the toe. As the simulations are linear, the complex displacements calculated at the location of the measurements can be put together to generate a complex matrix $\mathbf{D}$:

$$\mathbf{D}\,\mathbf{f} = \mathbf{d} \tag{4.24}$$

where $\mathbf{D}$ = displacement matrix,
$\mathbf{f}$ = force vector, and
$\mathbf{d}$ = displacement vector.

The post-processing of section 4.2 yields the amplitude and phase of the displacement measurements, which can be used to build the complex vector $\mathbf{d}$. The system of equation 4.24 is overdetermined (five accelerations at least are available to determine two forces). The least square solution is obtained as follows:

$$\mathbf{f} = (\mathbf{D}^*\,\mathbf{D})^{-1}\,\mathbf{D}^*\,\mathbf{d} \tag{4.25}$$

This process is performed for all the calculated damping values. The residue r is the norm of the difference between the calculated displacement and the measurements:

$$r = \|\mathbf{d} - \mathbf{D}\,\mathbf{f}\| \tag{4.26}$$

where r = residue of the least square solution.

4.4. Results and comparisons

The accelerations measurements of each experiment with a welded sheet pile are thus used to calibrate each model. Some results of the models can be compared between the different experiments:

- the amplitude of the top forces,
- the amplitude of the toe forces, and
- the residues of the least square fitting.

The quality of the results can be assessed in three ways:

- The top force amplitude can be compared with the force theoretically generated by the vibrator.
- The toe force can be modelled as a spring-damper system and its features can be inspected.
- If a proportional damping is assumed, the minimum of the residue should determine the damping constant of the system.

4.4.1. Accordance of the toe amplitude

The amplitude of the toe force is shown in figure 4.18.

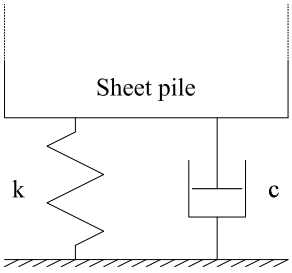

Figure 4.15.: Spring-damper system

The system of woodblocks and conveyor belts can be modelled as a spring-damper system (see figure 4.15). Such a model was earlier used as a model of the soil [52]. Furthermore, the composition of a conveyor belt (steel cables and rubber) reminds this model.
In order to determine the spring stiffness k and the damping constant c, the average displacement d_{toe} of the nodes of the toe section of the FE model is calculated and used with the toe force f_{toe}:

$$f_{toe} = -k\ d_{toe} - i\ \omega\ c\ d_{toe} \tag{4.27}$$

where f_{toe} = resultant force applied at the toe section (obtained by FEM simulations and the regression analysis) $[N]$,
k = spring stiffness $[N/m]$,
d_{toe} = average displacement of the section (obtained by FEM simulations and the regression analysis) $[m]$, and
c = damping constant of the damper.

The results displayed in figures 4.16 and 4.17 show that the damping constant is negative for a lot of experiments, inducing a power source at the bottom of the sheet pile. This observation is not consistent with the hypothesis of a passive behaviour of the woodblocks and the conveyor belt.

It is deduced that the toe force is poorly approximated. Another regression analysis can thus be performed by setting the toe force to 0 kN and by fitting the top force only. A comparison is made in the next sections.

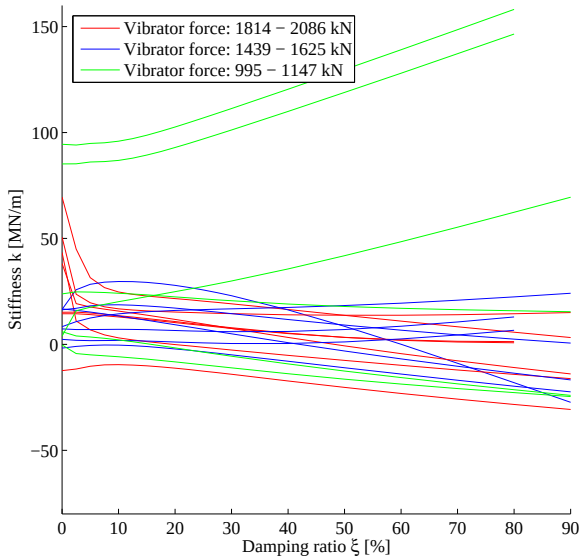

(a) Spring stiffness

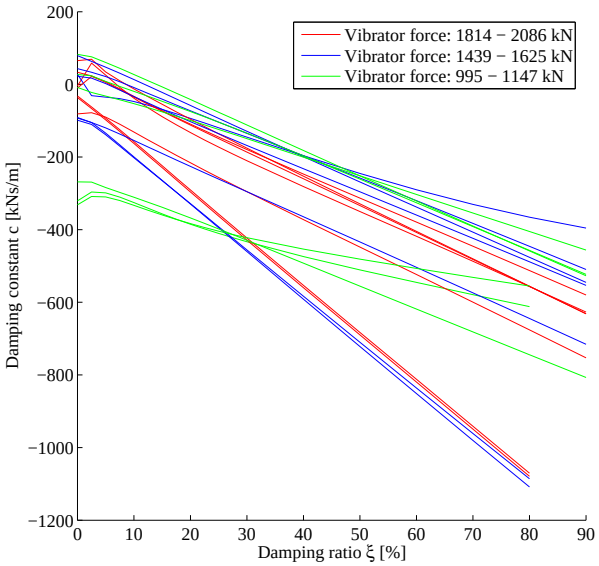

(b) Damping constant of the damper

Figure 4.16.: Spring-damper properties during the first experiment session

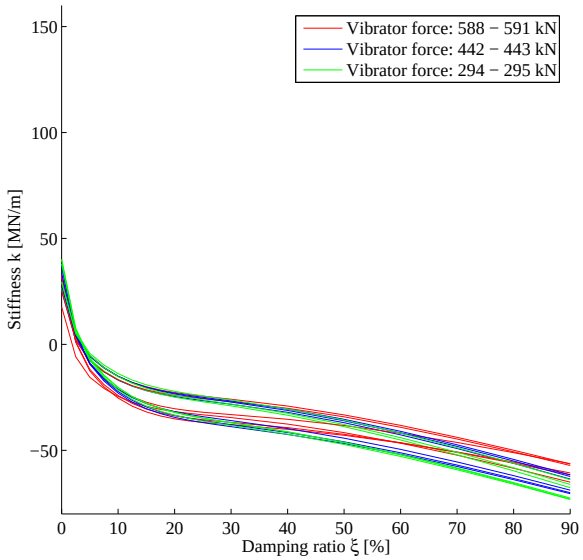

(a) Spring stiffness

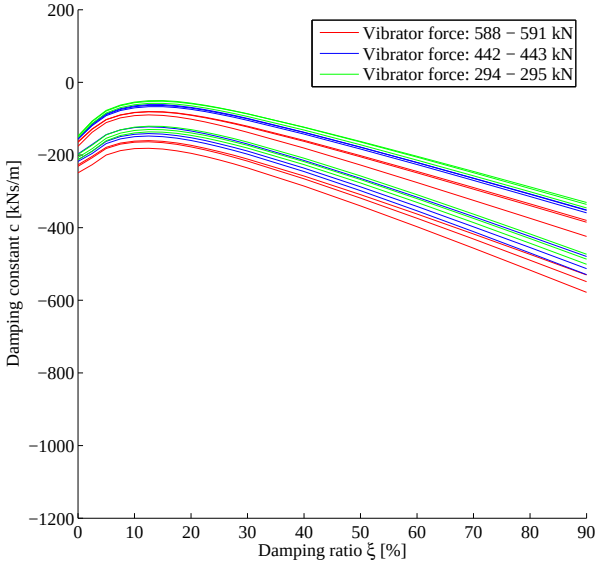

(b) Damping constant of the damper

Figure 4.17.: Spring-damper properties during the second experiment session

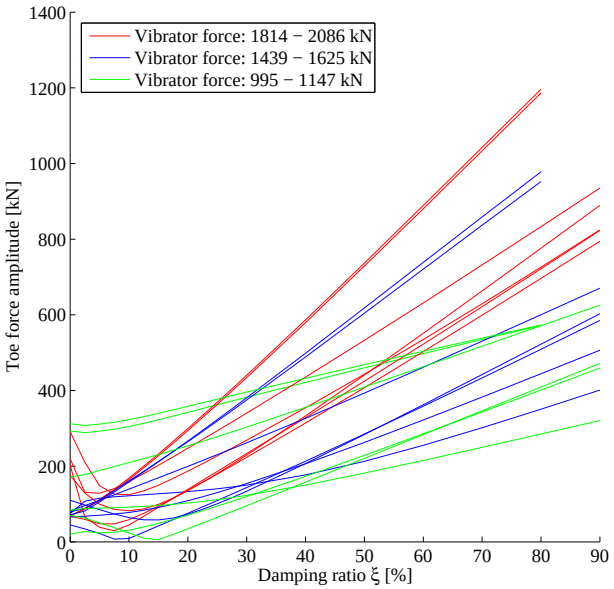

(a) First experiment session

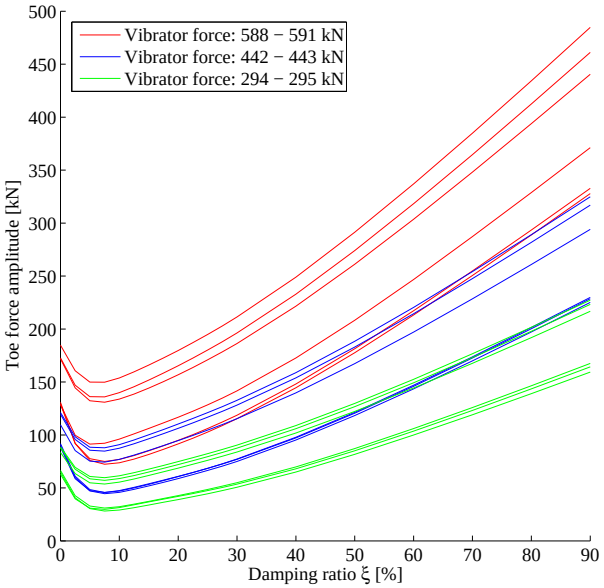

(b) Second experiment session

Figure 4.18.: Toe force amplitudes

4.4.2. Accordance of the top amplitude

Two vibrator parameters govern the vibrator force (see equation 2.5): the frequency and the eccentric moment. Six combinations of the parameters were used and yield different vibrator forces:

- between 2086 and 2103 kN (one experiment had a level around 1814 kN);
- between 1599 and 1625 kN (two experiments had a level around 1439 and 1466 kN);
- between 1115 and 1147 kN (one experiment had a level around 995 kN);
- between 588 and 591 kN;
- between 442 and 443 kN;
- between 294 and 295 kN.

When comparing these values with results in figures 4.19 and 4.20, it can be seen that the forces are underestimated for the first experiment session and overestimated for the second one.
A larger dispersion of the results is observed for the first experiment session; indeed, less vertical accelerations were measured (five measurements for the first experiment session and ten for the second one) and more various configurations were processed:

For the first session: experiments `1`, `2`, `3`, `31`, `32`, `37`, `38`, `39`, `42`, `43`, `44`, `47`, `48`, `49`, `50`, `54` (2×), `55` (2×), and `56` (2×);

For the second session: experiments `193` (2×), `196` (2×), `199` (2×).

The fitting without any toe forces yields almost constant top forces. So the processing is robust in this case against damping variations.

4.4.3. Residue

The residues of the regression analysis calculated by equation 4.26 are shown in figures 4.21 and 4.22.

The minimum of the residue occurs in a wide range: mainly between 0 and 20 %. This method cannot be used to identify the damping.
It can also be seen that the residue is not much larger in the model without any toe forces, especially for the second experiment session: a maximum increase of 18 % is observed for this session. So neglecting the toe forces in the model has not a large impact on the regression analysis and it is an acceptable approximation; indeed, the top forces is the main energy input in the system.

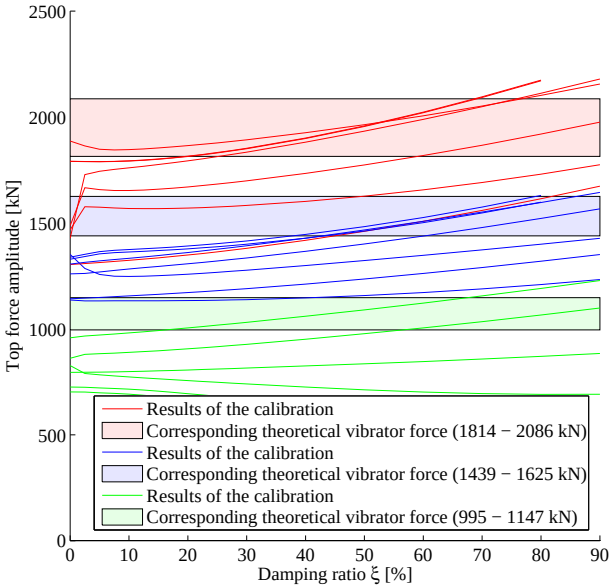

(a) With a toe force in the model

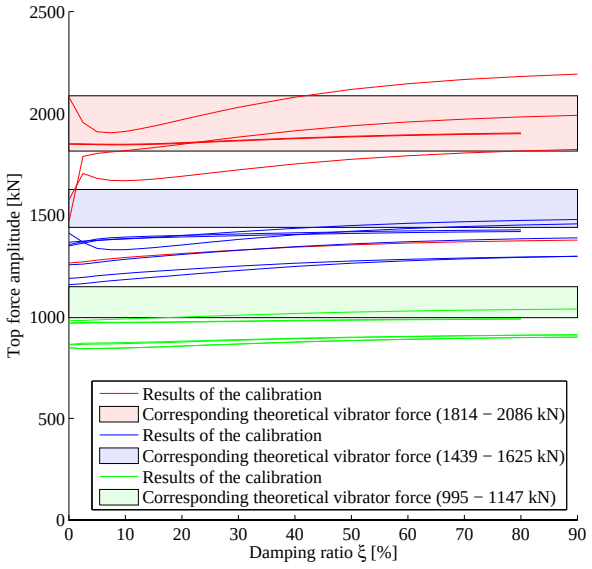

(b) Without any toe force in the model

Figure 4.19.: Top force amplitudes of the first experiment session

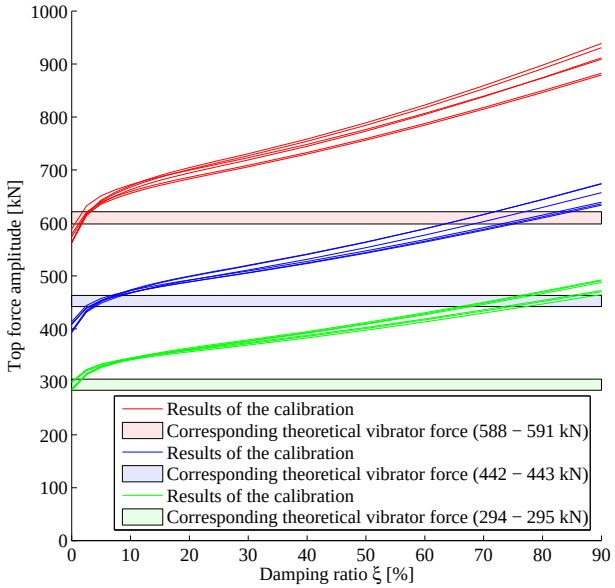

(a) With a toe force in the model

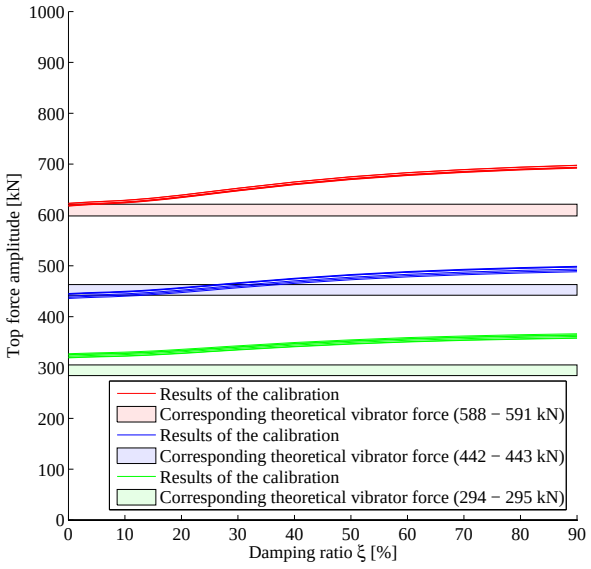

(b) Without any toe force in the model

Figure 4.20.: Top force amplitudes of the second experiment session

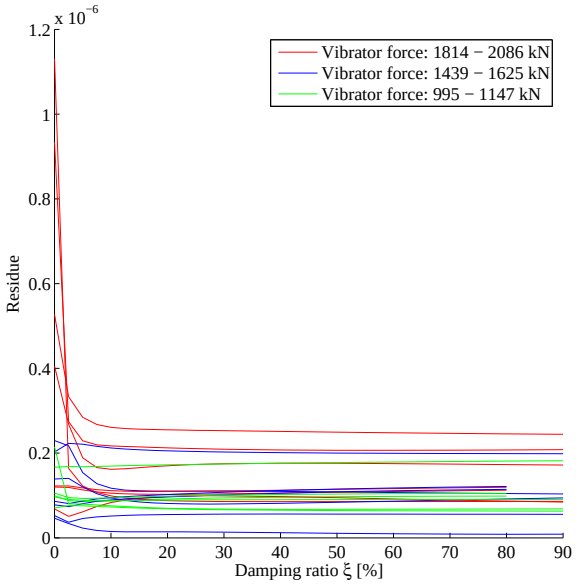

(a) With a toe force in the model

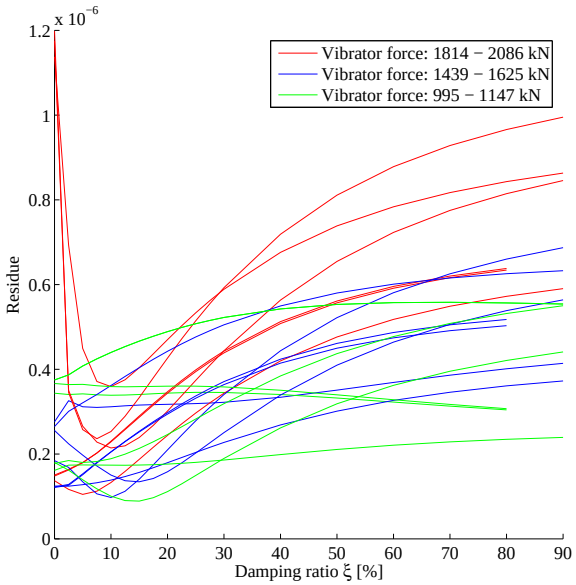

(b) Without any toe force in the model

Figure 4.21.: Residues of the first experiment session

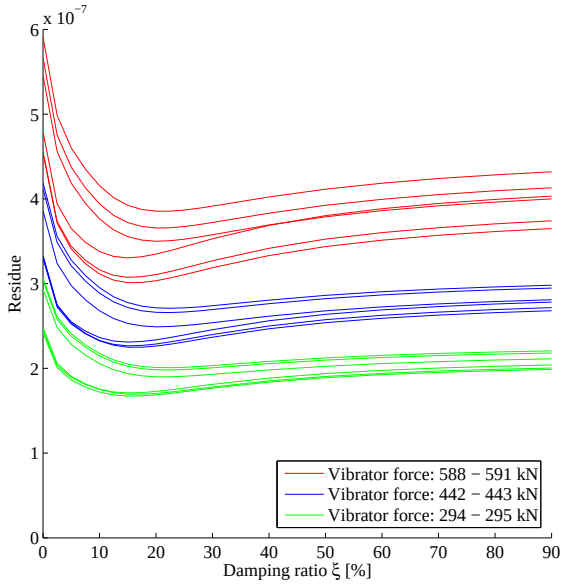

(a) With a toe force in the model

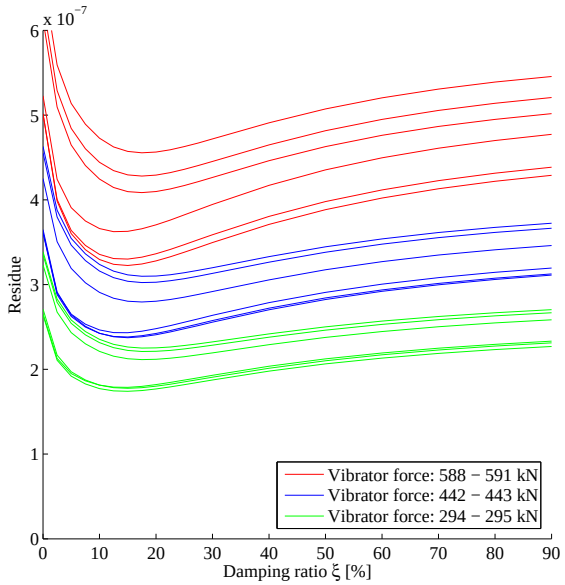

(b) Without any toe force in the model

Figure 4.22.: Residues of the second experiment session

4.5. Conclusion

By carefully post-processing measurements of vertical accelerations, the vertical forces applied at the ends of the sheet pile can be calculated. But this process gives only satisfying results for the top forces (the largest ones).

No information is obtained from the measurements of horizontal acceleration: large phase differences are observed between the horizontal and the vertical accelerations, when close or opposite phase differences are waited for a linear system. The observed large phase differences would imply a large damping or strong nonlinearities in the system. Moreover, horizontal motions are more sensitive to the shape variation and the location of the measurement. So finding precise correspondences for these horizontal motions between the calculation and the measurements is a challenge that cannot be achieved:

- The exact shape of the sheet pile and the exact positioning of the clamping system should be taken into account; indeed, hammer modal analyses showed that shape variations in the tolerances were important for the horizontal motions.
- The soil action on the sheet pile toe should be modelled and the possible slope of the sheet pile should be taken into account.
- The horizontal measurements could have been modified by the transverse sensitivity and the large amplitude of the vertical motions, or by the supports of the accelerometers.

Without any external horizontal force, horizontal motions of some millimetres are generated by the vertical forces in the simulations. Horizontal forces do not need to be introduced in the model to obtain horizontal motions. The reasons of such a generation are studied in section 5.1. Because of the approximations included in the model, a lot of variations should be calculated and the results should be statistically processed to deduce an average behaviour.

Chapter 5.

Simulation of the impacts

Chapter 4 showed that vertical forces of the vibrator can generate horizontal motions. But the mechanisms implied in this generation must be identified: this is made in section 5.1. These motions can induce impacts in the common interlock. By using the explanations of section 5.1, calculations are performed to estimate the probabilities of impact occurrences in section 5.2 (with the help of confidential appendix F). Several parameters are studied:

- the sheet pile type,
- the sheet pile length,
- the clamping device,
- the vibrator mass,
- the vibrator frequency,
- the damping, and
- the spacing between the welds of the common interlock.

The threshold observed in the acoustic measurements (see section 2.3.3) can be identified and related to parameters of the sheet pile. Section 5.3 studies the optimisation that can be performed on a chosen type of sheet pile. It is shown that few improvements can be reached: more improvements are obtained when working on the spacing between the welds.

5.1. Mechanisms generating horizontal motions

To know how the horizontal motions are generated, the modes of the frequency range are studied in section 5.1.1. The way used to excite these modes is investigated in section 5.1.2.

5.1.1. Characterization of the modes

When inspecting the modes given by a *Finite Element* (FE) modal analysis of a single sheet pile, two types of modes appear:

- bending modes about the two principal axes of the section (see figures 5.2a and 5.2c), and
- torsion modes around the shear centre (see figure 5.2b.

It is known that the wave implied in these modes are independent of each other if the shear centre of the section is merged with the centre of gravity of the section [39, 53], which is rather the case for a single sheet pile (as shown in figure 2.17). As modes are generated because of the interaction of waves, a deeper knowledge of these waves is needed.

Bending modes

Bending waves in a beam are represented by four field variables describing the motion and the stresses of a cross-section; for example in figure 5.1:

- the transversal velocity v_y of the section $[m/s]$,
- the angular velocity w_z about the axis perpendicular both to the axis of the beam and to the transverse displacement $[rad/s]$,
- the bending moment M_z, which acts about the same axis $[Nm]$, and
- the shear force F_y transmitted across the section $[N]$.

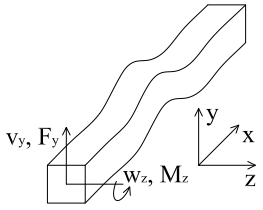

Figure 5.1.: Field variables describing the bending behaviour

Several assumptions are made:

- The sheet pile behaves like a beam.
- The rotational inertia of the section is neglected; it must be taken into account for high frequencies.
- The contour of any cross-section of the beam remains distortion free.
- Shear deformation of the thin wall in its own plan is negligible.
- The section is considered as rigid.

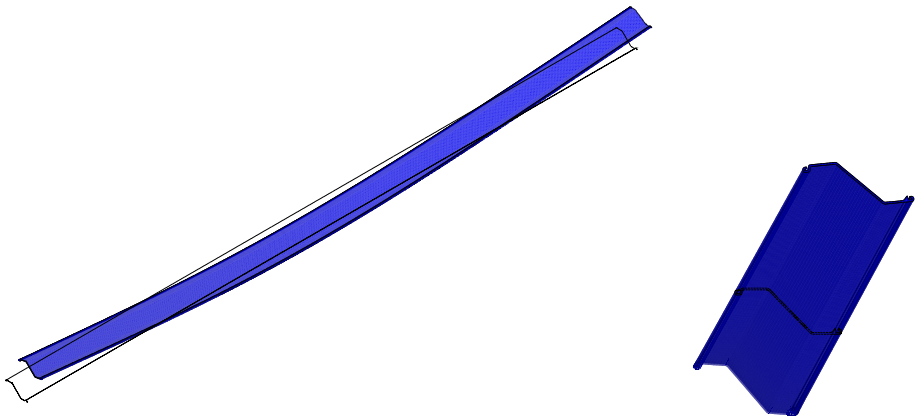

(a) First bending mode (about the weakest principal axis)

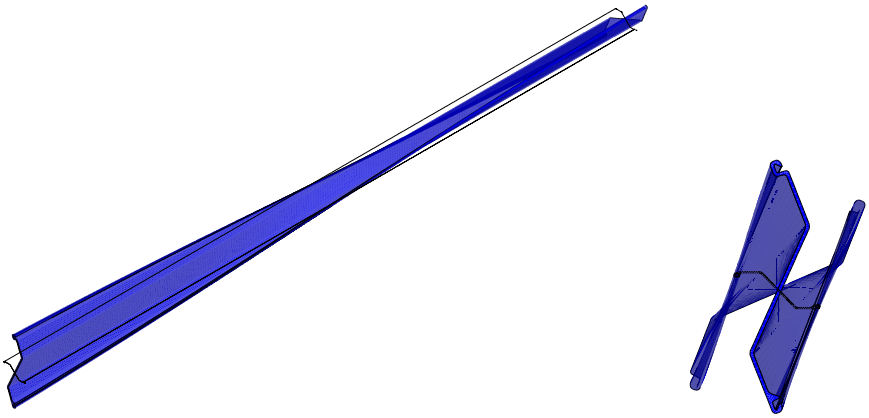

(b) First torsion mode (around the shear centre)

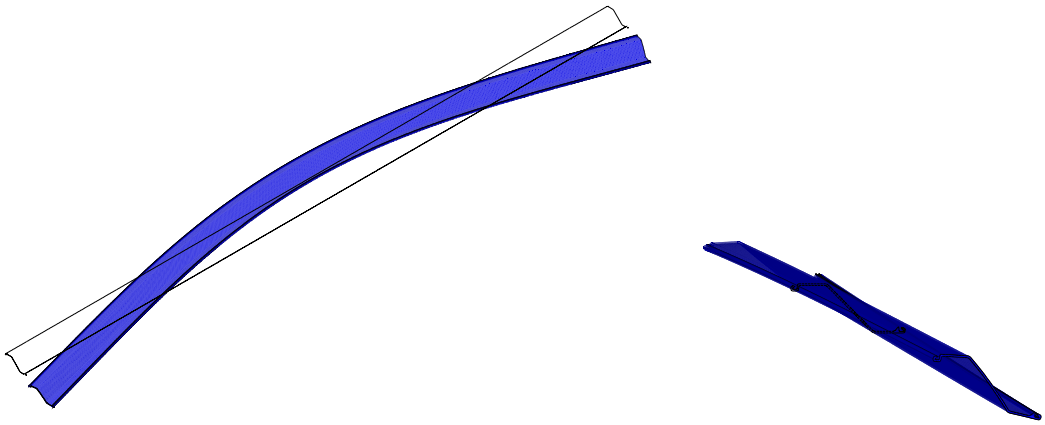

(c) First bending mode (about the strongest principal axis)

Figure 5.2.: Modes of a single sheet pile of 20 m (axonometric projection and section view)

The equation of the motion is the same for these four field variables [50]:

$$E\ I\frac{\partial^4}{\partial x^4}(v_y, w_z, M_z, F_y) + \rho\ A\frac{\partial^2}{\partial t^2}(v_y, w_z, M_z, F_y) = 0 \tag{5.1}$$

where E = Young's modulus $[N/m^2]$,
I = second moment of area $[m^4]$,
v_y = transversal velocity $[m/s]$,
w_z = angular velocity $[rad/s]$,
M_z = bending moment $[Nm]$,
F_y = shear force $[N]$,
ρ = density $[kg/m^3]$, and
A = section area $[m^2]$.

From this equation, the bending phase speed c_B and the bending wavelength λ_B (characteristics of the section) can be calculated:

$$c_B = \sqrt[4]{\frac{E\ I}{\rho\ A}}\ \sqrt{\omega} = \sqrt[4]{\frac{E\ I}{\rho\ A}}\ \sqrt{2\pi f} \tag{5.2}$$

$$\lambda_B = \frac{c_B}{f} = \sqrt[4]{\frac{E\ I}{\rho\ A}}\ \sqrt{\frac{2\pi}{f}} \tag{5.3}$$

where c_B = bending phase speed $[m/s]$,
ω = angular frequency $[rad/s]$,
f = frequency $[Hz]$, and
λ_B = bending wavelength $[m]$.

An example of variation of the bending phase velocity c_B and wavelength λ_B is available in figure 5.3.

All the assumptions made before the calculations can be verified by controlling the frequency occurrence between the analytical formula and a FE modal simulation. For a sheet pile with free boundary conditions, the bending natural frequencies $f_{B,n}$ are given as follows [50]:

$$f_{B,n} = \frac{\mu_n^2}{2\pi\ L^2}\sqrt{\frac{E\ I}{\rho\ A}} \tag{5.4}$$

where $f_{B,n}$ = bending natural frequency $[Hz]$,
n = number of nodes n of the mode shape,
μ_n = factor depending on n (see table 5.1),
L = sheet pile length $[m]$,

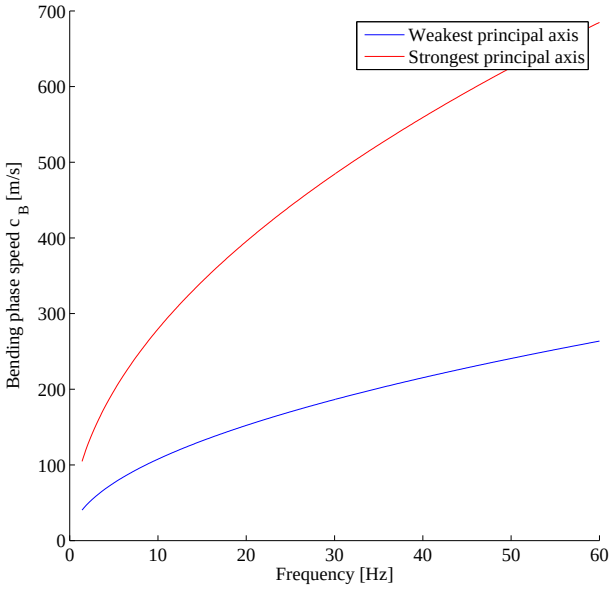

(a) Bending phase speed

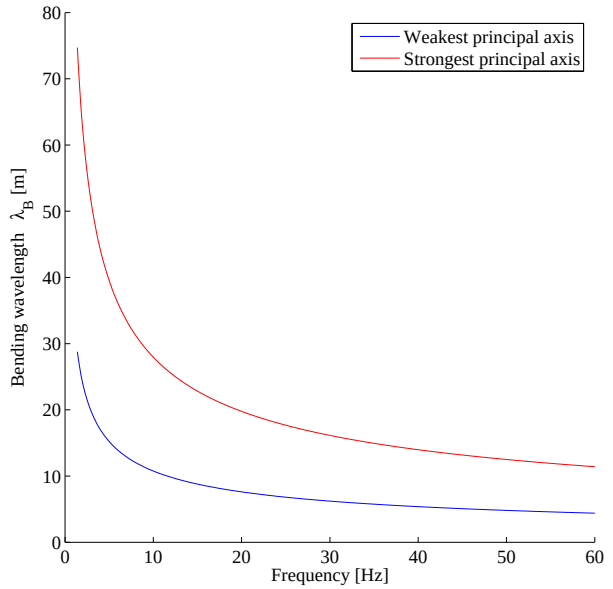

(b) Bending wavelength

Figure 5.3.: Bending wave properties for a single Z sheet pile

n	$\frac{\mu_n}{2\pi}$
2	0.753
> 2	$\approx \frac{n}{2} - \frac{1}{4}$

Table 5.1.: Factor μ_n for a beam with free boundary conditions

Figure 5.4 shows a good accordance between the FE simulation and the analytical model for the modes occurring in the low frequency range. For higher frequencies, the fitting between the simulations and the analytical model becomes bad and the model is considered not valid anymore. Indeed, the first section mode interacts with the bending behaviour and the section is assumed to remain rigid in the beam theory. This mode (occurring at 77.7 Hz in plain strain condition for the studied single sheet pile) is shown in figure 5.5.

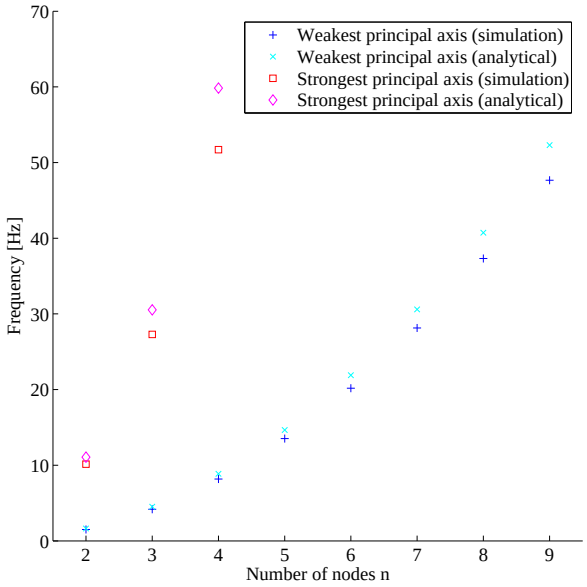

Figure 5.4.: Bending natural frequencies for a single sheet pile of 20 m

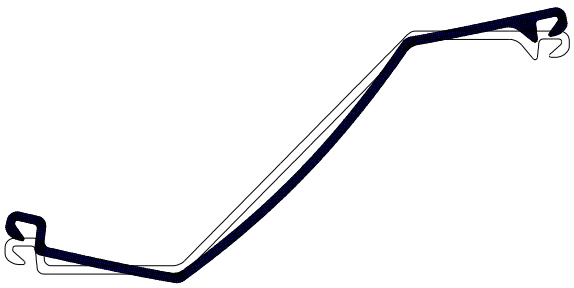

Figure 5.5.: First section mode of a single sheet pile (in plane strain condition)

Torsion modes

For open sections, a torsion theory modelling the warping phenomenon must be used, because the sections do not remain plain and this deformation interacts with the other slices of the beam.

For a Vlassov's beam with a shear centre merged with the centre of gravity of the section, the torsion is independent of the bending and the equation of the motion is given as follows [36]:

$$E\ I_\omega\ \frac{\partial^4\ w_x}{\partial x^4} - G\ K\ \frac{\partial^2\ w_x}{\partial x^2} + \rho\ I_p\ \frac{\partial^2\ w_x}{\partial t^2} - \rho\ I_\omega\ \frac{\partial^4\ w_x}{\partial x^2 \partial t^2} = 0 \tag{5.5}$$

where I_ω = warping stiffness (also called principal sectorial moment of inertia);
$I_\omega = \int_A \omega_W^2\ dA$ (ω_W is defined further in equation 5.12) $[m^6]$,
w_x = rotational velocity (see figure 5.6) $[rad/s]$,
G = shear modulus $[N/m^2]$,
K = Saint Venant's torsional stiffness $[m^4]$, and
I_p = polar moment of inertia $[m^4]$.

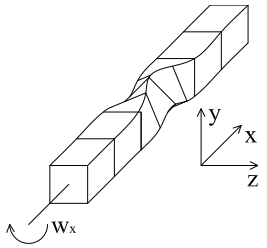

Figure 5.6.: Field variable describing the torsion behaviour

As in the case of the bending waves, the rotational inertia (the last term of equation 5.5) can be neglected in the low frequency range[1]. In this case, the torsion phase speed c_T and the wavelength λ_T is calculated as follows:

$$c_T = \omega \sqrt{\frac{2\ E\ I_\omega}{\sqrt{G^2\ K^2 + 4\ E\ I_\omega\ \rho\ I_p\ \omega^2} - G\ K}} \tag{5.6}$$

$$\lambda_T = 2\pi \sqrt{\frac{2\ E\ I_\omega}{\sqrt{G^2\ K^2 + 4\ E\ I_\omega\ \rho\ I_p\ \omega^2} - G\ K}} \tag{5.7}$$

where c_T = torsion phase speed $[m/s]$, and
λ_T = torsion wavelength $[m]$.

An example of variation of the torsion phase velocity c_T and wavelength λ_T is available in figure 5.7; the torsion properties I_ω and K are calculated with an FE simulation designed to obtain such results. The torsion properties of the section can be evaluated analytically only for simple geometries.

[1] This term limits the torsion speed to the traction-compression speed $\sqrt{\frac{E}{\rho}}$ for high frequencies.

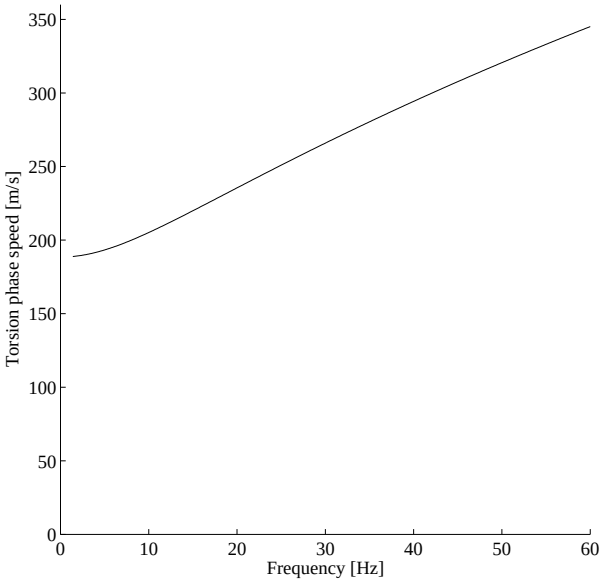

(a) Torsion phase speed

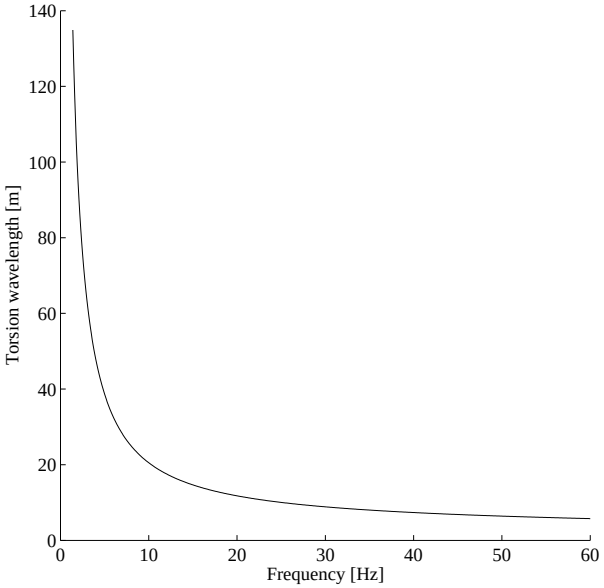

(b) Torsion wavelength

Figure 5.7.: Torsion wave properties for the studied single sheet pile

In order to verify the assumptions of the model by comparing the natural frequency occurrences between the analytical formula and the FE modal simulation, one should identify constants ν_n similar to constants μ_n of equation 5.4: they are the non-trivial solutions (given in table 5.2) of the following equation:

$$\cos(\nu)\ \cosh(o) + \frac{o^6 - \nu^6}{2\ \nu^3\ o^3}\ \sin(\nu)\ \sinh(o) = 1 \quad \text{with } o = \sqrt{\nu^2 + \frac{G\ K\ L^2}{E\ I_\omega}} \tag{5.8}$$

n	$\frac{\nu_n}{2\pi}$
1	0.497
2	0.980
3	1.451
4	1.916
5	2.384
6	2.857
7	3.336
$n \to +\infty$	$\frac{n}{2} - \frac{1}{4}$

Table 5.2.: Factor ν_n for the studied single sheet pile of 20 m with free boundary conditions

The resonance frequencies are thus:

$$f_{T,n} = \frac{1}{2\pi}\sqrt{\frac{E\ I_\omega\ \nu_n^4}{\rho\ I_p\ L^4} + \frac{G\ K\ \nu_n^2}{\rho\ I_p\ L^2}} \tag{5.9}$$

where $f_{T,n}$ = torsional natural frequency $[Hz]$, and
ν_n = factor depending on n (see table 5.2).

Figure 5.8 shows a good accordance between the FE simulation and the analytical model. Like the case of the bending, the first section mode shown in figure 5.5 could influence in the higher frequency range.

5.1.2. Excitation of the modes

As already observed in chapter 4, vertical forces can generate horizontal motions. If the stresses in the beam were generated by a uniform pressure over the section, then only a horizontal motion due to the Poisson's effect would be observed. But the vertical forces are transferred by a clamping device with a bending moment and/or a torsion bi-moment (depending on its exact position).

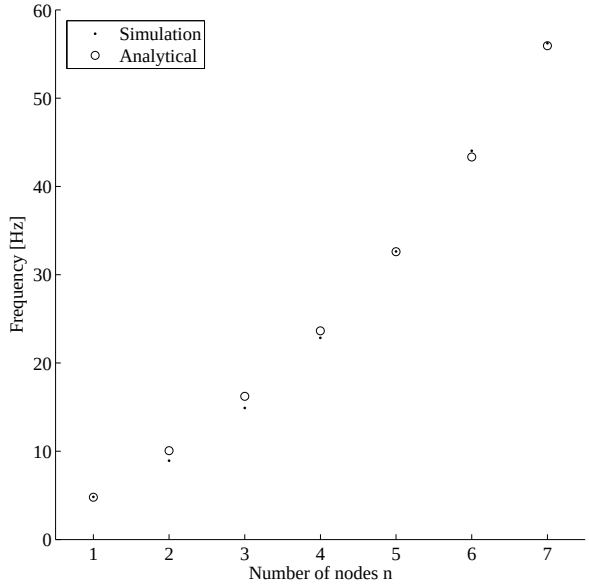

Figure 5.8.: Torsion natural frequencies for the studied single sheet pile of 20 m

A pressure distribution $p(y, z)$ can be integrated in the principal axes over the section to obtain a bending moment as follows:

$$M_y = \int_A z\ p(y,z)\ dA \quad M_z = \int_A y\ p(y,z)\ dA \tag{5.10}$$

where M_y = bending moment about principal y-axis $[Nm]$,
A = area of the section $[m^2]$,
$p(y, z)$ = pressure distribution $[Pa]$, and
M_z = bending moment about principal z-axis $[Nm]$.

A torsion bi-moment is obtained similarly:

$$B_z = \int_A \omega_W(y,z)\ p(y,z)\ dA \tag{5.11}$$

where B_z = torsion bi-moment about principal x-axis $[Nm^2]$, and
$\omega_W(y, z)$ = normalized sectorial area $[m^2]$.

The sectorial area $\omega_W(y, z)$ is a function defined over the section as follows [36]:

$$\frac{\partial^2\ \omega_W}{\partial y^2} + \frac{\partial^2\ \omega_W}{\partial z^2} = 0 \tag{5.12}$$

Boundary conditions applied to the function $\omega_W(y,z)$ can be found in the literature [36]. The function $\omega_W(y,z)$ is normalized so that:

$$\int_A \omega_W(y,z)\ dA = 0 \tag{5.13}$$

Figure 5.9 shows such a function for the section of the studied double sheet pile; this function is not exactly symmetrical with the principal axes of the section because of the clutches.

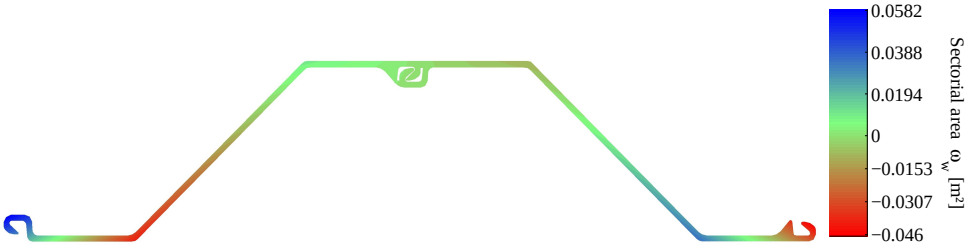

Figure 5.9.: Normalized sectorial area for the section of the studied double sheet pile

Because of this lack of symmetry, bending moments and a torsion bi-moment are generated by a double clamping device, even if its position is exactly centred. Moreover, on site, the position of the clamps and the symmetry of the section are more approximate and induce thus larger moments and bi-moments.

A bending moment or a torsion bi-moment can generate the following waves:

For a single sheet pile: As the shear centre of the section is almost merged with the centre of gravity, the bending and torsion waves can be considered as independent.

For a double sheet pile: As the shear centre is close to one principal axis of the section, coupled bending-torsion waves are generated with pure bending waves.

For a weld: The waves of the two single sheet piles are then transferred with appropriated impedance and may change their type partly. If the weld is large, the welded section can be considered as a double sheet pile.

Simulations performed in section 5.2 study the differences between a single clamping device and a double one.

5.2. Study of the occurrence of impacts

The mechanism explained in section 2.3.3 is partly proved in section 5.1: during a vibratory pile driving, the vibrator uses a frequency range that excites modes with a substantial horizontal motion. In this section, the link between the bending wavelength and the threshold spacing between the welds found in section 2.3.3 is established. Indeed, the bending wavelength influences the resonance frequency of bending local-modes.

By using linear FE simulations of harmonic motions, the maximum difference of the motions of the clutches of one interlock can be calculated. By comparing it with the average clearance defined in confidential appendix F, the probability of impacts occurrence can be assessed.

5.2.1. A theory for the local-mode resonances

Between two welds, the single sheet piles are assumed to behave like two independent beams with torsion and bending motions, inducing a local-mode behaviour. Impacts can occur if the difference of the displacement is larger than the available clearance (see confidential appendix F for a study of this clearance). For harmonic FE simulations without damping[2], the harmonic motion is described as follows:

$$\mathbf{K}\ \mathbf{x} - \omega^2\ \mathbf{M}\ \mathbf{x} = \mathbf{f} \tag{5.14}$$

where $\mathbf{K}$ = stiffness matrix,
$\mathbf{x}$ = response vector, defined as $[x(t)] = \mathbf{x}\ \mathrm{e}^{\ i\ \omega\ t}$,
ω = angular frequency $[rad/s]$,
$\mathbf{M}$ = mass matrix, and
$\mathbf{f}$ = excitation force vector, defined as $[f(t)] = \mathbf{f}\ \mathrm{e}^{\ i\ \omega\ t}$.

For a given excitation, the harmonic motion can be obtained by two ways:

- Equation 5.14 can be solved by the direct inversion for each studied angular frequency:
$$\mathbf{x} = [\mathbf{K} - \omega^2\ \mathbf{M}]^{-1}\ \mathbf{f} = \boldsymbol{\alpha}(\omega)\ \mathbf{f} \tag{5.15}$$
where $\boldsymbol{\alpha}(\omega)$ = receptance matrix.
- N resonance angular frequencies ω_k and modes $\boldsymbol{\Psi}_k$ can be calculated and used to obtain the receptance matrix $\boldsymbol{\alpha}(\omega)$ [54]:
$$\boldsymbol{\alpha}(\omega) = \sum_{k=1}^{N} \frac{\boldsymbol{\Psi}_k\ \boldsymbol{\Psi}_k^T}{\boldsymbol{\Psi}_k^T\ \mathbf{M}\ \boldsymbol{\Psi}_k}\ \frac{1}{\omega_k^2 - \omega^2} \tag{5.16}$$

[2] If the damping is considered, more complex formulas are obtained with similar processes.

where N = number of modes,
$\mathbf{\Psi}_k$ = mode shape vector of mode k, and
ω_k = angular frequency of mode k $[rad/s]$.

Equation 5.16 shows that a mode has less influence on the displacement if its frequency is far from the excitation frequency. The sheet pile can be designed by choosing the modes far from the excitation range (between 22 and 50 Hz, see section 5.2.2). But the motion due to the global-mode resonances cannot be removed: figures 5.4 and 5.8 shows that some of them occur in the frequency range of excitation (between 22 and 50 Hz). Only the occurrence of local-mode resonances can be removed from this range by using enough welds in the common interlock. When considering the wavelengths obtained in figures 5.3b and 5.7b, only the bending behaviour about the weakest principal axis is relevant and should be studied.

Two models can be used to predict how the first local-mode can occur [37, 38].

- The resonance is considered as similar to the resonance of a bi-articulated beam and the welds are then considered as a ball and socket joint (see figure 5.10).

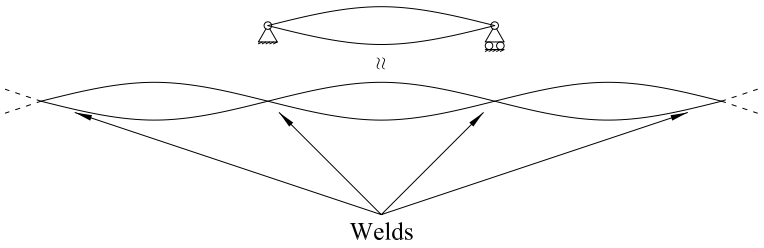

Figure 5.10.: Local-mode resonance of a double sheet pile similar to a bi-articulated beam

In this case, the bending frequency resonances are characterized by a factor $\mu_n = (n-1)\ \pi$ with $n \in \mathbb{N} \setminus \{0, 1\}$ (see equation 5.4), i.e. for the first resonance:

$$\ell = \frac{\mu_2}{2\pi}\ \lambda_B = \frac{1}{2}\ \lambda_B \tag{5.17}$$

where ℓ = beam length (between two welds) $[m]$.

- The resonance can also be considered as similar to the resonance of a bi-clamped beam and the welds are thus considered as a clamping (see figure 5.11).
  In this case, μ_n is given in table 5.3 and the condition for resonance occurrence is now:

$$\ell = \frac{\mu_2}{2\pi}\ \lambda_B = 0.753\ \lambda_B \tag{5.18}$$

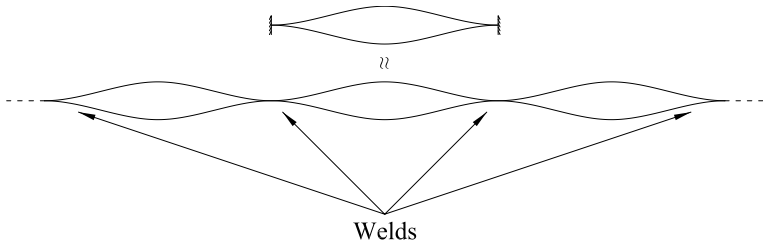

Figure 5.11.: Local-mode resonance of a double sheet pile similar to a bi-clamped beam

n	$\frac{\mu_n}{2\pi}$
2	0.753
> 2	$\approx \frac{n}{2} - \frac{1}{4}$

Table 5.3.: Factor μ_n for a bi-clamped beam (n is the number of nodes)

This occurrence is studied in the next sections to determine which model is the correct one. It is made by observing the differences of the motions between the two clutches of the common interlock, as a function of the spacing between the welds and of the frequency (as the wavelength depends on the frequency, see equation 5.3).

5.2.2. Used model

The model uses a double sheet pile of a chosen type. No force is applied at the toe (see figure 5.12), because it was shown in section 4.4.1 that such a force plays a minor role for the vertical accelerations for the investigated experiments.

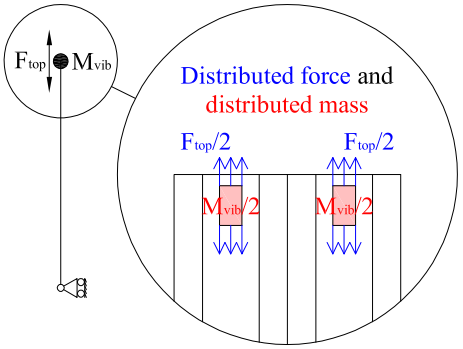

Figure 5.12.: Model of the sheet pile toe and the vibrator

The welds of the common interlock have a length of 0.2 m (the usual length of a triple crimping point) and are positioned so that the spaces between them are constant. Two welds are set at the ends of the sheet pile in order to avoid large motions that can be observed usually at a free end: in this case, they are welded to avoid large motions differences between the interlocked clutches. As in section 4.3.3, the horizontal motion of the toe section is avoided, as shown in figures 5.12 and 5.13b.

The vibrator is modelled as in section 4.3.3 (see figure 5.12). Two configurations are tested: a single clamping system (as in figure 4.14a) and a double one (as in figure 5.13b). The moment of inertia of the vibrator is neglected: indeed, the vibrator mass itself is the main influence on the motion of the nodes of the clamping device in the simulations (several tons for 4 dm^2); moreover, most of the energy is introduced in the system by traction-compression forces, and the moment of inertia cannot influence such motions directly in the case of a sheet pile.

The mass of the vibrator is chosen as follows:

1. When looking to the vibrators on the market, a relationship between the vibrating mass and the generated force can be found. In fact, the empty acceleration (without any sheet pile) is always around 300 m/s^2 (the slope of the curve of figure 5.14a).

2. This feature is independent of the maximum frequency of the vibrator. Two ranges can be distinguished: low and high frequency vibrators; the covered range[3] is between 22 and 50 Hz (see figure 5.14b).

   The frequency range of the simulations is chosen as between 22 and 50 Hz (the maximum frequencies used for vibrators). Lower frequencies can be performed by vibrators with a variable frequency; such frequencies are not relevant, because the operators on site will normally choose the highest frequency, as the highest force is generated in this case (see equation 2.5).

3. For a chosen sheet pile, the mass of the vibrator depends on the wanted vertical acceleration. If the sheet pile and the vibrator are considered as punctual masses, the obtained vertical acceleration is calculated as follows:

$$a_{wanted} = a_{empty} \frac{m_{vib}}{m_{vib} + m_{sp}} \tag{5.19}$$

   where a_{wanted} = wanted vertical acceleration $[m/s^2]$,
   a_{empty} = empty acceleration of the vibrator $[m/s^2]$,
   m_{vib} = vibrating mass of the vibrator $[kg]$, and

[3]Vibrators with a frequency of 55 Hz are mounted on an excavator and are not used drive large piles.

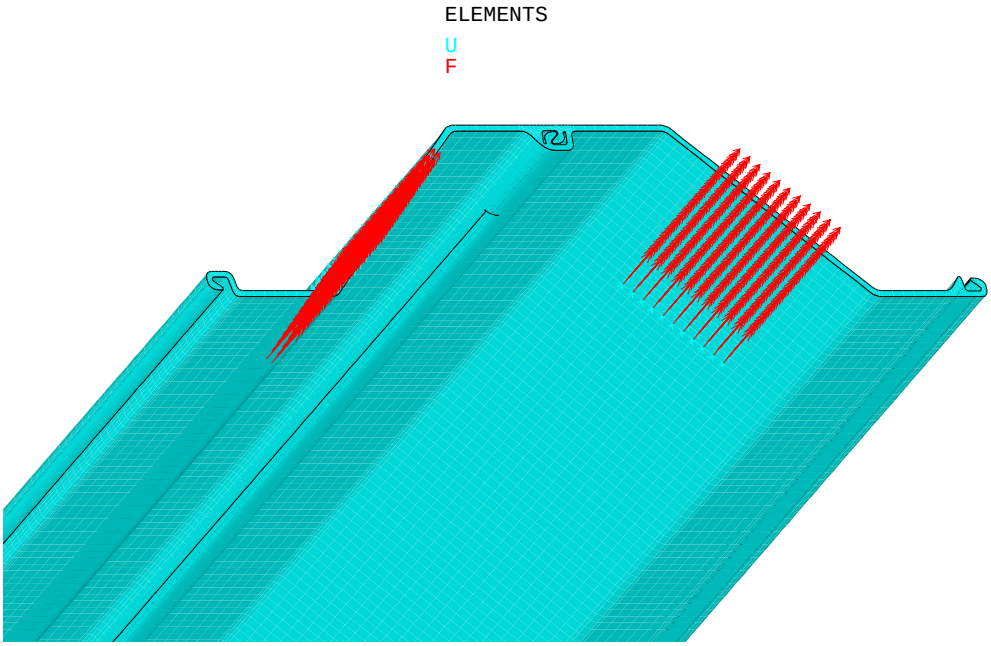

(a) Top boundary condition

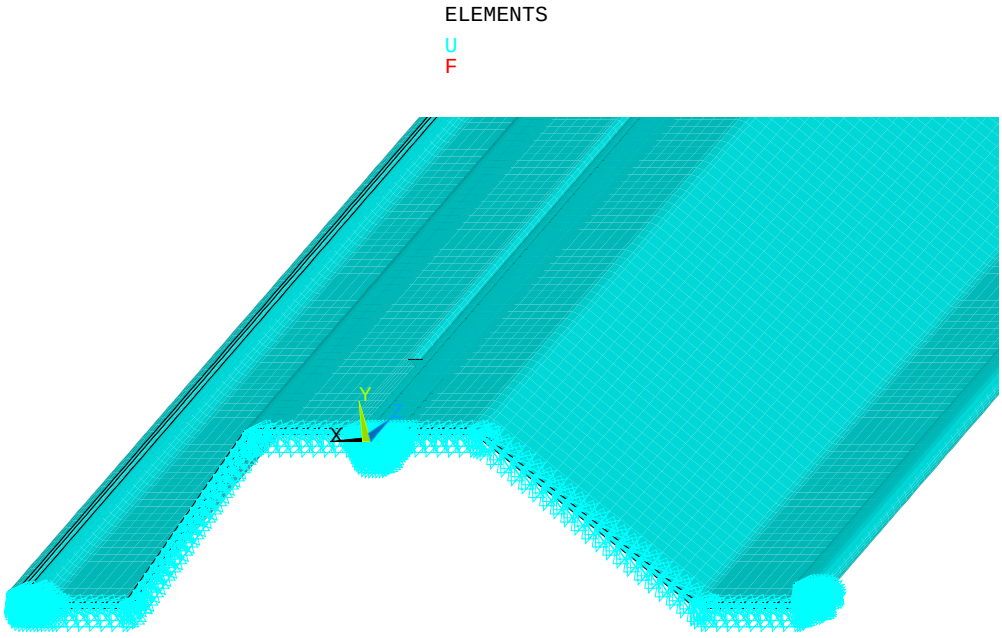

(b) Toe boundary condition

Figure 5.13.: Example of boundary conditions

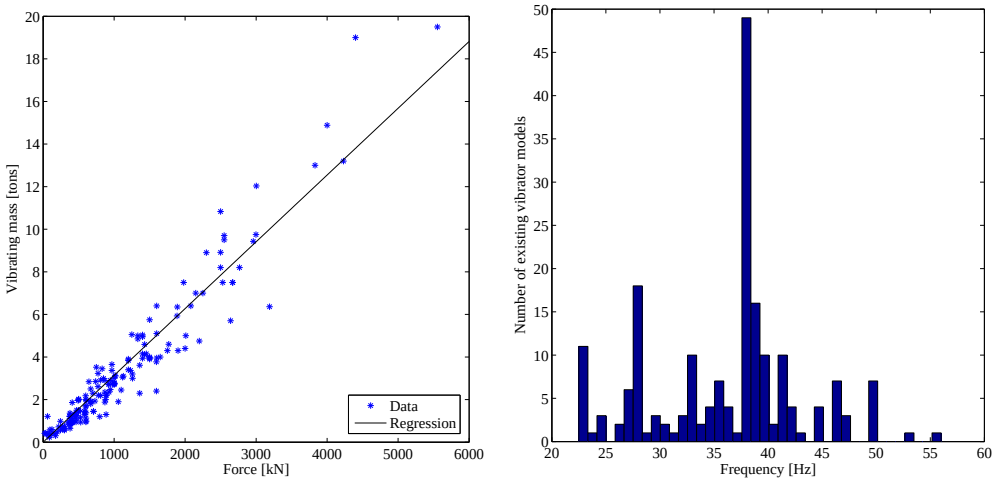

(a) Relationship between the vibrating mass and the generated force

(b) Frequency range

Figure 5.14.: Properties of the vibrators on the market [55, 56, 57, 58, 59, 60, 61, 62]

m_{sp} = sheet pile mass $[kg]$.

A mass of the vibrator can be calculated:

$$m_{vib} = \frac{a_{wanted}}{a_{empty} - a_{wanted}} m_{sp} \tag{5.20}$$

So several vertical accelerations are tested (100, 150, 200 and 250 m/s^2) and the vibrator mass is chosen with equation 5.20 to generate such accelerations.

5.2.3. Post-processing

The FE harmonic simulation calculates the displacements of the sheet pile (real and imaginary parts). They are processed to obtain the motions in the interlock and to conclude about the impact occurrence.

The first step is to associate a curvilinear coordinate to the nodes of the FE simulation. This is made by calculating the perimeter of the section of the clutch where impacts can occur (see figure 5.15). The straight and curved interlock have the same profile in this part. Each node is associated with the closest point on the contour of the other clutch.
The results of this point are obtained by extrapolating the results of the nodes neighbouring the associated point with the curvilinear coordinate. The difference of the motions is thus calculated between one node and its associated point on

the other clutch.
In fact, for any sheet piles, the real geometry of the interlock might deviate from the nominal shape due to manufacturing tolerances. This has a large influence on the clearance of the interlock (see confidential appendix F), but a small one on the modes of the sheet pile.

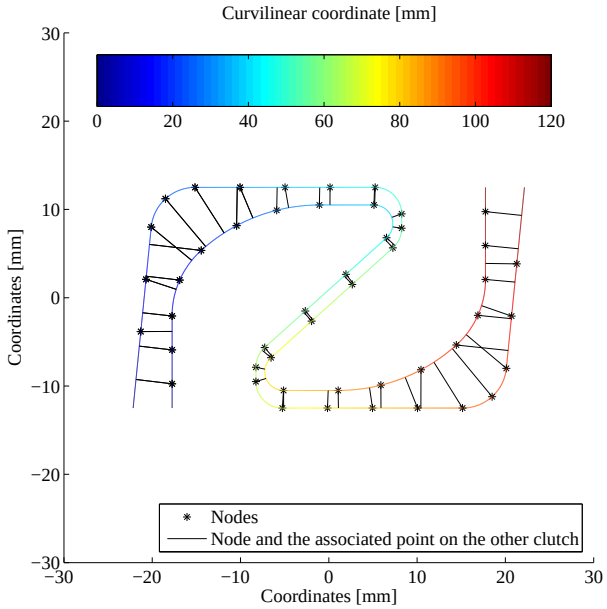

Figure 5.15.: Section where impacts can occur and an example of the location of the nodes

The difference of the motions is calculated for the real and the imaginary parts of the motions. The maximum amplitude of the impacts d in the plan of the section is obtained by looking for its maximum; the result gives:

$$d = \max_{k\in\mathbb{Z}} \left(x_r \cos\Phi + x_i \sin\Phi\right)^2 + \left(y_r \cos\Phi + y_i \sin\Phi\right)^2$$
$$\text{with} \quad \Phi = \tfrac{1}{2} \arctan\left(2\, \tfrac{x_r\ x_i + y_r\ y_i}{x_r^2 + y_r^2 - x_i^2 - y_i^2}\right) + \tfrac{k\ \pi}{2} \quad (k \in \mathbb{Z}) \tag{5.21}$$

where d = maximum amplitude of the difference of the displacement of the studied node $[m]$,
x_r = real part of the difference of the displacement in the abscissa direction of figure 5.15 $[m]$,
x_i = imaginary part of the difference of the displacement in the abscissa direction of figure 5.15 $[m]$,
y_r = real part of the difference of the displacement in the ordinate direction of figure 5.15 $[m]$, and

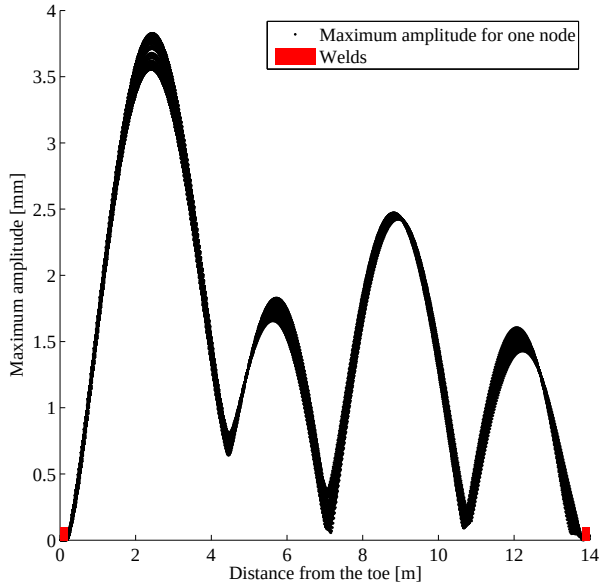

(a) For a sheet pile without any welds between the ends (spacing of 13.6 m between the welds)

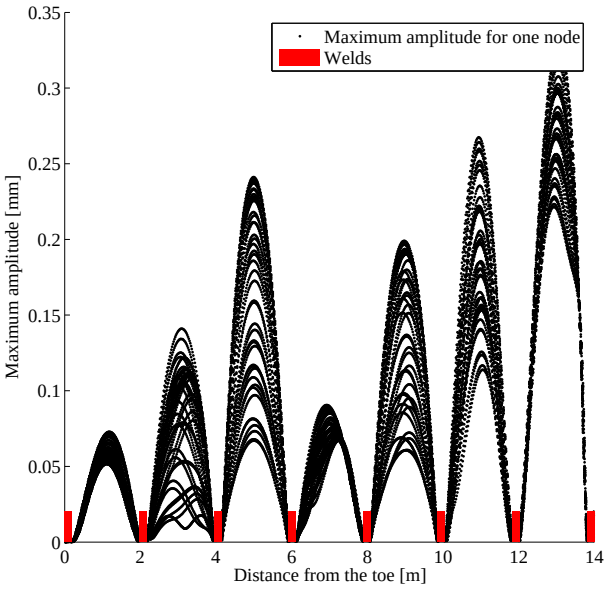

(b) For a sheet pile with 6 welds between the ends (spacing of 1.9 m between the welds)

Figure 5.16.: Examples of maximum amplitude of the nodes as a function of the distance between the node and the sheet pile toe for a Z sheet pile of 14 m, showing that one or several impacts can occur between two welds, depending on the spacing between the welds

y_i = imaginary part of the difference of the displacement in the ordinate direction of figure 5.15 $[m]$.

The amplitude of the difference of the displacement d (calculated for each node) is displayed as a function of the distance between the node and the sheet pile toe (see the two examples of figure 5.16).
In this figure, one or several local maxima can be observed between two welds. If the difference of motion exceeds the clearance in the interlock, then impacts can occur at the location of these maxima. It can be seen that several impacts occur between two welds for large spacing between the welds (13.6 m in figure 5.16a) and that only one impact is expected for a smaller spacing (1.9 m in figure 5.16b), as expected by the mechanism explained in section 2.3.3.

The maximum of figure 5.16 (the maximum amplitude of the impacts of the considered sheet pile, called "maximum impact amplitude" in the following text) is then taken and placed into a graphic as a function of the frequency and the spacing between the welds. Figure 5.17 is obtained; their values can be interpolated and compared to the bending wavelength (e.g. in figure 5.3b). It must be mentioned that this interpolation can miss some resonances.

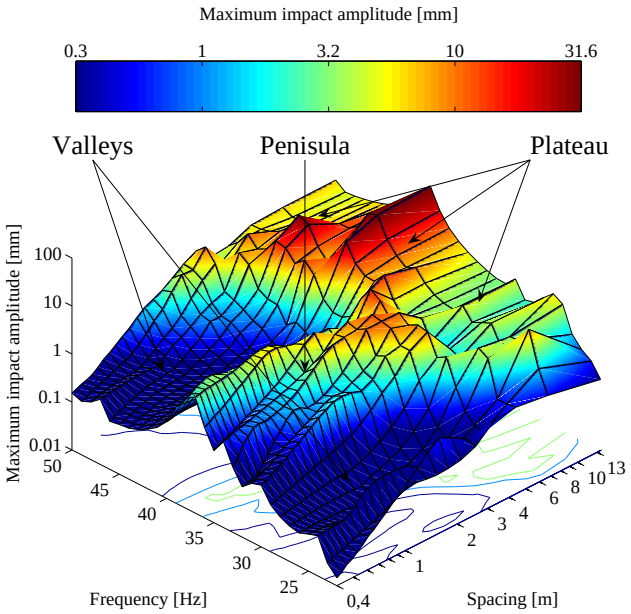

Figure 5.17.: Example of the interpolation of the maximum impact amplitudes of one sheet pile as a function of the frequency and the spacing between the welds (reference simulation: a Z sheet pile of 14 m with a single clamping device, 1 %of modal damping and 250 m/s^2 of wanted vertical acceleration)

5.2.4. Studied parameters

These simulations study a lot of parameters.

The sheet pile type: Several Z types are studied, as the wavelengths are different for each type.

The clamping device: As already mentioned, two clamping devices are applied to the model: a single clamping device (as in figure 4.14a) and a double one (as in figure 5.13b).

The sheet pile length: The model uses sheet pile lengths usually used during vibratory pile driving.

The vibrator amplitude: Equation 5.20 explains how the mass of the vibrator is chosen for a chosen vertical wanted acceleration a_{wanted}.

The damping: As section 4.4 was not able to indicate a value of the damping, several modal damping ratios are tested: 0, 1, 2, 5, 10 and 20 %.

5.2.5. Results

The relationship between the occurrence of impacts and the acoustic measurements is first demonstrated.
Then, by varying the parameters, conclusions about the occurrence of impacts and the influence of the local mode resonances can be obtained. For this study, the reference configuration is a Z sheet pile of 14 m with a single clamping device, 1 %of modal damping and 250 m/s^2 of wanted vertical acceleration, whose results are displayed in figure 5.17.
Because of the aspect of the results discussed further in this section, comparisons at one chosen frequency can yield wrong conclusions. Comparisons must be made statistically for all the considered frequency range.

Comparison with the experiments

The vibroimpact theory [43, 44, 63, 64] implies strong non-linearities and a lot of behaviours can be met (harmonic, pseudo-harmonic, chaotic, etc.). Here below, the way to study impact occurrences is different: when a mass m impacts vertically a horizontal beam with a velocity v_0 (as shown in figure 5.18), the exciting impulse I generating structure-borne sound (that can afterwards resonate as air-borne sound) is assumed resulting from a force-time history $F(t)$ [50]:

$$I = \int_{-\inf}^{\inf} F(t)\ dt \tag{5.22}$$

where I = exciting impulse $[Ns]$, and
$F(t)$ = contact force between the impact of the mass m on the beam $[N]$.

The exciting impulse I lies between $m\ v_0$ when no bounces take place and $2\ m\ v_0$ for a complete conservation of momentum.

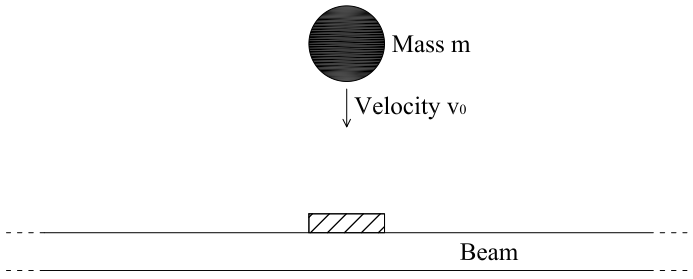

Figure 5.18.: Mass m impacting a beam at a speed v_0

Analogously, more violent is the impact between two clutches, more noise it will generate. The velocity before the impact can be related to the maximum amplitude difference with a linear simulation (so without taking into account the possible impacts).

Figures 5.19, 5.20 and 5.21 show the simulation of the sheet piles tested during the two experiment sessions: the welds and the vibrator are modelled as performed on site; the toe model is the one explained in section 5.2.2. For the experiments of the first experiment session (figures 5.19 and 5.20), the results are given as a range, because of the uncertainties about the frequencies.
When figures 5.19, 5.20 and 5.21 are compared to figures 2.14 and 2.17, a correspondence between the maximum impact amplitude and the generated noise can be found: the threshold space observed during the experiments is well reproduced by the simulations.

General aspect of the results

Figure 5.22 draws the results of figure 5.17 without interpolation (as it can miss resonances). This figure shows the general aspects of the simulations. Three parts can be identified; they are described wit a geographic analogy:

A plateau: On the right part of the graphic, large amplitudes can be observed. In this part, global- and local-mode resonances occur.

Valleys: On the left part, the maximum impact amplitudes mainly decrease when the spacing between the welds decreases (as it can be seen in figure 5.17).

A peninsula: In some cases, this decrease of the valley is not observed. This peninsula of the plateau is a global-mode resonance that generates large impact amplitudes even for small spaces between the welds.

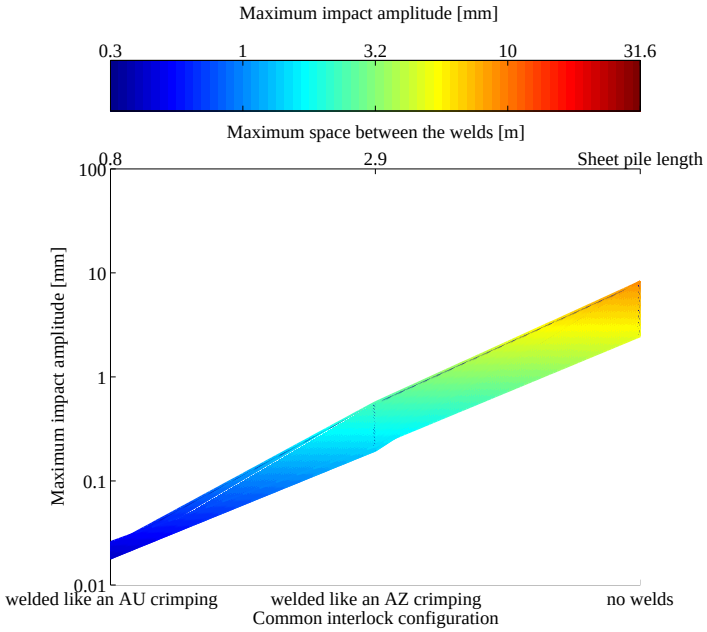

(a) Frequency around 38 Hz

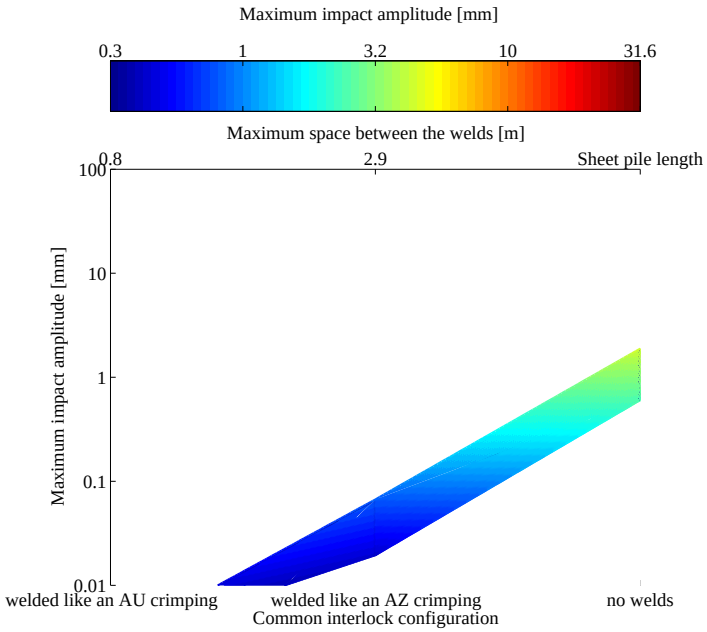

(b) Frequency around 33 Hz

Figure 5.19.: Simulation of the impacts during the first experiment (to compare with figure 2.14)

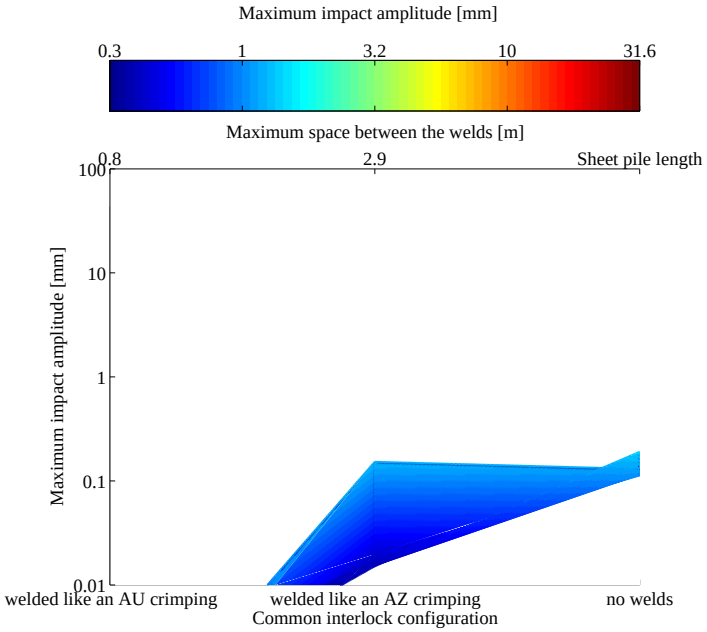

(a) Frequency around 28 Hz

Figure 5.20.: Simulation of the impacts during the first experiment (to compare with figure 2.14)

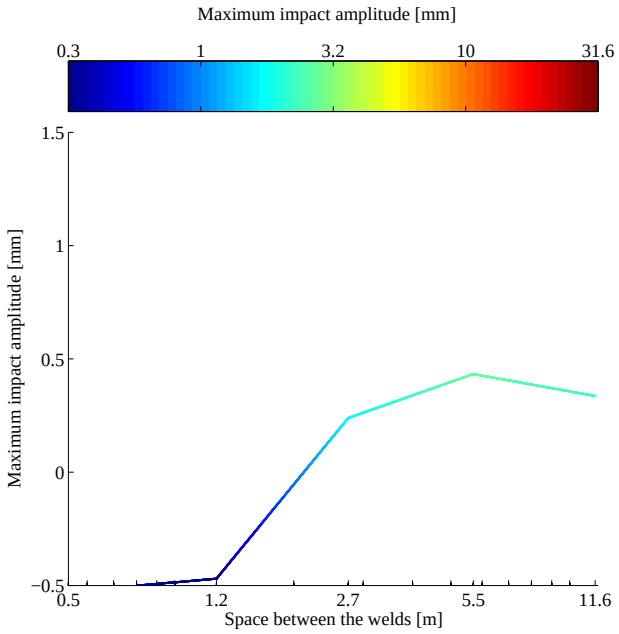

Figure 5.21.: Simulation of the impacts during the second experiment session (to compare with figure 2.17)

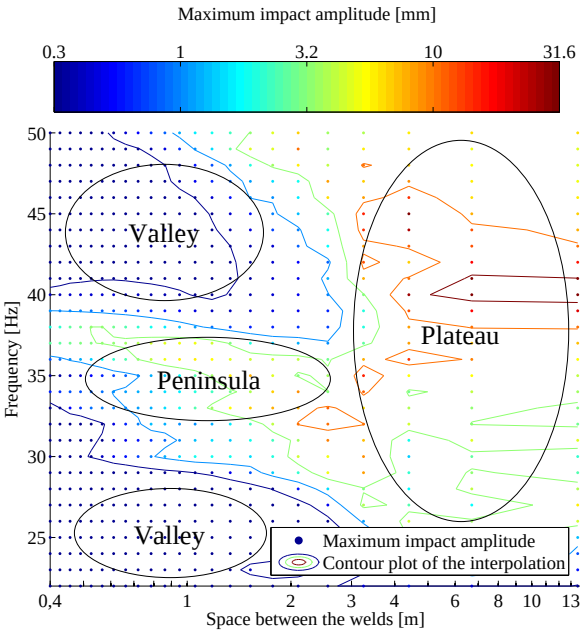

Figure 5.22.: Reference simulation with another layout of figure 5.17 showing different regions (Z sheet pile of 14 m with a single clamping device, 1 %of modal damping and 250 m/s^2 of wanted vertical acceleration)

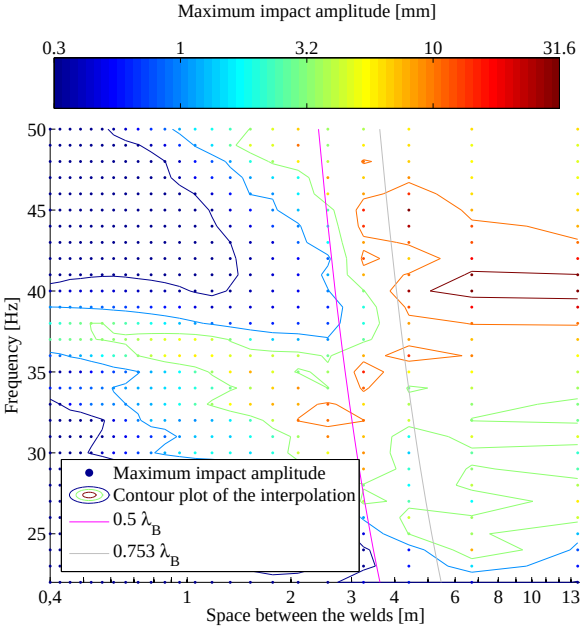

Figure 5.23.: Reference simulation (figure 5.22) with the associated bending wavelength, showing the boundary of the plateau as close to half of the bending wavelength

Link between the boundary of the plateau and the bending wavelength

To prove the theory of section 5.2.1, the bending wavelength about the weakest principal axis is multiplied by the factor μ_2 ($0.5\,\pi$ and $0.753\,\pi$) of the two presented hypotheses and drawn in figure 5.23.
It can be seen that the plateau can be delimited by half of the bending wavelength. The local-mode resonances seem to behave like the bending resonance of a bi-articulated beam (see figure 5.24 for an example of such local-modes). In this case, the parameters that do not modify the wavelength should have a weak influence on the boundary between the plateau and the valleys.

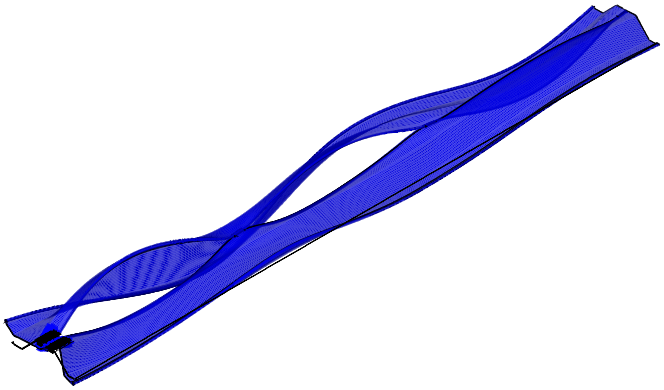

(a) Local-mode at 28 Hz

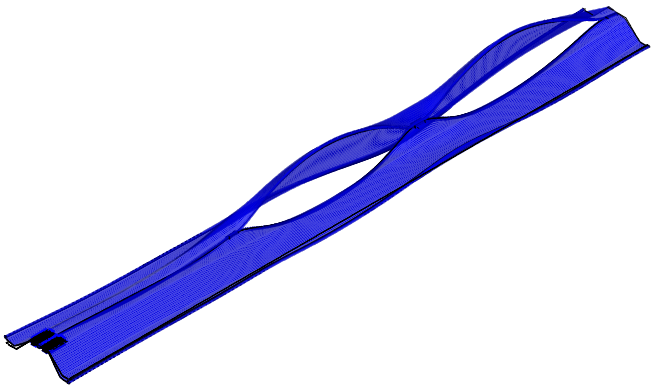

(b) Local-mode at 30.3 Hz

Figure 5.24.: First local-modes for a Z sheet pile of 14 m with 4.4 m of spacing between the welds

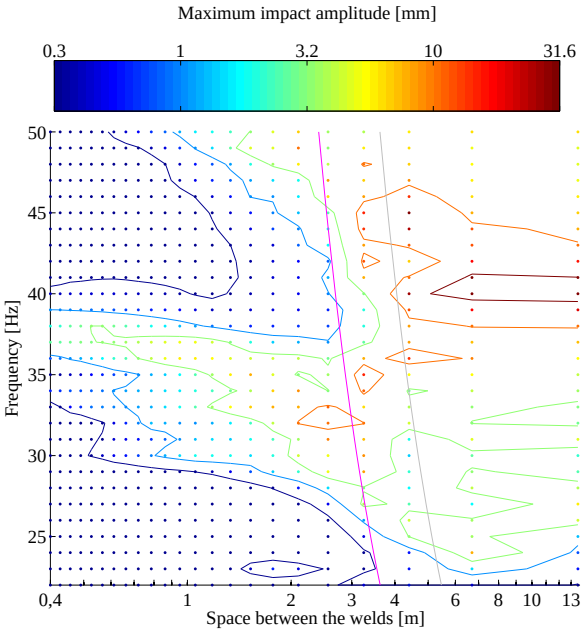

(a) With a single clamping device

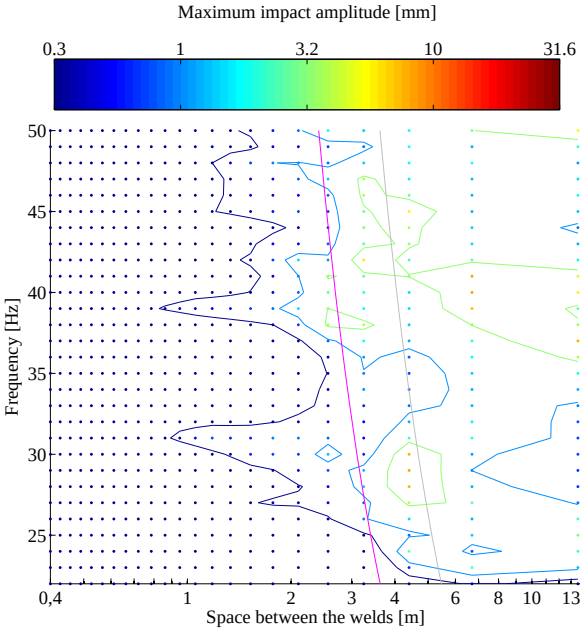

(b) With a double clamping device

Figure 5.25.: Influence of the clamping system on the maximum impact amplitude for the reference simulation, showing a decrease of the maximum impact amplitude

Influence of the clamping system

A double clamping system decreases the maximum impact amplitude (see the example of figure 5.25). But this configuration is not quiet in any cases: depending on the configuration, local- or global-modes can be excited and generate noise. Anyway, the boundary between the plateau and the valleys is still around half of the bending wavelength, as bending modes are excited even if the vibrator has a centred position on the section.

Influence of the sheet pile length

As shown in figure 5.27, the local-mode resonances are not substantially modified by a variation of the length: the boundary of the plateau is not moved. The global-mode resonances occur at lower frequencies for larger lengths (e.g. see equation 5.4 for the bending modes), thus more peninsulas can be observed.
Another effect of the increase of the length is the increase of the spacing resolution (more spacings can be computed), because the welds in section 5.2.2 were equally spaced on purpose.

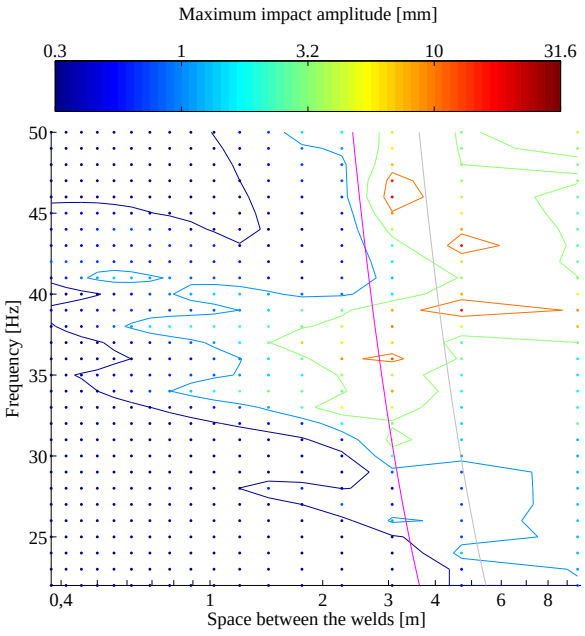

(a) Sheet pile with a length of 10 m

Figure 5.26.: Influence of the sheet pile length on the maximum impact amplitude for the reference simulation, showing the modification of the spacing resolution

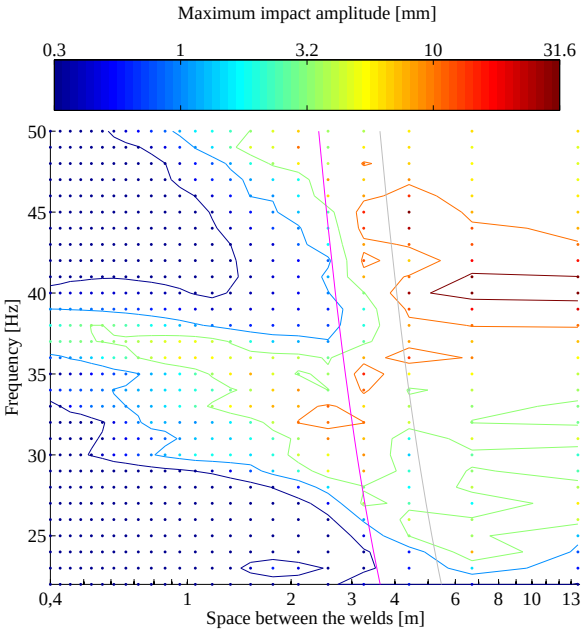

(a) Sheet pile with a length of 14 m

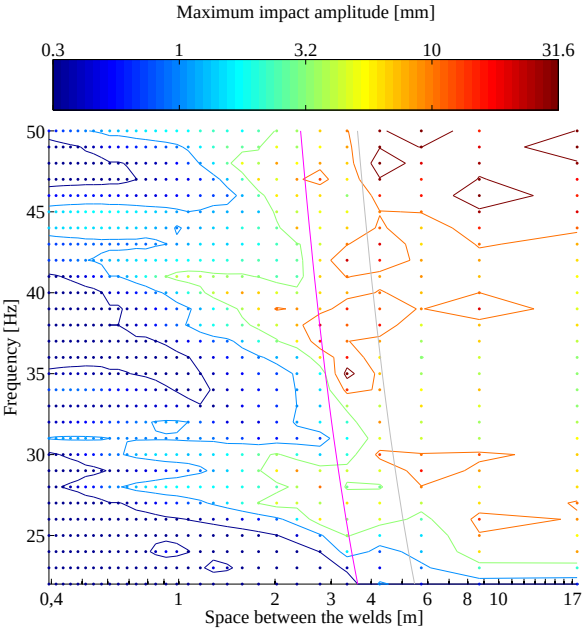

(b) Sheet pile with a length of 18 m

Figure 5.27.: Influence of the sheet pile length on the maximum impact amplitude for the reference simulation, showing the increase of peninsulas for a larger length

Influence of the wanted vertical acceleration amplitude

The wanted vertical amplitude is modified by changing the vibrator mass (see equation 5.20). If this modification was applied only by changing the force, only a vertical translation would have been observed in figure 5.17 (and thus a modification of the colours of figure 5.23).
But as the vibrator mass has been changed, the global-mode resonances have modified frequencies, i.e. the peninsulas are observed at modified frequencies (see figures 5.28 and 5.29). However, the boundary of the plateau (linked to the local-mode resonance) still occur around the resonance frequencies of a bi-articulated beam.
As the vertical forces applied to the sheet pile decrease in figures 5.28 and 5.29 compared to figure 5.23, the average level of the plateau decreases, but the boundary between the plateau and the valleys does not depend on the vibrator mass.

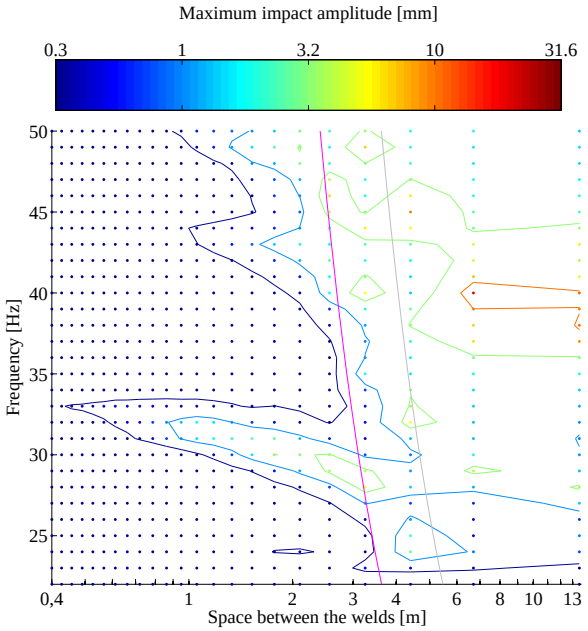

(a) With a wanted vertical acceleration of 100 m/s^2

Figure 5.28.: Influence of the wanted vertical amplitude on the maximum impact amplitude for the reference simulation, showing no clear modification of the boundary of the plateau

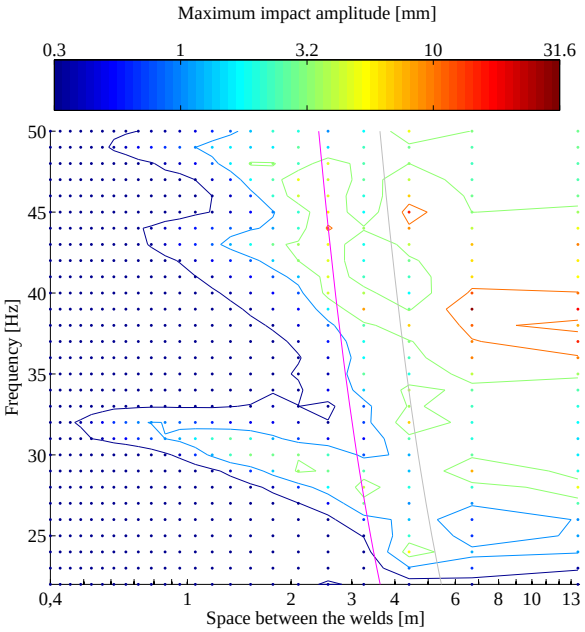

(a) With a wanted vertical acceleration of 150 m/s^2

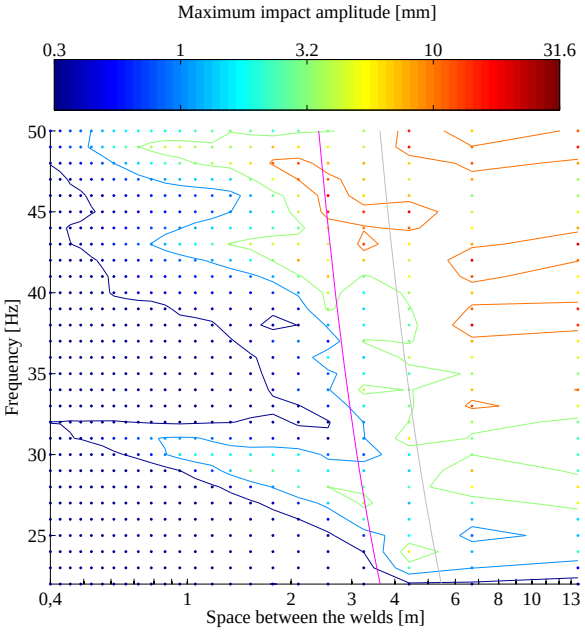

(b) With a wanted vertical acceleration of 200 m/s^2

Figure 5.29.: Influence of the wanted vertical acceleration on the maximum impact amplitude, showing no clear modification of the boundary of the plateau

Influence of the damping

The damping decreases the influence of the resonances modes; equation 5.16 is modified as follows in the case of a hysteretically damped and viscously damped model, respectively:

$$\boldsymbol{\alpha}(\omega) = \sum_{k=1}^{N} \frac{\boldsymbol{\Phi}_k \, \boldsymbol{\Phi}_k^T}{\omega_k^2 - \omega^2 + i \, \eta_k \, \omega_k^2} \tag{5.23}$$

$$\boldsymbol{\alpha}(\omega) = \sum_{k=1}^{N} \left(\frac{\boldsymbol{\Phi}_k \, \boldsymbol{\Phi}_k^T}{\omega_k \xi_k + i\omega - i\omega_k \, \sqrt{1-\xi_k^2}} + \frac{\boldsymbol{\Phi}_k^* \, \boldsymbol{\Phi}_k^{*T}}{\omega_k \xi_k + i\omega + i\omega_k \sqrt{1-\xi_k^2}} \right) \tag{5.24}$$

where η_k = hysteretic damping loss factor of mode k, and
ξ_k = viscous damping loss factor of mode k.

It can be seen in figure 5.30 that a higher viscous damping ratio removes the peninsulas and provides results that can be considered as more statistical, as they show more clearly the boundary between the plateau and the valley. It also decreases the general level of all the regions (plateau and valleys).

Influence of the section type

The sheet pile section influences the bending wavelength. But as it can be seen in figure 5.31, the same relationship can be found between a fraction of the wavelength and the boundary between the plateau and the valleys for other simulated types.
It can be seen further (in section 5.3.1) that the bending wavelengths increase for stronger sheet piles (i.e. with a higher elastic section modulus). So a stronger profile has statistically smaller maximum impact amplitudes for a given spacing between the welds.

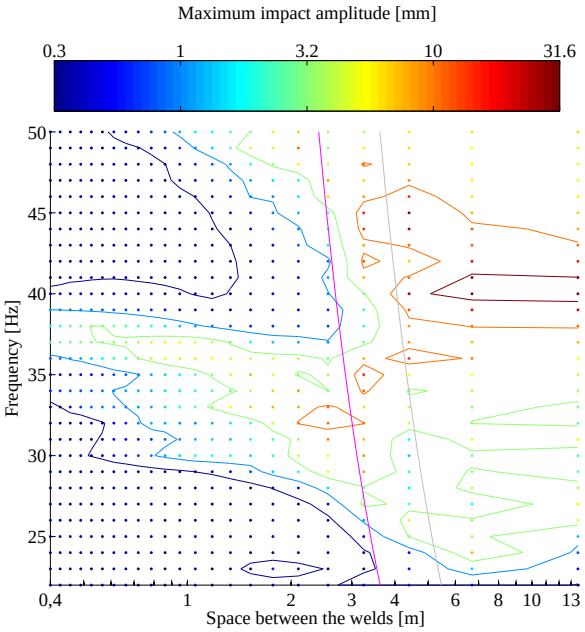

(a) With a modal damping of 1 %

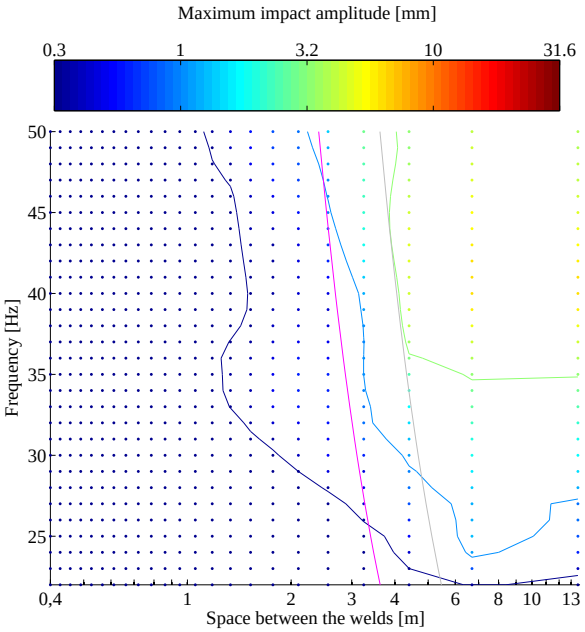

(b) With a modal damping of 10 %

Figure 5.30.: Influence of the damping on the maximum impact amplitude for the reference simulation, showing no clear modification of the boundary of the plateau, a removal of the peninsulas and a decrease of the average level for a higher modal damping

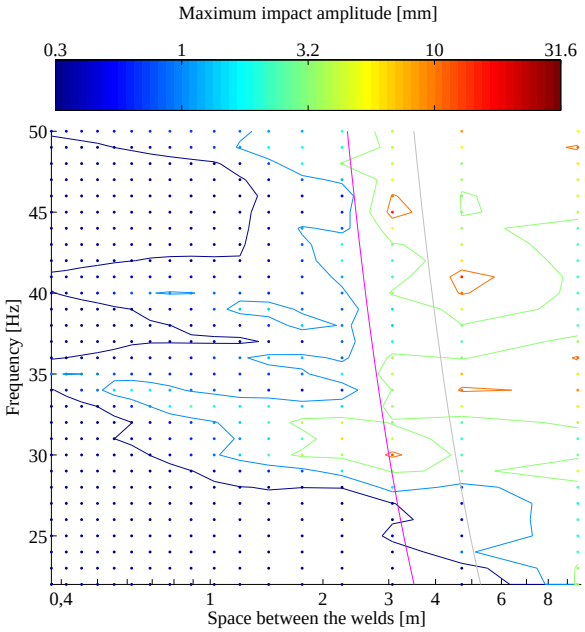

(a) For a Z sheet pile (reference type)

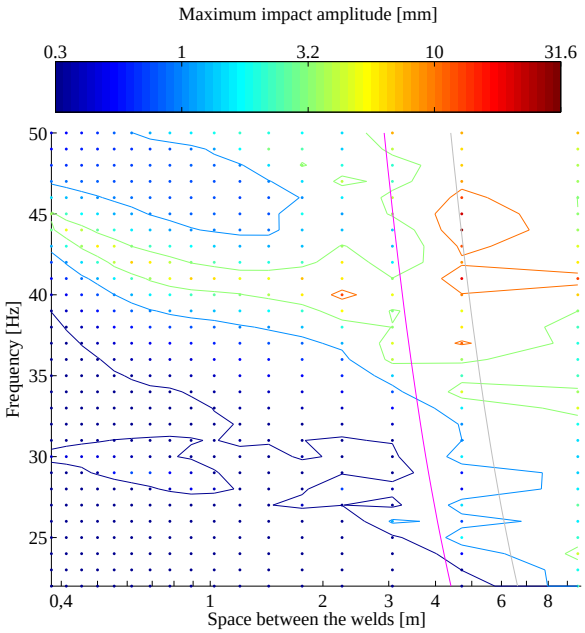

(b) For a Z sheet pile (higher elastic section modulus than the reference type)

Figure 5.31.: Influence of the section type on the maximum impact amplitude, showing always the relationship between the boundary of the plateau and half of the bending wavelength

5.2.6. Choice of an optimal spacing between the welds

Even if the ratio between the bending wavelength and the spacing between the welds is identified, nothing indicates how far of this ratio the spacing must be chosen to have behaviour without noisy impacts.

Equation 5.24 shows[4] that the influence of a mode depends on its resonance frequency and its damping loss factor. In case of low damping, a proportional damping can be assumed, i.e. the modes are real. Equation 5.24 becomes then:

$$\boldsymbol{\alpha}(\omega) = \sum_{k=1}^{N} \left(\frac{\boldsymbol{\Phi}_k \, \boldsymbol{\Phi}_k^T}{\omega_k^2 - \omega^2 + 2 \, i \, \xi_k \, \omega_k \, \omega} \right) \tag{5.25}$$

In this case, the reduction of the amplitude compared to resonance amplitude is a ratio of formula 5.25 in the two considered cases (at the resonance and at another frequency):

$$R = \frac{2 \, \xi_k}{\sqrt{1 + \left(\frac{\omega}{\omega_k}\right)^4 - 2 \, (1 - 2 \, \xi_k^2) \, \left(\frac{\omega}{\omega_k}\right)^2}} \tag{5.26}$$

where R = reduction factor.

For bending local-modes, the resonance frequency depends on the wavelength (equation 5.4), itself related to the spacing between the welds as shown in the previous section.

$$\frac{\omega}{\omega_k} = \frac{(2 \, s)^2}{\lambda_B^2} \tag{5.27}$$

$$R = \frac{2 \, \xi}{\sqrt{1 + \left(\frac{2 \, s}{\lambda_B}\right)^8 - 2 \, (1 - 2 \, \xi^2) \, \left(\frac{2 \, s}{\lambda_B}\right)^4}} \tag{5.28}$$

where ξ = maximum damping loss factor of the modes implied in the motion generation, and
s = spacing between the welds $[m]$.

Figure 5.32 shows this reduction factor for several damping loss factors. A decrease of 90 % for the impact amplitude (i.e. $R = 10^{-1}$) is possible only if the damping loss factor is weaker than 5 %. But it is difficult to modify the damping loss factor for a sheet pile.
So the choice of the spacing is made with another criterion. The asymptotic reduction factor for $s = 0$ is $2 \, \xi$. Twice this asymptotic reduction factor (thus $4 \, \xi$) is obtained for $s = 0.42 \times \lambda_B$. It seems to be a good choice, as a larger decrease

[4] The viscously damped model is usually used in simulations and in experimental modal analyses.

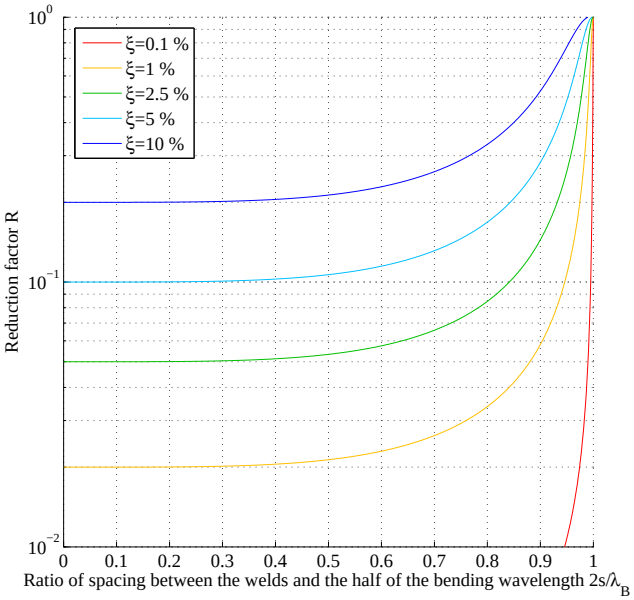

Figure 5.32.: Reduction factor as a function of the spacing between the welds

of the impact amplitude will induce a prohibitive decrease of the spacing between the welds.
The role of this reduction factor is similar to a security coefficient.

5.2.7. Conclusion

The study of the spacing between the welds showed that the local-mode resonances can be related to half of the bending wavelength of a sheet pile. This wavelength depends only on the sheet pile type and on the vibrator frequency, not on the sheet pile length or on the vibrator mass.

The clamping device has an influence: a single clamping device excites the modes more and larger impact amplitudes can be statistically observed. An increase of the wanted vertical acceleration behaves in the same way.

By increasing the damping, the relationship between the wavelength and the local-mode resonances can be seen more clearly.

A reduction factor is defined to choose the spacing between the welds far enough of the boundary of the plateau (half of the bending wavelength).

5.3. Optimisation of the sheet pile type

The determination of the optimisation potential is made in two steps:

1. The actual situation is evaluated.
2. An optimisation of the situation is performed.

5.3.1. Comparison of the existing types

Figure 5.33 shows a comparison of the ratio $\sqrt[4]{\frac{E\ I}{\rho\ A}}$ that partly determines the bending wavelength (see equation 5.3). The range of variation is small (around 20 %), even if the compared types are very different. No substantial difference between the old types and the new ones is found.

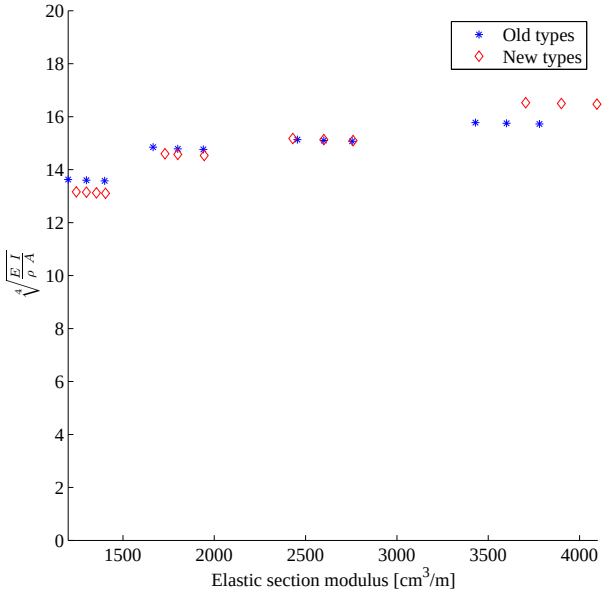

Figure 5.33.: Ratio $\sqrt[4]{\frac{E\ I}{\rho\ A}}$ of Z sheet piles

5.3.2. Optimisation of a sheet pile section

For a simple design, some parameters completely define the sheet pile section; for example (see figure 5.34):

- the web angle,
- the web thickness,

- the flange thickness,
- the section width,
- the section height, and
- the clutch geometry.

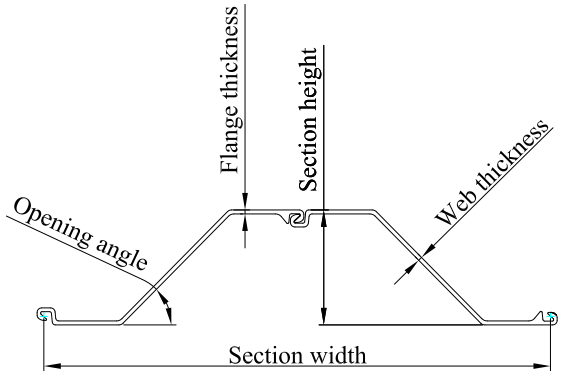

Figure 5.34.: Parameters of a section of a Z type

Three features are crucial for the contractors and the salesmen:

- the section width,
- the wall mass, and
- the elastic section modulus.

Analytical relationships between the variables of the two lists can be set. If the clutch geometry is assumed depending only on the flange thickness, an allowed range of variation can be defined for chosen parameters (section width, wall mass and elastic section modulus). Figure 5.35 shows such variations for the features of the reference Z sheet pile (section width, wall mass and elastic section modulus).

The obtained range of variation of the coefficient $\sqrt[4]{\frac{E\ I}{\rho\ A}}$ is shown in figure 5.36. This short study shows that the potential of optimisation is not large: to optimise the reference sheet pile, a right angle for the web angle and the thinnest flange thickness must be chosen. But the limits of the manufacturing processes should be considered and the gain is only 36 % on the bending wavelength compared to the actual design.

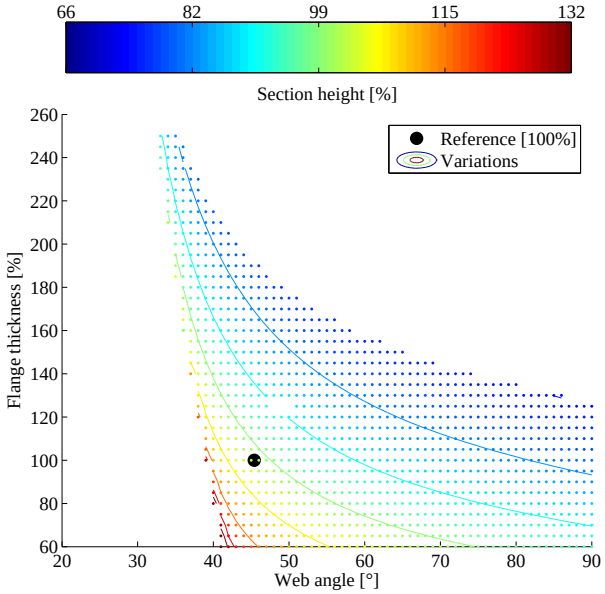

(a) Section height as a function of the web angle and the flange thickness

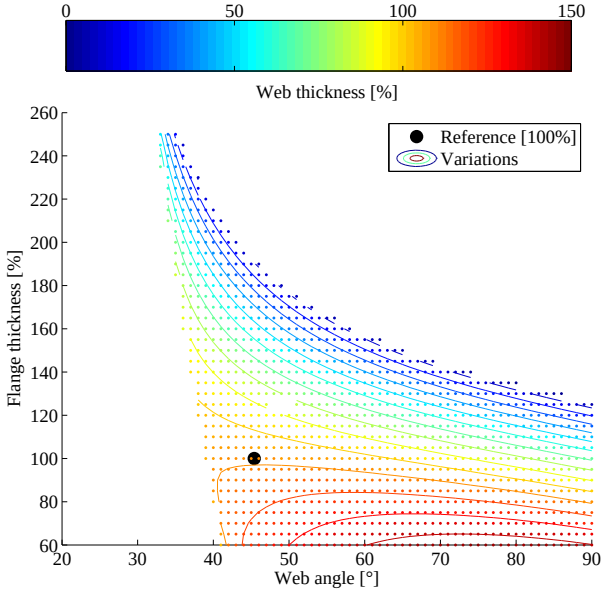

(b) Web thickness as a function of the web angle and the flange thickness

Figure 5.35.: Combinations of the section parameters to obtain the features of the reference Z sheet pile

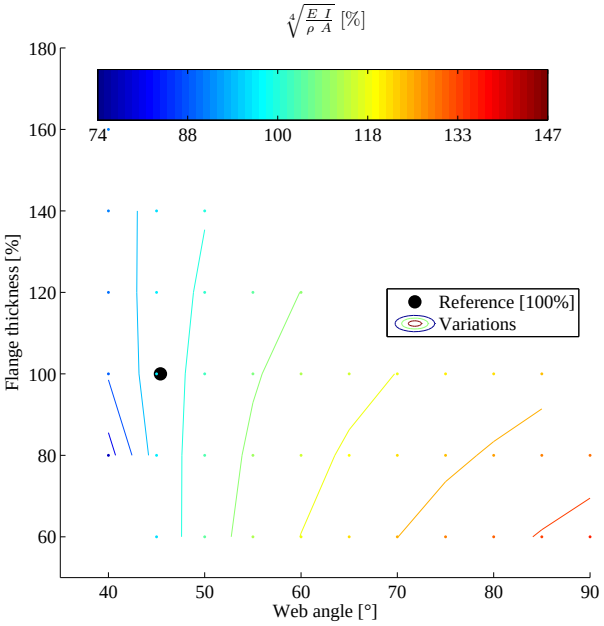

Figure 5.36.: Factor $\sqrt[4]{\frac{E\,I}{\rho\,A}}$ for the combination of features given in figure 5.35

5.4. Conclusion

This chapter studies how impacts are generated.

1. The clamping device transmitting the forces of the vibrator generates a bending moment and/or a torsion bimoment on the top of the double sheet pile.
2. Bending and/or torsion waves are propagating along the sheet pile. Depending on the configuration and on the boundary conditions, they are able to generate global- and/or local-mode resonances.
3. These resonances contribute to the motion of the clutches if their frequency is close to the excitation frequency.
4. Impacts occur because of the difference of the motion of the straight and curved clutches of the common interlock.

A comparison between the acoustic measurements and simulations of the impact occurrences validates this theory.

Other simulations are made to study the influence of several parameters. Some hypotheses of the model should be kept in mind:

- The ends of the simulated sheet pile were welded.

- The space between the welds of the common interlock was constant.
- The studied clutches were drawn with the nominal geometry.
- The vertical forces of the soil were not taken into account.
- Horizontal motions of the toe section were prevented.

It is shown that:

- a decrease of the wanted vertical acceleration or the use of a double clamping device statistically makes impacts that are less violent;
- modifying the spacing between the welds has a more important effect: if the spacing between the welds is chosen shorter than half of the bending wavelength of a single sheet pile, then a decrease of the violence is almost always obtained (a security factor is defined to facilitate this choice);
- the section geometry of the sheet pile plays a role in the determination of this bending wavelength: the study of the potential of optimisation is made to show that an increase of the wavelength of 36 % can be obtained.

It seems that the simplest way to improve the acoustic of a double sheet pile is to carefully choose the spacing between the welds. Other improvements are less efficient. However, it should be kept in mind that global-mode resonances can always occur with a short spacing between the welds, and so the improvements remain statistical improvements.
Such a choice is made as follows:

1. The parameters of the section can be used to calculate the factor $\sqrt[4]{\frac{E\ I}{\rho\ A}}$. It can be also be obtained in figure 5.33 for existing sections (the minimum for the existing sections: $\sqrt[4]{\frac{E\ I}{\rho\ A}} = 13$) .
2. The highest frequency f of the used vibrator is taken into account ($f = 50\ Hz$ when considering figure 5.14b).
3. A reduction factor R is chosen by taking into account the modal damping ratio ξ. It was shown that a factor $R = 0.84$ is a good compromise.
4. The space s between the welds is obtained as follows:

$$s = \frac{R}{2} \sqrt[4]{\frac{E\ I}{\rho\ A}} \sqrt{\frac{2\ \pi}{f}} \tag{5.29}$$

This calculation gives a spacing between the welds $s = 1.9\ m$, for a reduction factor $R = 4\ \xi$.

General conclusion

It is shown in this thesis that the noise generated during the vibratory pile driving of Z double sheet piles has several sources, with various sound levels:

- Impact noise can be generated in the common interlock of a double sheet pile or with an existing wall.
- Impacts were also observed during the experiments with the security device. The accessories (security device, guides, pipes for experiments session, etc.) can drastically increase the noise of a vibratory pile driving.
- If no impacts are generated, the structure-borne sound that resonates in the sheet pile comes from the vibrator and from the interaction with the soil.

The impacts in the common interlock of a double sheet pile are studied in a more detailed way. The mechanism involved in this noise generation is recalled:

- Due to the location of the clamping system on the top section, the vibrator generates traction-compression waves as well as bending and torsion waves. The configuration of the system (boundary conditions, configuration of the common interlock, sheet pile length, etc.) conditions the occurrence of resonances.
- When propagating along the sheet pile, these waves move the section along the principal axes and around the shear centre for the bending and torsion motions, respectively. Depending on their interaction, resonance modes occur at different frequencies.
- The two interlocked clutches moves in two different ways: impacts can occur and provoke a lot of noise.
- Between two connections (welds or crimping points), several impacts can occur at different locations:
  - If the spacing between the connections is large, then several impacts can occur between two welds, showing that one or several local-modes have resonance frequencies close to the vibrator frequency. One or several impacts with a substantial amplitude (and thus noise) can occur as the local-modes are excited.
  - If the spacing is small enough (around half of the bending wavelength or smaller), only one impact is observed between two welds. In this case,

the shorter the spacing between the welds, statistically the smaller the violence of the impacts and thus the noise that could be generated; indeed, the resonance frequencies of the local-modes are set at higher frequencies for a smaller spacing between the welds and the local-modes are less excited.

A reduction factor of the impacts is defined as a function of the configuration of the sheet pile. It plays the role of a security coefficient.
It should be kept in mind that this method works only on the impacts generated by the local-modes. The effect of the global-modes remains and the improvements must be considered statistically.

Guidelines for the contractors

Noise can be decreased on construction sites with the following tips, given in the order of importance:

- The configuration of the common interlock of the sheet pile is very important: the spacing between the welds (or the crimping points) should be short enough to avoid any effect of the first local-mode resonance.
- Any impact source should be removed or insulated. This concerns the security device (chain or shackle) as well as guides. Contractors can use wooden guides instead of steel guides, as recommended by the technical guide of the vibratory pile driving [4] (Experiments that were not representative of the most encountered cases were made and show the wooden guide as an improvement.). The use of a leader-mounted system instead of a free-hanging system allows driving without any guide in most of the cases, but it is mainly used with a single clamping device.
- The height of the wall above the ground should be as small as possible to decrease the impacts in the connection.
- The lower the frequency, the larger the allowed spacing between the welds. Low frequency vibrators statistically make less noise but more vibrations in the soil.
- The use of a double clamping system instead of a single one statistically decreases the violence of the impacts in the common interlock; it has a weak and statistical influence.
- The smaller the eccentric moment, the less violent the impacts if they occur. But such a modification affects also the vibro-driveability. A vibrator should never be oversized for the performed application.

- The filling of the common interlock with a watertightness joint could soften the impacts and the generated noise.

However, even if all these recommendations are followed, global-mode resonances of the sheet pile can occur, depending on the configuration, the frequency, etc. Two solutions remain in this case: to weld the entire common interlock of the sheet pile and/or to change the vibrator frequency.

It seems difficult to generate a sound power level below 105-110 dBA (equivalent sound pressure level: 77-82 dBA at 10 m of the source). The press driving or other methods could be used in areas with more strict limits.

Development directions for the manufacturers

The first objective of the manufacturers should be the supply of sheet piles with a crimping pattern (spacing between the triple crimping points) adapted to avoid the first local mode resonance. The geometry of the triple crimping point itself could influence this behaviour and should be investigated. Tools to choose such a pattern are given in chapter 5.

As shown in section 5.3, an improvement of the section will not induce a spectacular increase of the wavelength (only 20 % can be expected), but more difficulties for the rolling of such sheet piles though. This parameter should only be supervised when a new design is developed.

The influence of the different sealants on the violence of impacts should be quantified.

All the developments that could decrease the free motions in the common interlock should be considered: welding, continuous crimping, etc.

Scope of future researches

Subsection 5.2.5 showed a direct relationship between the expected impact amplitude and the observed generated sound. Deeper investigations should explain how vibroimpacts generate air-borne sound as well as structure-borne sound resonating in the air. The first one, known as acceleration (or deceleration) noise, is due to the rapid change in velocity of the moving body (the clutches and a part of the sheet pile in the case of a vibratory pile driving) during the impact process, i.e. the sound emanates from the impacting elements. The second one, known as ringing noise, is due to sound radiation form resonant structural modes of the workpiece or any attached structures (mainly the sheet pile in the case of a

vibratory pile driving) [27] excited by the contact force during the impact. Such investigations should try to obtain the spectra of the air-borne sound and of the contact force generated during the impacts.

The use of a sealant to soften impacts should be investigated further. The sealant of the common interlock is added after the crimping. It could not get everywhere along the section interlock. New designs of joints (how to fill the interlock, material, etc.) could be developed for quiet applications.

This thesis studied only stationary situations. But the sheet piles do not stay out of the soil during a vibratory pile driving. Even if a decrease of the sound is expected in this case, this decrease should be quantified to know the average situation and the worst case.

A clutch design could be developed to prevent that the air-borne sound (acceleration noise) propagates in the surrounding area. In this case, the structure-borne sound (the ringing noise) could become the relevant noise source. The sheet pile should then be acoustically studied. As the role of the clearance was not clearly established, this one could also be studied further.

Appendices

Bibliography

[1] Arcelor Commmercial RPS S.à r.l., Esch-sur-Alzette (Luxembourg), Piling Handbook, 8th edition, reprint 2008 (2008) [cited February 15, 2010].
URL http://www.arcelormittal.com/sheetpiling/uploads/files/ArcelorMittal%20Piling%20Handbook_rev08.pdf

[2] Pile driver [cited February 15, 2010].
URL http://en.wikipedia.org/wiki/Pile_driver

[3] K. Viking, Vibro-driveability - a field study of vibratory driven sheet piles in non-cohesive soils, Ph.D. thesis, Division of Soil and Rock Mechanics, Royal Institute of Technology, Stockholm, Sweden (2002).

[4] P. Arnould, J. Canou, H. Gonin, D. Guillaume, P. Keller, Y. Legendre, C. Legrand, F. Rocher-Lacoste, J.-G. Stieffert, D. Vié, Vibratory pile-driving - 2006 technical guide, Presse de l'école nationale des ponts et chaussées, 2006.

[5] M. G. Tseitlin, V. O. Izofoz, Vibro pile-driving of metallic sheet piles under reconstruction and urban development conditions, Soil Mechanics Foundation Engineering 26 (2) (1989) 37–40.

[6] K. Funk, Expertensystem für Lärm- und Erschütterungsprognosen beim Einbringen von Spundbohlen, Ph.D. thesis, Institut für Statik und Dynamik, Leibniz Universität Hannover, Germany (1996).

[7] G. A. Athanasopoulos, P. C. Pelekis, Ground vibrations from sheetpile driving in urban environment: measurements, analysis and effects on buildings and occupants, Soil Dynamics and Earthquake Engineering 19 (5) (2000) 371–387.

[8] S. Bonnefoy-Claudet, F. Cotton, P.-Y. Bard, The nature of noise wavefield and its applications for site effects studies. a literature review, Earth-Science Reviews 79 (3-4) (2006) 205–227.

[9] A. Ahlqvist, E. Enggren, Impact on surrounding environment from vibro driven sheet piles, in: International Symposium on Vibratory Pile Driving and Deep Soil Vibratory Compaction - Transvib 2006, Paris, France, 2006, pp. 317–330.

[10] H. R. Masoumi, G. Degrande, G. Lombaert, Free field vibrations due to vibratory pile driving in layered soil medium, in: International Symposium

on Vibratory Pile Driving and Deep Soil Vibratory Compaction - Transvib 2006, Paris, France, 2006, pp. 343–352.

[11] F. Rocher-Lacoste, A. Braham, J.-F. Semblat, Modélisation de la propagation des ondes en cours de vibrofonçage, in: International Symposium on Vibratory Pile Driving and Deep Soil Vibratory Compaction - Transvib 2006, Paris, France, 2006, pp. 373–385.

[12] H. R. Masoumi, G. Degrande, G. Lombaert, Prediction of free field vibrations due to pile driving using a dynamic soil-structure interaction formulation, Soil Dynamics and Earthquake Engineering 27 (2) (2007) 126–143.

[13] F. Rocher-Lacoste, Étude expérimentale en vraie grandeur et étude numérique des pieux vibrofoncés: vibrations dans l'environnement et capacité portante., Ph.D. thesis, Laboratoire Central des Ponts et Chaussées, École Nationale des Ponts et Chaussées, France (2008).

[14] V. Whenham, L. Areias, F. Rocher-Lacoste, D. Vié, M.-P. Bourdouxhe, A. Holeyman, Full scale sheet pile vibro-driving tests, in: Proceedings of the 17th International Conference on Soil Mechanics & Geotechnical Engineering, Vol. 2, Alexandria, Egypt, 2009, pp. 1354–1357.

[15] The European Parliament and the Council of the European Union, Directive 2002/49/EC of the European Parliament and of the Council of 25 June 2002 relating to the assessment and management of environmental noise, Official Journal of the European Communities L 189 [cited March 1, 2010].
URL `http://eur-lex.europa.eu/LexUriServ/LexUriServ.do?uri=OJ:L:2002:189:0012:0025:EN:PDF`

[16] World Health Organization, Guidelines for Community Noise (1999) [cited March 1, 2010].
URL `http://www.who.int/docstore/peh/noise/Comnoise-4.pdf`

[17] B. Mériel, B. Bonhomme, Le bruit des chantiers, Bulletin des Laboratoires des Ponts et Chaussées 208 (1997) 87–98.

[18] R. Boittin, DV Construction - Suppression du PN. 186 à la Riche (37) - Mesure de bruit, unpublished technical report obtained through personal communications (October 2002).

[19] J.-P. Joris, Battage de palplanches à Zeebrugge - Mesures comparatives du bruit - Rapport, unpublished technical report obtained through personal communications (January 2004).

[20] C. Crispin, B. Ingelaere, Measurement of the noise levels generated by the vibrodriving and the impact driving of different sheetpile's types, unpublished technical report of the Belgian Building Research Institute (BBRI) obtained through personal communications (November 2004).

[21] The European Parliament and the Council of the European Union, Directive 2000/14/EC of the European Parliament and of the Council of 8 May 2000 on the approximation of the laws of the Member States relating to the noise emission in the environment by equipment for use outdoors, Official Journal of the European Communities L 162 [cited March 1, 2010].
URL `http://eur-lex.europa.eu/LexUriServ/LexUriServ.do?uri=OJ:L:2000:162:0001:0078:EN:PDF`

[22] ISO 3744, Acoustics - Determination of sound power levels of noise sources using sound pressure - Engineering method in an essential free field over a reflecting plane, International Organization for Standardization (1994).

[23] ISO 6395, Acoustics - Measurement of exterior noise emitted by earth-moving machinery - Dynamic test conditions, International Organization for Standardization (1988).

[24] H. S. Gill, Assessment of noise from "quiet" pile drivers, Journal of Sound and Vibration 65 (2) (1979) 193–202.

[25] M. J. Ballesteros, M. C. Fernández, S. Quintana, J. A. Ballesteros, I. González, Noise emission evolution on construction sites. measurement for controlling and assessing its impact on the people and on the environment, Building and Environment 45 (3) (2010) 711–717.

[26] A. Schwartz, P. Leonov, Acoustic aspects of building sites, Applied Acoustics 7 (4) (1974) 281–294.

[27] M. Norton, D. Karczub, Fundamentals of noise and vibration analysis for engineers, Cambridge University Press, 2003, Ch. 4, pp. 151–155,162–164,247,274–275.

[28] R. Kruse, S. Sauerzapf, Reducing the Influence of Microphone Errors on In-Situ Ground Impedance Measurements, Acta Acustica united with Acustica 94 (2008) 151–155.

[29] K. Heutschi, Calculation of Reflections in an Urban Environment, Acta Acustica united with Acustica 95 (2009) 644–652.

[30] International Organization for Standardization (ISO), ISO 266: Acoustics - Preferred frequencies (1997).

[31] International Electrotechnical Commission (IEC), IEC 61672-1: Electroacoustics - Sound level meters - Part 1: Specifications (2002).

[32] T. Le Thiet, J. Canou, J.-C. Dupla, Fréquence de sollicitation et vibrofonçabilité des pieux, in: International Symposium on Vibratory Pile Driving and Deep Soil Vibratory Compaction - Transvib 2006, Paris, France, 2006, pp. 177–184.

[33] Arcelor Commmercial RPS S.à r.l., Esch-sur-Alzette (Luxembourg), Steel Sheet Piling - General Catalogue - Edition 2006-2 (2006) [cited February 15, 2007].
URL `http://www.arcelorprojects.com/ADNL/PDF/general_EN.pdf`

[34] ArcelorMittal Commmercial RPS S.à r.l., Esch-sur-Alzette (Luxembourg), Foundation Solutions - Steel Sheet Piling - General Catalogue 2008 - 2nd Edition (2008) [cited Februaty 15, 2009].
URL `http://www.arcelorprojects.com/ADNL/PDF/general_EN.pdf`

[35] ArcelorMittal Commmercial RPS S.à r.l., Esch-sur-Alzette (Luxembourg), Foundation Solutions for Projects - Steel Sheet Piling - General Catalogue 2009 (2009) [cited February 15, 2010].
URL `http://www.arcelorprojects.com/ADNL/PDF/general_EN.pdf`

[36] T. Kawai, Y. Fujitani, Some considerations on the modern beam theory. Theoretical studies., Report of the Institute of Industrial Science, University of Tokyo 32 (2) (1986) 1–78.

[37] R. H. Lyon, R. G. DeJong, Theory and application of Statistical Energy Analysis, 2nd Edition, RH Lyon Corp, Cambridge, MA, 1995, Ch. 3, pp. 65–67.

[38] Y. Lu, H. Hao, G. Ma, Y. Zhou, Local-mode resonance and its structural effects under horizontal ground shock excitations, Journal of Sound and Vibration 254 (1) (2002) 51–68.

[39] E. Dokumaci, An exact solution for coupled bending and torsion vibrations of uniform beams having single cross-sectional symmetry, Journal of Sound and Vibration 119 (3) (1987) 443–449.

[40] M. B. S. Magalhães, R. A. Tenenbaum, Sound sources reconstruction techniques: a review of their evolution and new trends, Acta Acustica united with Acustica 90 (2) (2004) 199–220.

[41] J. Christensen, J. Hald, Beamforming, Brüel & Kjær Technical Review 1 (2004) 1–48 [cited March 1, 2010].
URL `http://www.bksv.com/pdf/bv0056.pdf`

[42] InfraTec GmbH, Dresden (Germany), VarioCAM® hr basic [cited February 15, 2010].
URL `http://www.infratec.de/fileadmin/downloads/pdf/Flyer_VC2_basic_en_mail.pdf`

[43] I. A. Mahfouz, F. Badrakhan, Chaotic behaviour of some piecewise-linear systems, part II: systems with clearance, Journal of Sound and Vibration 143 (2) (1990) 289–328.

[44] F. Peterka, J. Vacík, Transition to chaotic motion in mechanical systems with impacts, Journal of Sound and Vibration 154 (1) (1992) 95–115.

[45] S. Natsiavas, On the dynamics of oscillators with bi-linear damping and stiffness, International Journal of Non-Linear Mechanics 25 (5) (1990) 535–554.

[46] PCB Piezotronics^{INC}, New York (USA), Model 352C03 - Specification Sheet [cited February 15, 2010].
URL `http://www.pcb.com/contentstore/docs/PCB_Corporate/Vibration/products/specsheets/352C03_E.pdf`

[47] K. I. AG, Data sheet, Type 8702B..., 8704B..., Kistler Instrument Corporation, Amherst (USA) [cited February 15, 2010].
URL `http://www.kistler.com/mediaaccess/8702B100__000-239e-03.08.pdf`

[48] PCB Piezotronics^{INC}, New York (USA), Model 352C33 - Specification Sheet [cited February 15, 2010].
URL `http://www.pcb.com/contentstore/docs/PCB_Corporate/Vibration/products/specsheets/352C33_E.pdf`

[49] F. J. Harris, On the Use of Windows for Harmonic Analysis with the Discrete Fourier Transform, Proceedings of the IEEE 66 (1) (1978) 51–83.

[50] L. Cremer, M. Heckl, B. A. T. Peterson, Structure-Borne Sound, 3rd Edition, Springer-Verlag, Berlin Heidelberg, 2005, Ch. 3, pp. 37–38,54–55,67–74,306–318.

[51] E. Mettler, Dynamic buckling, Handbook of engineering mechanics, McGraw-Hill, New York, 1962, Ch. 62, pp. 4–6.

[52] E. A. L. Smith, Pile-driving analysis by the wave equation, Journal of the Soil Mechanics and Foundations Divisions - Proceedings of the ASCE 86 (1960) 35–61.

[53] R. E. D. Bishop, S. M. Cannon, S. Miao, On coupled bending and torsional vibration of uniform beams, Journal of Sound and Vibration 131 (3) (1989) 457–464.

[54] N. M. M. Maia, J. M. M. e Silva, et al., Theoretical and Experimental Modal Analysis, Research Studies Press LTD, 1997, Ch. 1, pp. 63–70.

[55] ABI. Products - MOBILRAM-System - Attachments [online, cited May 1, 2010].
URL `http://www.abi-gmbh.com/abi-attachments.html`

[56] Dawson. Excavator Mounted Vibrators [online, cited May 1, 2010].
URL `http://dawson-engineering.net/driving/vibrators/`

[57] ICE-Holland. Vibratory hammers ICE-Holland [online, cited May 1, 2010].
URL `http://www.ice-bv.nl/products/indexvh.htm`

[58] Pajot. Our Products - Hydraulic Vobrators [online, cited May 1, 2010].
URL `http://www.pajot.com/en/hydraulic-piling-vibrators.html`

[59] PTC. Vibrodrivers - Technical Data [online, cited May 1, 2010].
URL `http://www.ptc.fayat.com/1-1465-1566-1662/Technical-Data.htm`

[60] PVE. Dieseko's Piling & Vibro Equipment - Products [online, cited May 1, 2010].
URL `http://www.dieseko.nl/pve.html`

[61] Soilmec. Attachements - Vibrators [online, cited May 1, 2010].
URL `http://www.soilmec.com/viewdoc.asp?co_id=154`

[62] ThyssenKrupp Steelcom. Products - Vibro Hammers [online, cited May 1, 2010].
URL `http://www.tk-steelcom.com.au/vibro-hammers.htm`

[63] C. N. Bapat, N. Popplewell, Several similar vibroimpact systems, Journal of Sound and Vibration 113 (1) (1987) 17–28.

[64] D. P. Hess, A. Soom, Normal Vibrations and Friction Under Harmonic Loads: Part I — Hertzian Contacts, Journal of Tribology - Transactions of the ASME 113 (1991) 80–86.

[65] Brüel & Kjær, Nærum (Denmark), Product Data - The Falcon™ Range 1/2" Microphones - Types 4188 to 4193 [cited February 15, 2010].
URL `http://www.bksv.com/pdf/Bp1380.pdf`

[66] Brüel & Kjær, Nærum (Denmark), Product Data - DeltaTron® Microphone Preamplifier - Type 2671 [cited February 15, 2010].
URL `http://www.bksv.com/pdf/Bp1446.pdf`

[67] PCB Piezotronics^{INC}, New York (USA), Model 377B02 - Specification Sheet [cited February 15, 2010].
URL `http://www.pcb.com/contentstore/docs/PCB_Corporate/Vibration/products/specsheets/377B02_D.pdf`

[68] PCB Piezotronics^{INC}, New York (USA), Model 426E01 - Specification Sheet [cited February 15, 2010].
URL `http://www.pcb.com/contentstore/docs/PCB_Corporate/Vibration/products/specsheets/426E01_C.pdf`

[69] PCB Piezotronics^{INC}, New York (USA), Model 378B02 - Condenser Microphone - Installation and Operating Manual [cited February 15, 2010].
URL `http://www.pcb.com/contentstore/docs/PCB_Corporate/Vibration/products/Manuals/378B02.pdf`

[70] PCB Piezotronics^{INC}, New York (USA), Model 130D20 - Specification Sheet [cited February 15, 2010].

URL http://www.pcb.com/contentstore/docs/PCB_Corporate/Vibration/products/specsheets/130D20_D.pdf

[71] International Construction Equipment BV, Almere (The Netherlands), 36RF Vibratory Hammer - Specification Sheet [cited February 15, 2010].
URL http://www.ice-bv.nl/MACHINES/M36RF0014/..%5CM36RF%5CSPECSHEET.PDF

[72] International Construction Equipment BV, Almere (The Netherlands), 1000RF Power Pack - Specification Sheet [cited February 15, 2010].
URL http://www.ice-bv.nl/MACHINES/M1000RF010/..%5CM1000RF%5CSPECSHEET.PDF

[73] International Construction Equipment BV, Almere (The Netherlands), 80TU Clamp - Specification Sheet [cited February 15, 2010].
URL http://www.ice-bv.nl/MACHINES/M80TU011/..%5CM80TU%5CSPECSHEET.PDF

[74] International Construction Equipment BV, Almere (The Netherlands), 130TU Clamp - Specification Sheet [cited February 15, 2010].
URL http://www.ice-bv.nl/MACHINES/M130TU011/..%5CM130TU%5CSPECSHEET.PDF

[75] ABI GmbH, Niedernberg (Germany), Applications for the ABI MOBILIRAM-SYSTEM TM 10/12,5.

Appendix A.

Measurement equipment

A.1. Acoustic measurements

Six microphones have been used to measure the sound during the experiments:

Microphones 1 and 2: Brüel & Kjær microphones of type `4189-A-021` (composed of a free-field microphone of type `4189` [65] and of preamplifier of type `2671` [66]);

Microphones 3 and 4: PCB microphones (composed of a free-field microphone of type `377B02` [67] and of a preamplifier or type `426E01` [68]);

Microphone 5 and 6: PCB microphones of type `378B02` [69] (composed of a free-field microphone of type `377B02` [67] and of a preamplifier or type `426E01` [68]).

They have been used with the appropriated windscreen: Brüel & Kjær windscreens of type `UA0459` for the microphones 1 and 2, and PCB windscreens of type `079A06` for the microphones 3, 4, 5 and 6.

A.2. Beamforming measurements

The used microphones were PCB microphones of type `130D20` [70], which were mounted with the associated windscreens of type `079A07`.

A.3. Acceleration measurements

Details about the used accelerometers can be found in tables A.1 and A.2.

Orientation and position	**Mfr.**	**Type**
vertical at 10 m at right	PCB	352C03 [46]
lateral at 10 m at right	KISTLER	8702B100 [47]
front at 10 m at right	PCB	352C03 [46]
vertical at 10 m at left	PCB	352C33 [48]
lateral at 10 m at left	PCB	352C03 [46]
front at 10 m at left	PCB	352C03 [46]
vertical at 17.5 m at left	PCB	352C03 [46]
lateral at 17.5 m at left	PCB	352C03 [46]
front at 17.5 m at left	PCB	352C33 [48]
vertical at 17.5 m at right	PCB	352C03 [46]
lateral at 17.5 m at right	PCB	352C03 [46]
front at 17.5 m at right	PCB	352C03 [46]
vertical at 17.5 m at centre left	PCB	352C33 [48]
lateral at 17.5 m at centre left	PCB	352C33 [48]
front at 17.5 m at centre left	PCB	352C33 [48]

Table A.1.: Description of the accelerometers of the first experiment session

Orientation and position					Mfr.	Type
vertical	on	the vibrodriver	at	right	PCB	352C03 [46]
vertical	on	the vibrodriver	at	left	PCB	352C03 [46]
vertical	at	9 m	at	right	PCB	T352C03 [46]
lateral	at	9 m	at	right	PCB	T352C03 [46]
front	at	9 m	at	right	PCB	T352C03 [46]
vertical	at	9 m	at	centre	PCB	T352C03 [46]
lateral	at	9 m	at	centre	PCB	352C03 [46]
front	at	9 m	at	centre	PCB	352C03 [46]
vertical	at	7.5 m	at	right	PCB	352C03 [46]
vertical	at	7.5 m	at	centre	PCB	352C03 [46]
vertical	at	6 m	at	right	PCB	352C03 [46]
lateral	at	6 m	at	right	PCB	352C03 [46]
front	at	6 m	at	right	PCB	352C03 [46]
vertical	at	6 m	at	centre	PCB	352C03 [46]
lateral	at	6 m	at	centre	PCB	T352C03 [46]
front	at	6 m	at	centre	PCB	T352C03 [46]
vertical	at	4.5 m	at	right	PCB	352C03 [46]
vertical	at	4.5 m	at	centre	PCB	352C03 [46]
vertical	at	3 m	at	right	PCB	352C03 [46]
lateral	at	3 m	at	right	PCB	352C03 [46]
front	at	3 m	at	right	PCB	352C03 [46]
vertical	at	3 m	at	centre	PCB	352C03 [46]
lateral	at	3 m	at	centre	PCB	352C03 [46]
front	at	3 m	at	centre	PCB	352C03 [46]

Table A.2.: Description of the accelerometers of the second experiment session

Appendix B.

Description of the experiments

As a huge range of sound power levels can be measured during the experiments, it is important to specify the configuration of the performed experiments or of the simulation. The parameters can be sorted in three groups:

- the parameters of the sheet pile,
- the parameters of the vibrator, and
- the parameters of the vibratory pile driving.

A reference configuration was chosen for most of the parameters.

B.1. Parameters of the sheet pile

Three parameters are needed in order to characterise the sheet pile during the experiments:

- its type,
- its length, and
- the configuration of its interlock.

Another parameter was intended to be studied: an excessive error for the straightness of the sheet pile. But manufacturing difficulties prevented from testing such a bended sheet pile.

B.1.1. The sheet pile type

Five sheet pile types were used during the experiment sessions, with an elastic section modulus between 1200 and 3800 cm^3/m The reference type had an elastic section modulus of 1400 cm^3/m.

B.1.2. The sheet pile length

Several sheet pile lengths were tested:

- 10 m,
- 12 m,
- 15 m, and
- 20 m.

B.1.3. The common interlock configuration

The interlock configuration should be specified: it describes the assembly of the single sheet piles (by welding, by crimping, free, etc.) and the particularities of the interlock (grinding of the clutches, watertightness joint, etc.). The tested assembly configurations were:

- a totally welded common interlock;
- a crimped common interlock with a maximum space between the crimping points of 2.9 m, as shown in figure B.1a [33, 34, 35]:
  - the maximum distance between the first triple crimping point and the top is 500 mm,
  - then the distance between the triple crimping points is alternatively 700 and 2900 mm;
  - the maximum distance of a double crimping point from the toe is 450 mm;
  - 100 mm separates the points of one group from each other;
- a common interlock like the previous one, but with welds of 200 mm instead of the triple crimping points;
- a common interlock welded like with a maximum space between the welds of 0.8 m (welds of 200 mm), as shown for a crimping in figure B.1b [33, 34, 35]:
  - the maximum distance between the first triple crimping point and the top is 500 mm,
  - then the distance between the triple crimping points is alternatively 700 mm and 800 mm;
  - 100 mm separates the points of one group from each other;

- a free common interlock (no welding nor crimping); to ensure the security, a bolt placed at the toe maintained the sheet pile of 20 m and the sheet pile of 12 m had a weld of 400 mm at its two ends (i.e. a space of 11.2 m between the two welds);
- a partly welded common interlock with a constant spacing between the welds (welds of 200 mm); several configurations were tested:
  - spaces of 5.5 m,
  - spaces of 2.7 m,
  - spaces of 1.2 m, and
  - spaces of 0.5 m.

Some particularities of the interlock were also applied to some sheet piles:

- A crimped common interlock or a partly welded common interlock can be filled by a watertightness joint. Two products were used during the experiments [33, 34, 35]:
  - a polyurethane sealant, and
  - a bituminous sealant.
- A grinding was applied to the clutches in order to increase the clearance.

The reference configuration is a totally welded interlock, with no watertightness joint or grinding. Most of the common interlocks were welded instead of being crimped in order to increase the reproducibility of the assembly.

B.2. Parameters of the vibrator

The two experiment sessions were not performed with the same equipment. Before explaining the parameters, the used equipment must be presented.

First session experiment: The used system was a free-hanging system with the vibrator ICE 36RF-ts [71] and its hydraulic power pack ICE 1000RF [72]. Their main features are listed in table B.1.
Most of the sheet piles were intended to be driven with a double clamp (and not the standard single clamp ICE 320TU). As the sheet pile angle between the web and the flanges depends on the sheet pile type, several double clamps were combined with several plates in order to give the right combination: double clamps ICE 80TU [73] were used for sheet piles with a web angle of 55 °, and double clamps ICE 130TU [74] were used for sheet pile with a web angle of 45 or 63 °.

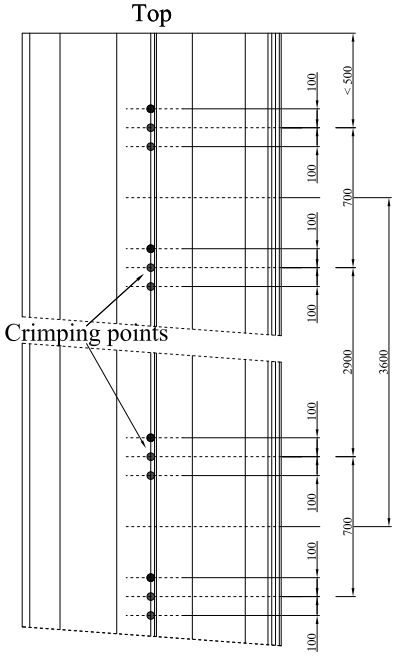

(a) Crimping with a maximum space between the welds of 2.9 m

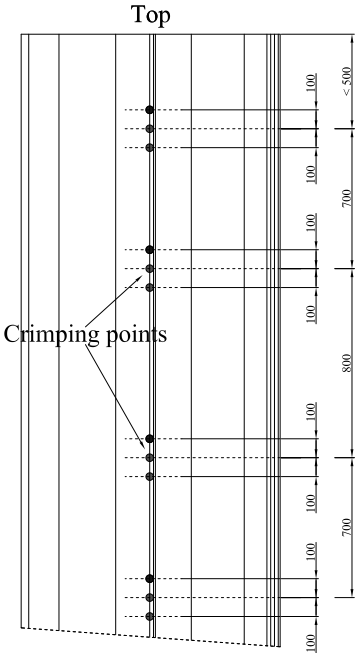

(b) Crimping with a maximum space between the welds of 0.8 m

Figure B.1.: Used crimpings [33, 34, 35]

Eccentric moment	:	0 - 36	kgm
Centrifugal force	:	0 - 2080	kN
Maximum frequency	:	2300	rpm
Dynamic weight (incl. the standard single clamp)	:	6400	kg
Total weight (incl. the standard single clamp)	:	8400	kg
Weight of the hydraulic hoses	:	500	kg

Table B.1.: Technical specifications of the used vibrator [71]

Second session experiment: The used system was the leader-mounted system ABI TM 10/12,5 [75] with the vibrator MRZV 600V. With such a system, the sheet piles were driven with a single clamp. The main features are listed in table B.2.

Eccentric moment	:	0 - 8	kgm
Centrifugal force	:	0 - 600	kN
Maximum frequency	:	2620	rpm
Dynamic weight (incl. the standard jaw assembly)	:	1950	kg
Total weight (incl. the standard jaw assembly)	:	2900	kg

Table B.2.: Technical specifications of the used vibrator [75]

B.2.1. The frequency

Four vibrator frequencies were used. These frequencies could vary in a short range (1 or 2 Hz), depending on the mass of the sheet pile, the power absorbed by the soil, the features of the motor, etc.

For the first experiment session:

- ± 38 Hz,
- ± 33 Hz, and
- ± 28 Hz.

For the second experiment session:

- ± 43 Hz.

For each experiment session, the reference frequency was the maximum available frequency: ± 38 Hz for the first experiment session and ± 43 Hz for the second experiment session.

B.2.2. The eccentric moment

As these vibrators had a variable eccentric moment, several driving forces were tested.

For the first experiment session:

- the maximum eccentric moment (36 kgm).

For the second experiment session:

- the maximum eccentric moment (8 kgm),
- 70% of the maximum eccentric moment (5.6 kgm), and
- 50% of the maximum eccentric moment (4 kgm).

For each experiment session, the reference eccentric moment was the maximum available eccentric moment: 36 kgm for the first experiment session and 8 kgm for the second experiment session.

B.2.3. The clamping system

Two types of clamping devices were used:

- a system with a double clamping system , and
- a system with a single clamping system.

For the first experiment session, the used clamping system was a double clamping system, except for one experiment (performed to make comparisons). For the second experiment session, the used clamping system was a single clamping system (as it is more difficult to place a double clamping system on a leader-mounted system).

B.3. Parameters of the vibratory pile driving

Many parameters related to this driving method could influence the noise generation. Only three of them were studied: the static surcharge force, the vibratory pile driving and the wall.

The influence of a guide (in wood or in steel) was intended to be measured, but the performed experiments were not representative of the guides used by the contractors.

B.3.1. The static surcharge force

For the first experiment session: Two static surcharge forces[1] F_0 were applied to the sheet pile during the vibratory pile drivings. For a free-hanging system, the static surcharge force is defined as follows [3]:

$$F_0 = g\ m_0 - T \tag{B.1}$$

where F_0 = static surcharge force $[N]$,
g = gravity $[m/s^2]$,
m_0 = bias mass $[kg]$, and
T = suspension force of the carrier (crane) $[N]$.

- For the reference case, a little suspension force was applied to maintain the sheet pile vertical; the static surcharge force was then around 26 kN.
- In the other case, the sheet pile had no contact with the conveyor belts: the static surcharge force was then equal to the opposite of the weight of the sheet pile (-31 kN).

For the second experiment session: In the case of a leader-mounted system, the static surcharge force F_0 is defined as follows [3]:

$$F_0 = g\ m_{sh} + P_0\ A_{cyl} \tag{B.2}$$

where F_0 = static surcharge force $[N]$,
g = gravity $[m/s^2]$,
m_{sh} = weight of the suppressor housing $[kg]$,
P_0 = hydraulic oil pressure $[N/m^2]$, and
A_{cyl} = area of hydraulic cylinder $[m^2]$.

The static surcharge force was always set at the maximum value: the maximum pressure delivered by the cylinders of the leader and the weight of the suppressor housing (more than 70 kN).

B.3.2. The vibratory pile driving

In section 1.2 was presented a method to drive sheet pile in a reproducible way and independently of the soil properties (on woodblocks and conveyor belts, see figure 1.8).

[1] The static surcharge force is defined as the average static force applied by the vibrator to the sheet pile.

To verify that similar levels were obtained (compared to the normal method used to drive), vibratory pile drivings with a downward and/or an upward motion were performed in the soil.

B.3.3. The wall

Four wall configurations were used:

- the sheet pile was tested without any connection to the wall,
- the sheet pile was interlocked with an existing wall of 1 m above ground level,
- the sheet pile was interlocked with an existing wall of 1 m above ground level by using a clutch filled by a bituminous sealant, and
- the sheet pile was interlocked with an existing wall of 3 m above ground level.

During these experiments, the downward motion of the sheet pile was still stopped by woodblocks and conveyor belts buried in the soil, even if the wall had been driven to a larger depth. The reference configuration was without any connection to the wall.

For the first experiment session: The wall was built by cutting a sheet pile a sheet pile of 20 m in three parts. So the wall of 1 m above the ground level had 5.6 m of penetration depth and the wall of 3 m above the ground level had 3.6 m of penetration depth. The clutch of the vibrating sheet pile that was interlocked with the wall was the curved one.

For the second experiment session: The wall was built by cutting a sheet pile of 12 m in three parts. So the walls of configurations of 1 m above the ground level had 3 m of penetration depth. The clutch of the vibrating sheet pile that was interlocked with the wall was the straight one for experiments with bituminous sealant in the connection with the wall and the curved one for experiments without bituminous sealant in the connection with the wall.

Appendix C.

The section principle for a harmonic behaviour

When performing harmonic *Finite Element* (FE) simulations, the following matrix problem is solved (the process gives similar results when considering the damping):

$$\mathbf{K}\ \mathbf{x} - \omega^2\ \mathbf{M}\ \mathbf{x} = \mathbf{f} \tag{C.1}$$

where $\mathbf{K}$ = stiffness matrix,
$\mathbf{x}$ = response vector, defined as $[x(t)] = \mathbf{x}\ \mathrm{e}^{\ i\ \omega\ t}$,
ω = angular frequency $[rad/s]$,
$\mathbf{M}$ = mass matrix, and
$\mathbf{f}$ = excitation force vector, defined as $[f(t)] = \mathbf{f}\ \mathrm{e}^{\ i\ \omega\ t}$.

For a given excitation, the harmonic motion can be obtained by two ways as already explained in section 5.2.1:

- Equation C.1 can be solved by the direct inversion for each studied angular:

$$\mathbf{x} = [\mathbf{K} - \omega^2\ \mathbf{M}]^{-1}\ \mathbf{f} = \boldsymbol{\alpha}(\omega)\ \mathbf{f} \tag{C.2}$$

  where $\boldsymbol{\alpha}(\omega)$ = receptance matrix.

- N resonance angular frequencies ω_k and modes $\boldsymbol{\Psi}_k$ can be calculated and use to obtain the receptance matrix $\boldsymbol{\alpha}(\omega)$ [54]:

$$\boldsymbol{\alpha}(\omega) = \sum_{k=1}^{N} \frac{\boldsymbol{\Psi}_k\ \boldsymbol{\Psi}_k^T}{\boldsymbol{\Psi}_k^T\ \mathbf{M}\ \boldsymbol{\Psi}_k}\ \frac{1}{\omega_k^2 - \omega^2} \tag{C.3}$$

  where N = number of modes,
  $\boldsymbol{\Psi}_k$ = mode shape vector of mode k, and
  ω_k = natural angular frequency of mode k $[rad/s]$.

  N is equal to the number of *Degrees Of Freedom* (DOF). A good approximation is obtained by choosing the modes with frequencies ω_k close to ω.

C.1. Splitting of the initial system into several parts

When splitting a static system into several parts, forces are added to the system where the splitting occurs in order to replace the internal forces transmitted by the removed element. It is the section principle.
Analogously, forces can be added to a harmonic model when splitting it. But the description of the system with resonances is changed (the resonance depends on the boundary conditions and on the structure) as well as the mass and the stiffness matrices. It is shown here below that, even if the modal description is changed, the same displacements (and thus harmonic behaviour) are obtained by adding forces where the system was cut.
To demonstrate it, a simple system with a finite number n of DOF is split into two parts like in figure C.1: part I with P DOF and part II with Q DOF. When removing spring k_2 in figure C.1, two forces $F(\omega)$ are added in order to have the same response of the two parts: these forces $F(\omega)$ are set to the value of the force generated before the splitting by spring k_2 at the angular frequency ω.

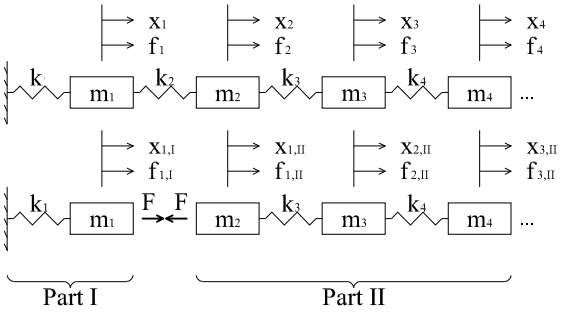

Figure C.1.: Splitting of a system

The description of the new parts is made similarly to equation C.2:

$$\mathbf{x}_I = [\mathbf{K}_I - \omega^2\ \mathbf{M}_I]^{-1}\ (\mathbf{f}_I + \mathbf{F}_I) = \boldsymbol{\alpha}_I(\omega)\ (\mathbf{f}_I + \mathbf{F}_I) \tag{C.4}$$

$$\mathbf{x}_{II} = [\mathbf{K}_{II} - \omega^2\ \mathbf{M}_{II}]^{-1}\ (\mathbf{f}_{II} + \mathbf{F}_{II}) = \boldsymbol{\alpha}_{II}(\omega)\ (\mathbf{f}_{II} + \mathbf{F}_{II}) \tag{C.5}$$

where $\mathbf{x}_I$ = response vector of part I,
$\mathbf{K}_I$ = stiffness matrix of part I,
$\mathbf{M}_I$ = mass matrix of part I,
$\mathbf{f}_I$ = excitation force vector of part I,
$\mathbf{F}_I$ = excitation force vector of the forces added to part I,
$\boldsymbol{\alpha}_I(\omega)$ = receptance matrix of part I,
$\mathbf{x}_{II}$ = response vector of part II,

$\mathbf{K}_{II}$ = stiffness matrix of part II,
$\mathbf{M}_{II}$ = mass matrix of part II,
$\mathbf{f}_{II}$ = excitation force vector of part II, and
$\mathbf{F}_{II}$ = excitation force vector of the forces added to part II,
$\boldsymbol{\alpha}_{II}(\omega)$ = receptance matrix of part II.

A relationship exists between $\mathbf{x}$ and $\mathbf{x}_I$: it is a $P \times N$ matrix $\mathbf{R}_I$ (called here "reduction matrix") filled only by some 0 and 1 placed in such a way that:

$$\mathbf{x}_I = \mathbf{R}_I \, \mathbf{x} \tag{C.6}$$

where $\mathbf{R}_I$ = reduction matrix of part I.

The following relationship can be obtained:

$$\mathbf{f}_I = \mathbf{R}_I \, \mathbf{f} \tag{C.7}$$

$$\mathbf{F}_I = \mathbf{R}_I \, \mathbf{F} \tag{C.8}$$

$$\mathbf{I}_P = \mathbf{R}_I \, \mathbf{R}_I^T \tag{C.9}$$

$$\mathbf{M}_I = \mathbf{R}_I \, \mathbf{M} \, \mathbf{R}_I^T \tag{C.10}$$

where $\mathbf{F}$ = excitation force vector replacing the removed springs (i.e. spring k_2 in figure C.1), and
where $\mathbf{I}_P$ = $P \times P$ identity matrix.

It has to be written that[1]:

$$\mathbf{K}_I \neq \mathbf{R}_I \, \mathbf{K} \, \mathbf{R}_I^T \tag{C.11}$$

Similarly,

$$\mathbf{x}_{II} = \mathbf{R}_{II} \, \mathbf{x} \tag{C.12}$$

$$\mathbf{f}_{II} = \mathbf{R}_{II} \, \mathbf{f} \tag{C.13}$$

$$\mathbf{F}_{II} = \mathbf{R}_{II} \, \mathbf{F} \tag{C.14}$$

$$\mathbf{I}_Q = \mathbf{R}_{II} \, \mathbf{R}_{II}^T \tag{C.15}$$

$$\mathbf{M}_{II} = \mathbf{R}_{II} \, \mathbf{M} \, \mathbf{R}_{II}^T \tag{C.16}$$

$$\mathbf{K}_{II} \neq \mathbf{R}_{II} \, \mathbf{K} \, \mathbf{R}_{II}^T \tag{C.17}$$

where $\mathbf{I}_Q = Q \times Q$ identity matrix.

The same masses belong to the initial system and the group of the split parts,

[1] Indeed, one or several springs were deleted.

but this is not true for the springs:

$$\mathbf{M} = \sum_{i=I}^{II} \mathbf{R}_i^T \ \mathbf{M}_i \ \mathbf{R}_i \tag{C.18}$$

$$\mathbf{K} \neq \sum_{i=I}^{II} \mathbf{R}_i^T \ \mathbf{K}_i \ \mathbf{R}_i \tag{C.19}$$

C.2. Relationship between the initial system and split parts

A relationship[2] links $\boldsymbol{\alpha}$ to $\boldsymbol{\alpha}_I$: if $\boldsymbol{\alpha}$ is known, $\boldsymbol{\alpha}_I$ can be found.

The force vector $\mathbf{F}(\omega)$ is composed of the forces applied on the masses by the deleted springs:

$$\mathbf{F} = \left[\sum_{i=I}^{II} \mathbf{R}_i^T \ \mathbf{K}_i \ \mathbf{R}_i - \mathbf{K} \right] \ \mathbf{x} \tag{C.20}$$

When adding this force vector $\mathbf{F}(\omega)$ to the force vector $\mathbf{f}$ applied to the initial model (see equation C.1), the responses of the split systems are the same when considering the common DOF:

$$\mathbf{x}_i = \boldsymbol{\alpha}_i \ [\mathbf{f}_i + \mathbf{F}_i] = \boldsymbol{\alpha}_i \ \mathbf{R}_i \ [\mathbf{f} + \mathbf{F}] = \mathbf{R}_i \ \mathbf{x} = \mathbf{R}_i \ \boldsymbol{\alpha} \ \mathbf{f} \quad \text{for } i = I, II \tag{C.21}$$

$\mathbf{F}$ is replaced by its expression from equation C.20 in equation C.21:

$$\boldsymbol{\alpha}_I \ \mathbf{R}_I \ \left[\mathbf{f} + \left[\sum_{i=I}^{II} \mathbf{R}_i^T \ \mathbf{K}_i \ \mathbf{R}_i - \mathbf{K} \right] \ \mathbf{x} \right] = \mathbf{R}_I \ \boldsymbol{\alpha} \ \mathbf{f} \tag{C.22}$$

$$\boldsymbol{\alpha}_I \ \mathbf{R}_I \ \left[\mathbf{I}_N \ \mathbf{f} + \left[\sum_{i=I}^{II} \mathbf{R}_i^T \ \mathbf{K}_i \ \mathbf{R}_i - \mathbf{K} \right] \boldsymbol{\alpha} \ \mathbf{f} \right] = \mathbf{R}_I \ \boldsymbol{\alpha} \ \mathbf{f} \tag{C.23}$$

$$\boldsymbol{\alpha}_I = \mathbf{R}_I \ \boldsymbol{\alpha} \ \left[\mathbf{I}_N + \left[\sum_{i=I}^{II} \mathbf{R}_i^T \ \mathbf{K}_i \ \mathbf{R}_i - \mathbf{K} \right] \boldsymbol{\alpha} \right]^{-1} \ \mathbf{R}_I^T \tag{C.24}$$

Equation C.24 shows that the receptance matrix of the split models $\boldsymbol{\alpha}_I$ can be obtained from the receptance matrix of the initial model $\boldsymbol{\alpha}$ and some manipulations describing the splitting of the initial model. This implies that when playing

[2] This development is made for part I; the results for part II are obtained by replacing the subscripts I by II in the final results.

with complex boundary conditions: they can be replaced by well chosen harmonic forces applied on a free model and the obtained motion will be the same, even if the modal description is different.

A FE model is described by such matrices, and this implies that some boundary conditions can be replaced by forces; these forces can be adjusted, for example in order to fit measurements (displacements, velocities or accelerations, stresses or strains, etc.). The maximum number of forces that can be added at nodes is the number of measurements: if five measurements are available, then forces can be added at five nodes.